

Inside: **Energy Quarterly**



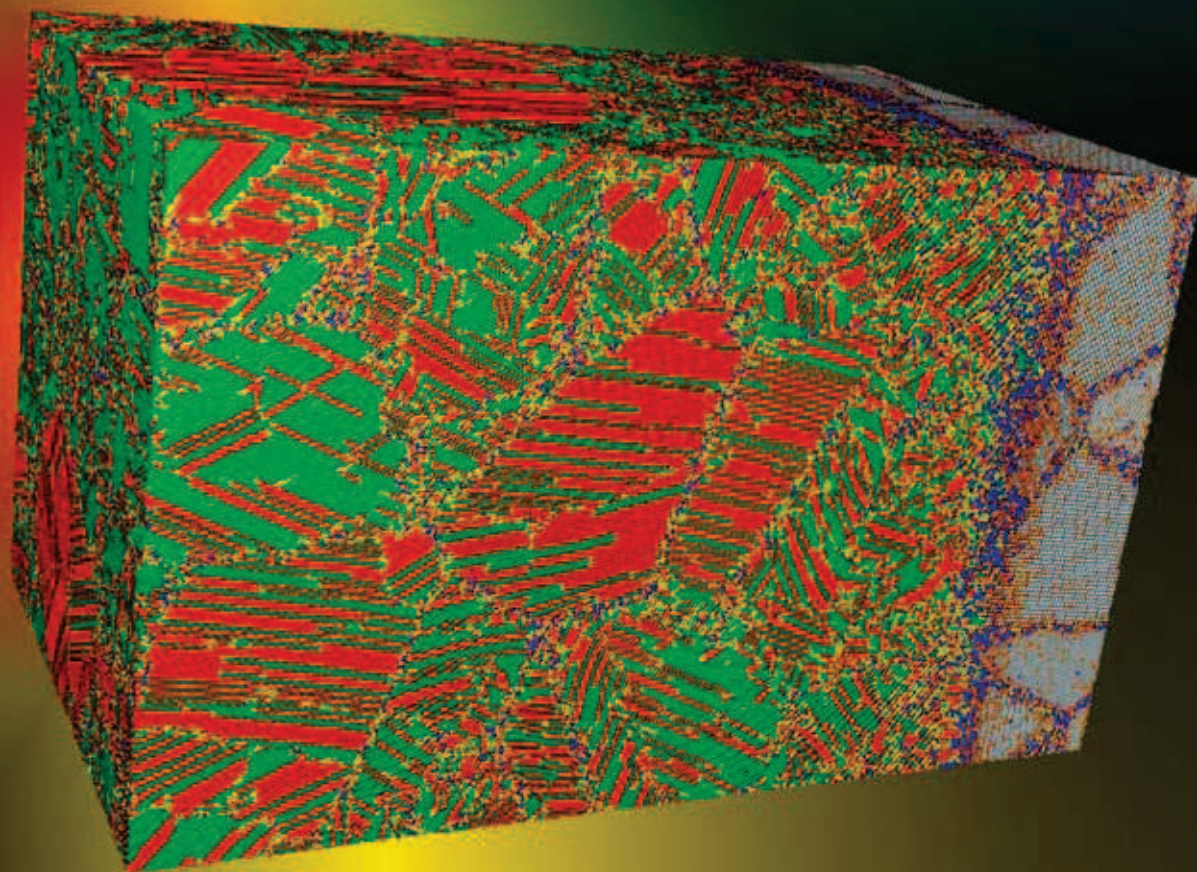
MRS **Bulletin**

December 2010 Vol. 35 No. 12
www.mrs.org/bulletin



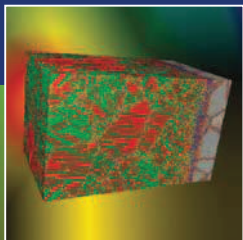
MATERIALS RESEARCH SOCIETY
Advancing materials. Improving the quality of life.

Structural metals at extremes



ALSO IN THIS ISSUE

**Materials for organic
and hybrid inorganic/
organic electronics**



Structural metals at extremes

Amit Misra and Ludovic Thilly, Guest Editors

Designing structural materials for tailored response at extreme conditions is a grand challenge in materials research. Such materials can be made using either “top-down” or “bottom-up” processes to create nanostructured metals and composites that contain atomically designed interfaces that not only block dislocation slip but also attract, absorb, and annihilate point and line defects. Such multifunctional material systems are not just high in strength but also tolerant of damage at extremes of irradiation, temperature, and mechanical stresses, and hence have applications as structural materials in nuclear power and other energy, transportation, and defense technologies. The exploration of these exceptional properties at extremes requires novel and unconventional methodologies, such as *in situ* experiments with high spatial and temporal resolution, complemented by simulation across multiple length and time scales.

Introduction

The topic of “materials under extreme environments” has received significant attention recently. Materials are key building blocks for the next generation of energy technologies, where they must feature enhanced performance at extremes of mechanical stress, strain, temperature, pressure, corrosive environments, particle radiation flux, and electric or magnetic fields.¹ For example, using supercritical steam significantly increases the efficiency of coal-fired power plants, but requires 50% higher operating temperatures and roughly double the operating pressure. Transportation applications, such as cars and aircraft, need lighter-weight and higher-strength structural materials to increase fuel efficiency and reduce CO₂ emission. For future nuclear-fission power plants, structural and cladding materials must perform at higher temperature and high dpa (displacements per atom). These increasingly extreme operating environments accelerate the aging process in materials, leading to reduced performance and eventually to failure.

Structural materials in defense, aerospace, construction, and other national-infrastructure applications also fail unpredictably, often at stresses less than 10% of the theoretical limit of strength for perfect crystals. Incremental changes in current structural materials may not produce the revolutionary breakthroughs needed for future applications. Innovative basic research that elucidates the fundamentals of how materials behave in extreme environments is required. Controlling the

matter-extreme environment interactions can help researchers to develop revolutionary new materials that perform in predictable ways at stresses approaching the theoretical limit of material strength, on the order of 10% of the elastic modulus, extending lifetimes, increasing efficiencies, providing novel capabilities, and lowering costs.^{1–3}

At a more fundamental level, the development of materials with a tailored response in extreme environments addresses one of the five grand challenges outlined in the recent Basic Energy Sciences Advisory Committee report⁴ titled “Directing Matter and Energy: Five Challenges for Science and the Imagination”: How do we design and perfect atom- and energy-efficient syntheses of revolutionary new forms of matter with tailored properties? Embodied in this grand challenge are specific science issues for structural materials at extremes, such as:

- How resistant to failure in extreme conditions of temperature, radiation, or environment exposure can we make a material?
- How do we make hard matter that heals damage or defects?
- How mechanically strong can we make materials yet keep them lightweight?

The field of “materials under extreme environments” is quite broad and may require more than one *MRS Bulletin* theme issue to capture the new developments. The focus of this issue is on metals, leaving out non-metals (ceramics for nuclear

Amit Misra, Los Alamos National Laboratory, New Mexico, USA; amisra@lanl.gov

Ludovic Thilly, Department of Physics and Mechanics of Materials, P-prime Institute, CNRS-University of Poitiers, SP2MI, Ave. Marie et Pierre Curie, 86962 Futuroscope, France; ludovic.thilly@univ-poitiers.fr

fuels, waste forms, and high-pressure synthesis of diamonds) and “chemistry at extremes” (e.g., chemistry of explosives at high-pressure, high strain rates). Keeping metals (especially nanostructured metals) as the focus, the set of articles in this issue highlights new developments in structural metals for radiation damage tolerance, shock, high magnetic fields, and high temperature stability. These articles capture three aspects of research in this field: (1) plastic deformation at extremes to synthesize bulk nano-metals and composites, (2) performance of nano-metals and composites (regardless of synthesis method) in some form of extreme environment such as particle radiation, high temperatures, high strain rates, and high magnetic fields, and (3) characterization methods (e.g., *in situ* x-ray diffraction or transmission electron microscopy [TEM]) for elucidation of damage processes under extreme environments.

Synthesis of new metal structures by severe plastic deformation bulk

During recent decades, the principal materials-design strategy has involved developing multifunctional structural materials with increased microstructure complexity. In this approach, the structural component also provides the functional property, such as reduction of mass, thermal insulation, electrical conduction, magnetic properties, acoustic damping, energy absorption, deformability, by adding selected new phases and refining the microstructure down to the nanometer scale. In this way, new nanocomposite materials have been developed, for instance, complex duplex steels or transformation-induced plasticity (TRIP) steels.⁵ The mechanical properties of each phase of these complex materials are strongly influenced by the high surface-to-volume ratio of the nanograins. Their flow strength, which is dislocation-mediated at large grain size, is increased by the so-called “size effect” (smaller is stronger).^{6–8} Moreover, the combination of different phases with different microstructure dimensions leads to complex co-deformation behavior.

Among the most promising fabrication techniques to obtain nanostructured metallic materials in the bulk form at the industrial scale are those based on severe plastic deformation (SPD), which by definition subjects materials to very large strains. In fact, researchers in this field talk in terms of “true strain,” which is the natural logarithm of the ratio of initial and final dimensions. The true strain is equal to the traditional “engineering strain,” or fractional change in dimension, only when these quantities are much less than one. In SPD, the true strain is typically larger than five, which breaks down the polycrystalline bulk material into crystalline units with dimensions of nanometers.

The article by Zhu et al. in this issue reviews the principal SPD techniques. Bulk nanostructured materials can be made using the severe deformations available in equal channel angular pressing (ECAP), high-pressure torsion (HPT), and accumulative roll bonding (ARB). Several variants of these SPD processes also exist: repetitive corrugation and straightening, co-shearing process, continuous confined strip shearing, twist extrusion, high-pressure tube twisting, asymmetric

rolling, and accumulative drawing and bundling. Nanostructured surface layers can be created on bulk metals using the repetitive pummeling known as surface mechanical attrition treatment (SMAT).

This “top-down” approach of SPD is based on the accumulation of lattice defects (dislocations) to achieve microstructure refinement. It contrasts with a “bottom-up” approach, where nanostructured materials are synthesized atom-by-atom, layer-by-layer, or via consolidation of small clusters.⁹ Metals are excellent candidates for SPD techniques, since they usually exhibit a ductile behavior at the strain rates and temperatures associated with these techniques. The details of the mechanisms involved in the grain refinement depend on the nature of the metals, such as crystallography, stacking fault energy, and strain hardening, and have been thoroughly studied during the past decades.^{10,11}

The view emerging from the earlier research is that SPD involves different stages of glide and interaction of dislocations, leading to their accumulation with increasing strain (**Figure 1a**), until a heterogeneous microstructure is formed, composed of regions with high or low dislocation density (Figure 1b). Upon further straining of the structure, loose tangles transform into dislocation walls by annihilation of dislocations with opposite Burgers vectors (via combined glide, cross-slip, and climb processes), separating dislocation-free regions or subgrains (Figure 1c).

In SPD techniques, this process is pushed to the limits by reaching the extreme stages of work hardening,^{10,11} where the thickness of the dislocation walls is further reduced (Figure 1d) until forming new grain boundaries. The formation of new grain boundaries suggests that grain refinement involves dynamic recovery of stored dislocations (Figure 1e). Along with the associated reduction of grain size, a typical feature of SPD-processed metals is the presence of a large fraction of grain boundaries (GBs) separating adjacent grains with crystallographic misorientation larger than 15°, referred to as high-angle grain boundaries (HAGBs).¹¹ HAGBs act as dislocation obstacles when the SPD-processed materials are subjected to service loading, giving them superior mechanical resistance.¹²

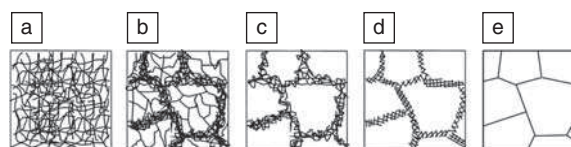


Figure 1. The main steps of grain refinement by severe plastic deformation (SPD). (a) Dislocations accumulate upon straining and (b) interact until forming a heterogeneous structure with high or low dislocation density regions. Further straining leads to the formation of (c) a typical microstructure with dislocation cells composed of dislocation walls separating dislocation-free regions (subgrains), the dislocation walls being (d) continuously refined until transformed into (e) grain boundaries when the SPD process is pushed to the limits to obtain a bulk ultrafine grain or nanostructured material.

The interest in studying SPD-processed materials is therefore twofold. First, the previously described microstructure refinement is a source for bulk materials with improved mechanical properties. Second, very large strains are imposed on the material in a confined geometry: the material is either forced to flow through a die with specific geometry (as in ECAP, ARB, and other variants) or to deform in a confined volume (as in HPT). In the case of SMAT, the material's surface is impacted by very energetic flying balls over a short period of time, and the bulk part of the material also confines the impacted region. In all cases, this confinement of metal flow leads to the creation of a complex stress state with intense hydrostatic and deviatoric components associated with high pressure and shear stresses. Such built-in pressure usually impedes massive fracture of the material, allowing copious plasticity.

Unique properties of nanostructured metals

Understanding how a metal responds to such severe and repeated deformation conditions is an important fundamental topic. Raabe et al. describe this issue in detail, with particular emphasis on the microstructure and the mechanical properties of metallic nanocomposites fabricated by SPD. By comparison to single-phase nanostructured metals, the study of composite materials is of interest since their mechanical properties generally result from a complex interplay between the properties of individual phases and the presence of interphase boundaries. In particular, internal stresses develop during co-deformation because of intra- and intergranular variations of plastic strain and have a strong impact on the strengthening mechanisms and macroscopic mechanical properties.

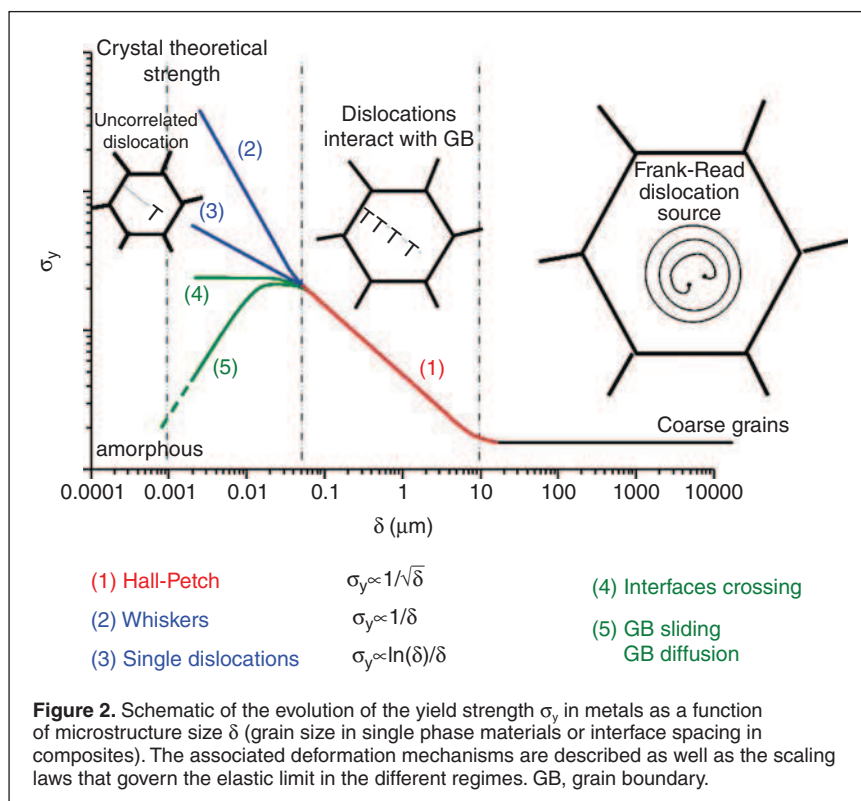
The first benefit in applying SPD to composite metals is the achievement of nanoscale phases leading to their improved mechanical strength. Among the oldest examples are the Damascus and Indian Wootz steels, or the steels obtained by pattern welding achieved by repeated folding in the early Middle Ages both in Europe and Asia.^{13,14} Similar exceptional mechanical properties are found in modern materials such as steel cords and piano wires and are now recognized as the effect of microstructure refinement on the plasticity mechanisms.

Indeed, it is now established that microstructure refinement exerts a strong influence on the mechanical properties of materials, as a result of the coupling between two length scales. One scale is the characteristic length of the physical phenomenon involved (in the case of plasticity, the mean free path of dislocations and the average distance between dislocations). The other scale is the microstructural dimension (grain size, grain boundary width, obstacle spacing, and radius). The interaction of these two quantities leads to deviations from conventional behavior.^{15,16}

The well-known Hall-Petch strengthening of polycrystalline materials is an example, in which a reduction of the grain size d (down to the micrometer regime) is accompanied by an increase of the yield stress, following a $d^{-1/2}$ dependence (Figure 2). With the development of new fabrication processes, the nanometer regime has been probed, and deviations from Hall-Petch strengthening have been recorded.

As GBs become more influential with grain-size reduction, the traditional plasticity mechanisms involving *intragrain* nucleation and propagation of dislocations become restricted. New strengthening mechanisms include deformation via uncorrelated dislocations (Orowan-type mechanism), with a grain-size dependence of the yield stress of $(1/d)\ln(d/b)$, where b is the length of the Burgers vector of the dislocations.^{17–22} Another mechanism involves whisker-type behavior, with a $1/d$ dependence.^{22,23} In the few-nanometer regime, a size-independent plateau in the yield stress is sometimes observed²¹ and attributed to easy dislocation transmission across GBs, while in some nanocrystalline materials, a softening (“inverse” Hall-Petch effect²⁴) has been reported as an indicator of diffusion processes or GB sliding associated with the large number of atoms located at GBs when the grain size is very small.

As pointed out in the article by Raabe et al., in nanocomposite metals, the heterophase interfaces provide an additional parameter to play with in the search for high-strength materials. Depending on the atomic species and the local crystallographic structure, these interfaces will transmit or trap dislocations, therefore modifying the strain-hardening behavior of the materials.



It is clear that the concept of interface engineering will be a key issue in the future development of nanocomposite materials, as discussed in the articles by Raabe et al. and Demkowicz et al.

Another remarkable feature exhibited by the nanostructured single phase or composite metals is the extension of the elastic-plastic transition, giving rise to a pronounced rounding of the stress-strain curves. This effect originates from very heterogeneous deformation taking place in these materials because of more-or-less extended grain- (or phase-) size distribution and complex internal stresses arising both from processing and from plastic incompatibilities between grains with different orientations relative to an externally applied stress.

At very small grain size, the probability that a grain experiences a plastic event (i.e., the emission of an individual dislocation at a GB, its gliding in the grain interior, and its absorption at the GB) is very small.^{25,26} As a consequence, nanostructured materials exhibit an extended microplastic regime characterized by early strain hardening. Hence the conventional criterion used to define the onset of macroplasticity, a macroyield strain equal to 0.2%, appears meaningless since at such strain, only a very small portion of grains have deformed plastically.^{25,26} This statement has been experimentally confirmed in nanocrystalline Ni, Cu/Ag multilayers, nanostructured Ni-Fe alloys, nanocomposite Cu/Nb wires, and nanocrystalline metal films. The amount of strain assigned to microplasticity was measured to significantly exceed the 0.2% convention for bulk metals.^{27–32} This phenomenon must be taken into account to define a stress value that does not underestimate the onset of macroplasticity in nanostructured materials.

The second benefit of applying SPD to composite metals is to study their microstructure evolution when subjected to extreme strains, beyond most normal service conditions. After SPD, a large elastic energy is stored via internal stresses and lattice defects (dislocations, vacancies), a situation where the materials are far from thermodynamic equilibrium. In such conditions, unexpected phenomena are likely to appear at interfaces, such as mechanical alloying or amorphization, even in the case of highly immiscible phases. Raabe et al. review observations made possible by state-of-the-art characterization techniques at the atomic scale: high-resolution TEM and atom probe tomography are ideal experimental tools and are well complemented by simulation techniques.

The models proposed to explain these observations either invoke purely diffusion-driven mechanisms, defect-enhanced diffusion or interface roughening, and plasticity-driven mechanical mixing. Independent of the validity of the models, these observations lead to the following contradiction with what was described earlier. After SPD and (partial) dissolution of previously sharp interfaces, the nanocomposite

metals continue to exhibit high strength. This phenomenon is still not fully understood, but it must be recognized in any process of interface engineering.

Nanostructured metals for high field magnets

As an illustration of how the SPD-processed nanocomposite metals are useful for applications that require extreme properties, we review the case of high-pulsed-field magnets. The generation of high magnetic fields (> 60 T) requires magnet winding materials with high electrical conductivity to minimize Ohmic heating effects. These fields are generally produced during a few milliseconds in pulsed magnets. At such fields, the Lorentz forces result in extreme Von Mises stresses on the winding material. At 60 T, the magnetic pressure is of the order of 1.5 GPa, and the Von Mises stress reaches 1 GPa; at 100 T, the magnetic pressure is 4 GPa, and the maximum stress on the magnet is larger than 2.2 GPa.^{33–35} Multifunctional materials with high electrical conductivity and high strength are therefore needed to safely survive these harsh operating conditions in nondestructive magnets.

The high electrical conductivity requirement demands copper-based materials for the magnet application. Among these materials, only nanocomposite wires can combine low electrical resistivity with an elastic limit high enough to withstand the Von Mises stress previously described.³⁴ **Figure 3**

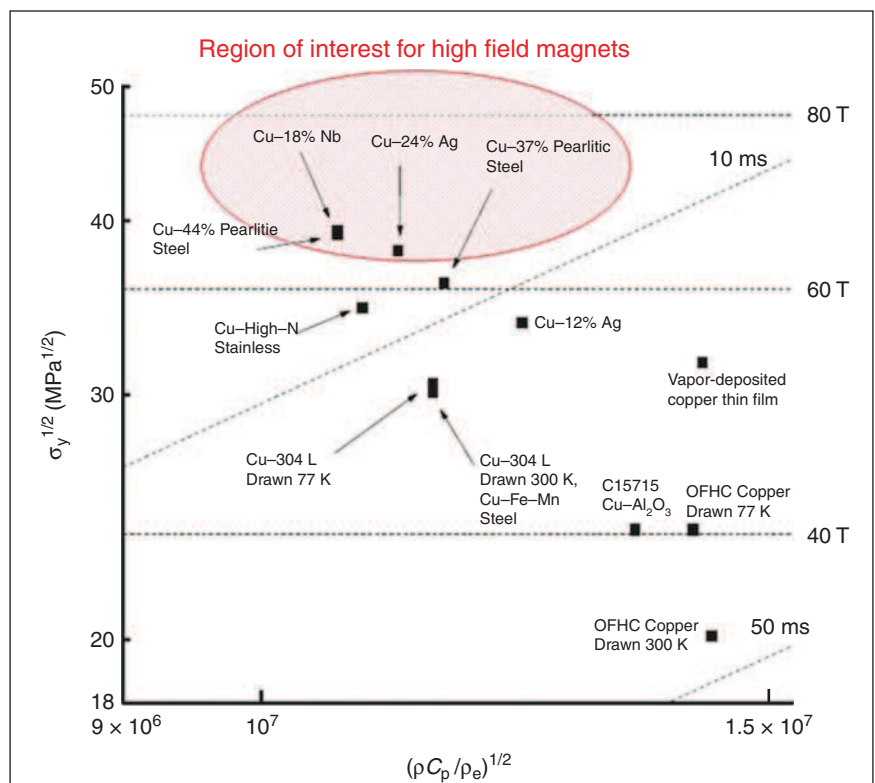


Figure 3. Materials-selection chart for high-field magnet development. Horizontal dashed lines indicate strength allowing a particular field intensity, while diagonal lines correspond to an allowable pulse duration. Only copper-based nanocomposite metals provide the necessary compromise between elastic limit ($\sigma_y^{1/2}$) and transport properties ($(\rho C_p/\rho_e)^{1/2}$), where ρ is the density, C_p is the volumetric heat capacity, and ρ_e is the electrical resistivity.³⁴

is a materials-selection chart showing the relative position of different copper-based material classes (from bulk cold-drawn Cu to highly complex composites and alloys) with respect to the two limiting factors: strength, σ_y , plotted as $\sigma^{1/2}$, and a quantity that quantifies Ohmic heating. Heavily cold-drawn Cu/Nb (Cu-18%Nb) and Cu/Ag (Cu-24%Ag) wires are the best candidates for a 60 T application; further improvements will still be required for higher fields.^{34,36}

One of the candidates, labeled Cu-18%Nb in Figure 3, is continuous Cu/Nb nanocomposite wire, composed of an architected multiscale Cu matrix reinforced by Nb nanofilaments or nanotubes. The wires were fabricated by SPD with the accumulative drawing and bundling process (SPD methods are reviewed in the article by Zhu et al.). A series of hot-extrusion/cold drawing/bundling cycles are repeated n times ($n \leq 5$) to obtain conductors containing $N = 85^n$ Nb nanostructures with a known distribution, separated by channels of pure copper. The process induces a multiscale structure, as illustrated in Figure 4 for a Cu/Nb wire.

This complex microstructure gives rise to extraordinary mechanical properties that have been studied by classical macroscopic tensile tests and nanoindentation, as well as *in situ* deformation in TEM and *in situ* deformation under neutron or synchrotron beam.^{18,22,30} The ultimate tensile strength reaches

2 GPa at 77 K (i.e., five times that of cold-worked pure Cu) for nanocomposite wires with a diameter of 2.5 mm that contain Nb nanofilaments with a diameter of 142 nm.¹⁸ The *in situ* experiments shed light on the specific elastic-plastic behavior of the different phases of the nanocomposites that are intimately connected to the local microstructure features (grain size). The micrometer-large Cu channels, with ultrafine grain structure (grain size from 200 nm to the micrometer range), exhibit strengthening following the Hall-Petch law; in the Cu nanochannels, the nucleation and propagation of dislocations are strongly affected by the reduced spacing between Cu-Nb interfaces, leading to a single-dislocation regime (Orowan-type) associated with increased yield stress; the Nb nanofilaments behave as whiskers with enhanced elastic limit.^{22,30,37}

Although the required mechanical and electrical properties are achieved in wires fabricated at laboratory scale, their mass production and use in magnets is still limited by processing obstacles (one must ensure the production of several tens of meters of defect-free wires), difficulties in winding these wires into the needed coils (the gain in strength is usually associated with the loss of ductility, as for most SPD processed materials), and the poor knowledge of their fatigue properties when subjected to thermomechanical cycling in real magnets. As for most of the materials reviewed in the article by Raabe et al.,

there is clearly space for materials improvement. Innovative strategies, such as the design of architected nanocomposite metals³ or interface engineering, should bring interesting results in the near future.

Response of nano-metals and composites to extreme environments

The size effects on mechanical strength described previously for single-phase nanostructured metals also have been explored for thin films metallic multilayers^{21,38–46} and nanotwinned fcc metals.^{47–51} When the size refinement produces grain or interphase boundaries that are thermally stable⁵² and can trap and annihilate point and line defects, the high strength can be combined with high damage tolerance in extreme environments. The article by Demkowicz et al. describes the atomic structures of boundaries that give rise to high damage tolerance.

Figure 5 and 6 show the increased damage tolerance of nanocomposites as compared with bulk metals. Bulk crystals or composites with coarse microstructure have very low strengths; nanostructuring leads to an increase in strength via the size effects discussed in Figure 2. For example, a Cu-Nb multilayer with an individual layer thickness of 5 nm has flow strength in excess of 2000 MPa, whereas the yield strengths of high purity, bulk single crystals of metals

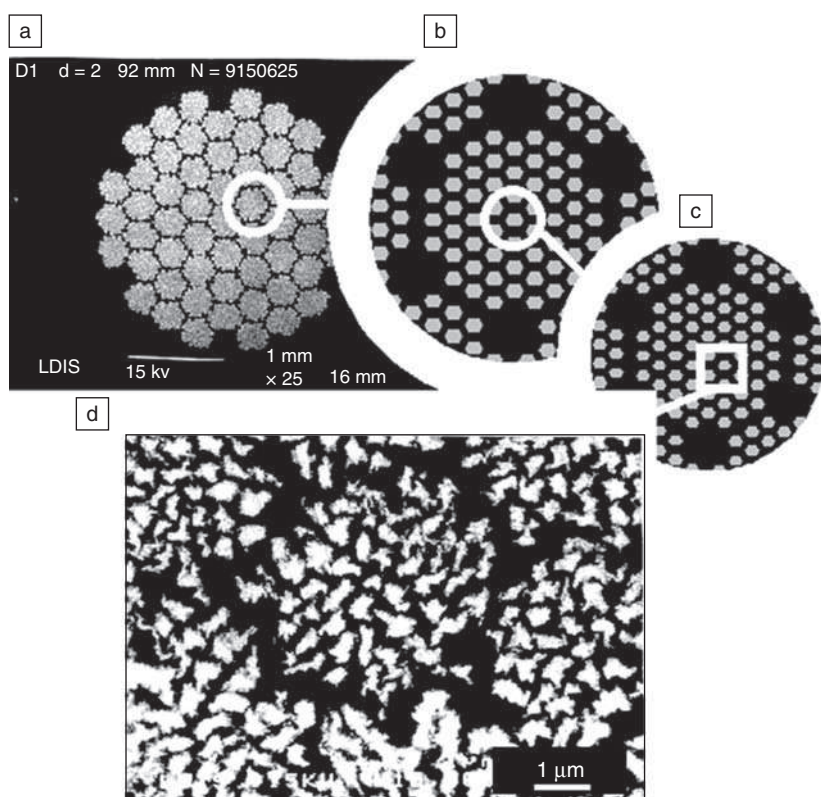


Figure 4. (a–c) Micrographs with successively higher magnification showing cross sections of the multiscale structure of Cu/Nb nanocomposite conductors for high-field pulsed magnets. (d) High magnification scanning electron micrograph showing Nb nanofilaments (white) embedded in the Cu matrix (black).³⁷

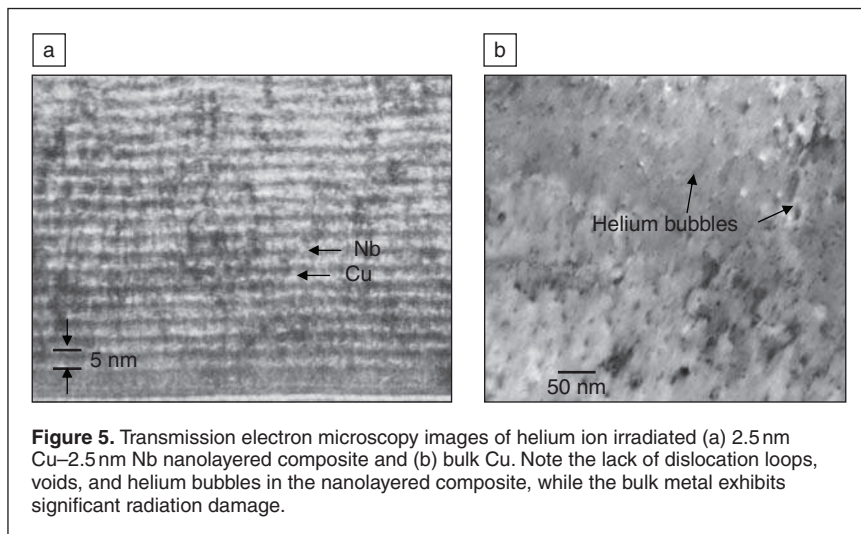


Figure 5. Transmission electron microscopy images of helium ion irradiated (a) 2.5 nm Cu–2.5 nm Nb nanolayered composite and (b) bulk Cu. Note the lack of dislocation loops, voids, and helium bubbles in the nanolayered composite, while the bulk metal exhibits significant radiation damage.

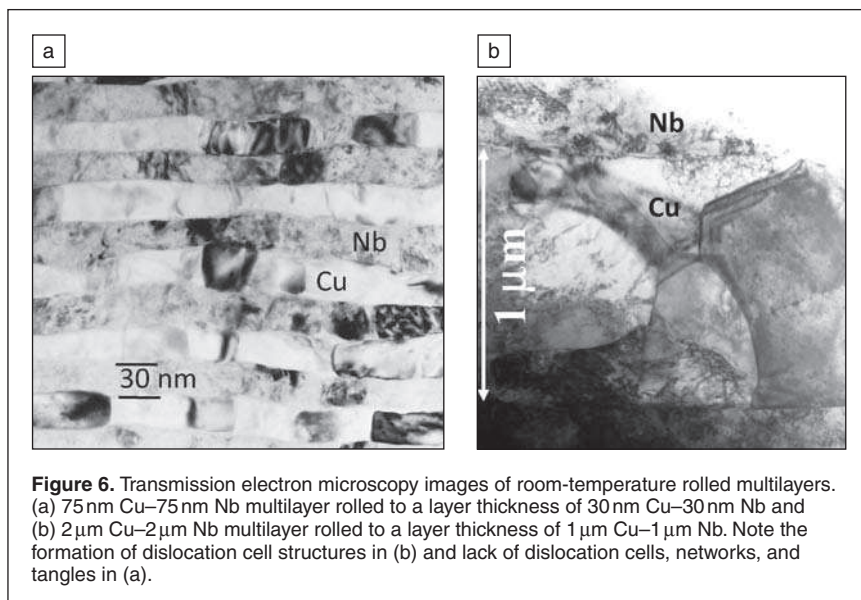


Figure 6. Transmission electron microscopy images of room-temperature rolled multilayers. (a) 75 nm Cu–75 nm Nb multilayer rolled to a layer thickness of 30 nm Cu–30 nm Nb and (b) 2 μm Cu–2 μm Nb multilayer rolled to a layer thickness of 1 μm Cu–1 μm Nb. Note the formation of dislocation cell structures in (b) and lack of dislocation cells, networks, and tangles in (a).

such as Cu are in the range of 10–50 MPa.^{21,53} Bulk crystals also have very low damage tolerance. For example, particle irradiation leads to the formation of interstitials and vacancies. The highly mobile interstitials can escape to the surfaces or cluster with other interstitials and collapse into dislocation loops. The vacancies aggregate as well and trap transmutation products such as helium, resulting in cavities. Overall, these radiation-induced defect phenomena lead to an increase in the mechanical yield strength, embrittlement, and swelling.^{54,55}

The article by Demkowicz et al. describes the atomic structures and energetics of interfaces that are super-sinks for radiation-induced defects, attracting, absorbing, and annihilating interstitials and vacancies, and thereby “self-healing” the material. As shown in Figure 5, for the same ion irradiation condition, pure Cu shows many defect agglomerates, but 2.5 nm Cu/2.5 nm Nb multilayers do not exhibit radiation damage.^{56,57} These interfaces are stable under high-temperature

ion irradiation as well.^{58,59} Similar effects have been observed at special grain boundaries in single-phase metals.^{60–65}

The same Cu–Nb interfaces are morphologically stable after room-temperature rolling to large plastic strains. Figure 6 shows that the micrometer-scale Cu–Nb multilayers developed dislocation-cell structures within the layers, leading to rotations away from the interface-plane normal. In contrast, the nanolayers (e.g., 75 nm layers rolled to 30 nm) showed no dislocation-cell structures and no rotation away from interface-plane normal.⁶⁶ Strain localization due to the formation of slip bands eventually leads to the initiation of cracks; hence, nanolayered materials with a more homogeneous distribution of slip and no accumulation of localized slip bands are more resistant to fracture.

Similarly, high strain-rate deformation increases the stress in a material to extremely high levels in a very short time. This results in excessive damage production, often via mechanisms such as twinning that are not activated at low stress levels.⁶⁷ The article by Rudd et al. in this issue discusses in more detail the behavior of materials at extremes of high strain rates. More work is needed to better understand the role of interfaces in controlling the behavior of materials at strain rate extremes.

All these findings suggest that nanostructured metals and composites can be designed to exhibit not just high strengths but also high damage tolerance, irrespective of whether the damage is introduced via plastic deformation or irradiation. The results reviewed here primarily highlight the fundamental mechanisms of defect interactions with interfaces in model systems.

These concepts can underpin the design of advanced engineering materials such as nanocomposites of steel, such as those discussed in the article by Demkowicz et al. and in other recent reviews by Odette and co-workers.^{68,69} For materials issues with current engineering materials in nuclear power reactors, the reader is referred to an earlier *MRS Bulletin* issue edited by Was, Zinkle, and Guérin.⁷⁰

Novel characterization methods for microstructure evolution at extremes

Although the microstructure of structural metals described in the different articles of this issue is well characterized in the as-processed state (from macroscopic to atomic scales), there is still a poorly known parameter: the microstructure stability of these materials in real service conditions. This stability is of crucial importance when the nanostructured materials are subjected to extreme conditions such as high strain rate

deformation, fast heating, high-dose irradiation, and high-frequency thermal and/or mechanical cycling. In many cases, post-mortem analysis can be of great help for characterizing the final state of microstructure evolution, but the evolution path cannot always be elucidated. Simulation tools can fruitfully complement this approach;⁷¹ however, the different simulation techniques have their own limitations, such as time and length scales of simulations, simplification of the microstructure, and validity of the interaction rules, and cannot fully replace experiments. Therefore to gain direct insight into the mechanisms governing the materials response under a given stimulus, *in situ* techniques have been widely developed during the last decades.^{72,73}

The challenge for *in situ* characterization techniques is to obtain the best possible temporal and spatial resolutions simultaneously. The characterization of the temporal evolution is essential for the discrimination of the kinetics laws involved in the observed microstructure evolutions and to better define the material's lifetime: *in situ* time-resolved techniques necessitate a probe with sufficient flux to enable fast recording of high statistics data. The recording speed becomes a possible limitation when the observed processes are ultrafast. On the other hand, spatial resolution is necessary first to locate exactly where the modifications take place but also to characterize the involved mechanisms at the proper scale (atomic scale in most cases). *In situ* spatially resolved techniques necessitate a focused probe with very well-defined shape.

The article from Browning et al. in this issue reviews recent advances in the *in situ* characterization of microstructure evolution in metals under extreme conditions such as rapid thermal gradients, irradiation, shock-driven void formation, and extreme pressure using dynamic TEM (DTEM), *in situ* TEM ion irradiation, electron tomography, and synchrotron radiation (small-angle x-ray scattering). A detailed description of the modifications brought to the conventional instruments provides insight into the challenges that these experiments are facing. For example, in DTEM, the fast temporal resolution is achieved by using two different nanosecond lasers, one to start the transformation in the sample and one to create the imaging pulse of electrons by photoemission. For *in situ* irradiation, ion accelerators must be linked to TEM; for *in situ* shock loading, a synchrotron beamline (at the Advanced Photon Source, Argonne National Laboratory, USA) is equipped with a drive laser, specific x-ray detector while a special synchrotron fill pattern is used to obtain highest flux and shortest x-ray pulse.⁷⁴ Similarly, the Linac Coherent Light Source (LCLS) beam at SLAC National Accelerator Laboratory, with its high peak brightness, short pulse duration (<100 fs), and tunable wavelength in the x-ray energy range, provides revolutionary capabilities to study the transient behavior of matter in extreme conditions. The particular strength of the matter in the extreme conditions (MEC) instrument is the combination of the unique LCLS beam with high-power optical laser beams to cover a broad range of extreme conditions such as intense pressure, temperature, stress, strain, and radiation.⁷⁵

These developments in the *in situ* characterization techniques have been applied to a diverse range of problems, as described in the article by Browning et al. The crystallization of amorphous films (nucleation rate and growth speed), the radiation damage mechanisms, the 3D defect density production in materials for nuclear-reactor applications (ferritic-martensitic and oxide-dispersion-strengthened steels), and the shock-generated submicron void formation in solids. These examples, and additional work reviewed in Reference 76, illustrate how the development of highly novel and unconventional methodologies pushes forward the frontiers of instrumentation and materials science.

Summary and future directions

Nanostructured metals and composites are known to be ultra-strong by virtue of the "smaller is stronger" trend. In addition to high strength, these materials can also be stable and damage tolerant at high irradiation doses at high temperatures, high strain rates, and large plastic strains. This unique combination of damage tolerance and high strength requires grain and/or interphase boundaries with atomic structures that make these boundaries strong obstacles to dislocations as well as strong sinks for point and line defects. Future developments of these multifunctional materials call for innovative strategies such as the design of architected nanocomposite metals and interface engineering. These approaches necessitate detailed experimental and simulation inputs, in particular continuous development of highly novel and unconventional *in situ* experimental capabilities that push simultaneously the limits in spatial and temporal resolution. Such capabilities will help elucidate the damage production and recovery mechanisms at interfaces under extremes conditions of irradiation, stress, and temperature.

Acknowledgments

A.M. acknowledges support at LANL from the U.S. Department of Energy, Office of Science, Office of Basic Energy Sciences. L.T. acknowledges support from the French Research Agency under contract ANR-06-MAPR-0013.

References

1. U.S. Department of Energy, *Basic Research Needs for Materials under Extreme Environments* (BES Workshop on Basic Research Needs for Materials under Extreme Environments Report, 11–13 June 2007); www.sc.doe.gov/bes/reports/abstracts.html#MUEE.
2. J.D. Madden, *Science* **318**, 1094 (2007).
3. O. Bouaziz, Y. Bréchet, J.D. Embury, *Adv. Eng. Mater.* **1–2**, 10 (2008).
4. U.S. Department of Energy, *Directing Matter and Energy: Five Challenges for Science and the Imagination* (BESAC Grand Challenges report, 25 January 2005); www.sc.doe.gov/bes/reports/abstracts.html#GC.
5. O. Bouaziz, J.D. Embury, *Mater. Sci. Forum* **42**, 539 (2007).
6. K.S. Kumar, H. Van Swygenhoven, S. Suresh, *Acta Mater.* **51**, 5743 (2003).
7. J.R. Weertman, *MRS Bull.* **29**, 616 (2004).
8. H. Van Swygenhoven, J.R. Weertman, *Mater. Today* **9**, 24 (2006).
9. M.A. Meyers, A. Mishra, D.J. Benson, *Prog. Mater. Sci.* **51**, 427 (2006).
10. U.F. Kocks, H. Mecking, *Prog. Mater. Sci.* **48**, 171 (2003).
11. J.A. Wert, X. Huang, G. Winther, W. Pantleon, H.F. Poulsen, *Mater. Today* **10–9**, 24 (2007).
12. R.Z. Valiev, Y. Estrin, Z. Horita, T.G. Langdon, M.J. Zehetbauer, Y.T. Zhu, *JOM* **58**, 33 (2006).


13. J.D. Verhoeven, *Metallography* **20**, 145 (1987).
14. W. Kochmann, M. Reibold, R. Goldberg, W. Hauffe, A.A. Levin, D.C. Meyer, T. Stephan, H. Müller, A. Belger, P. Paufler, *J. Alloys Comp.* **372**, L15 (2004).
15. E. Arzt, *Acta Mater.* **46**, 5611 (1998).
16. H. Gleiter, *Acta Mater.* **48**, 1 (2000).
17. K.S. Kumar, H. Van Swygenhoven, S. Suresh, *Acta Mater.* **51**, 5743 (2003).
18. L. Thilly, F. Lecouturier, J. Von Stebut, *Acta Mater.* **50**, 5049 (2002).
19. J. Gil Sevillano, *J. Phys. III* **1**, 967 (1991).
20. J.D. Embury, J.P. Hirth, *Acta Mater.* **42** (6), 2051 (1994).
21. A. Misra, J.P. Hirth, R.G. Hoagland, *Acta Mater.* **53**, 4817 (2005).
22. L. Thilly, O. Ludwig, M. Véron, F. Lecouturier, J.P. Peyrade, S. Askénazy, *Philos. Mag. A* **82** (5), 925 (2002).
23. S.S. Brenner, *J. Appl. Phys.* **27** (12), 1484 (1956).
24. A.H. Chokshi, A. Rosen, J. Karch, H. Gleiter, *Scripta Mater.* **23**, 1679 (1989).
25. G. Saada, *Mater. Sci. Eng. A* **400–401**, 146 (2005).
26. G. Saada, *Philos. Mag.* **85**, 3003 (2005).
27. S. Brandstetter, H. Van Swygenhoven, S. Van Petegem, B. Schmitt, R. Maaß, P.M. Derlet, *Advanced Mater.* **18**, 1545 (2006).
28. G. Saada, M. Verdier, G.F. Dirras, *Philos. Mag.* **87**, 4875 (2007).
29. H. Li, H. Choo, Y. Ren, T.A. Saleh, U. Lienert, P.K. Liaw, F. Ebrahimi, *Phys. Rev. Lett.* **101**, 015502 (2008).
30. L. Thilly, S. Van Petegem, P.O. Renault, F. Lecouturier, V. Vidal, B. Schmitt, H. Van Swygenhoven, *Acta Mater.* **57**, 3157 (2009).
31. J. Rajagopalan, C. Rentenberger, H.P. Karnthale, G. Dehm, M.T.A. Saif, *Acta Mater.* **58**, 4772 (2010).
32. C.C. Aydiner, D.W. Brown, N.A. Mara, J. Almer, A. Misra, *Appl. Phys. Lett.* **94**, 031906 (2009).
33. S. Askénazy, *Phys. B* **211**, 56 (1995).
34. K. Spencer, F. Lecouturier, L. Thilly, J.D. Embury, *Adv. Eng. Mater.* **6**, 290 (2004).
35. L. Thilly, F. Lecouturier, *Nanomaterials and Nanochemistry: High Field Coils*, (Springer, New York, 2007), p. 685.
36. J. Freudenberger, J. Lyubimova, A. Gaganov, H. Witte, A.L. Hickman, H. Jones, M. Nganb, *Mater. Sci. Eng. A* **527**, 2004 (2010).
37. L. Thilly, V. Vidal, S. Van Petegem, U. Stühr, F. Lecouturier, P.O. Renault, H. Van Swygenhoven, *Appl. Phys. Lett.* **88**, 191906 (2006).
38. W.D. Nix, *Math. Mech. Solids* **14**, 207 (2009).
39. S.M. Han, M.A. Phillips, W.D. Nix, *Acta Mater.* **57**, 4473 (2009).
40. J. Wang, R.G. Hoagland, A. Misra, *Scripta Mater.* **60**, 1067 (2009).
41. I.N. Mastorakos, H.M. Zbib, D.F. Bahr, *Appl. Phys. Lett.* **94**, 173114 (2009).
42. P.M. Anderson, J.S. Carpenter, *Scripta Mater.* **62**, 325 (2010).
43. Y.P. Li, G.P. Zhang, *Acta Mater.* **58**, 3877 (2010).

44. A.C. Lewis, C. Eberl, K.J. Hemker, T.P. Weihs, *J. Mater. Res.* **23**, 376 (2008).
45. B.M. Clemens, H. Kung, S.A. Barnett, *MRS Bull.* **24**, 20 (1999).
46. R.C. Cammarata, *Scripta Mater.* **50**, 751 (2004).
47. L. Lu, X. Chen, X. Huang, K. Lu, *Science* **323**, 607 (2009).
48. T. Zhu, J. Li, A. Samanta, H.G. Kim, S. Suresh, *Proc. Nat. Acad. Sci. U.S.A.* **104**, 3031 (2007).
49. O. Anderoglu, A. Misra, J. Wang, R.G. Hoagland, J.P. Hirth, X. Zhang, *Int. J. Plast.* **26**, 875 (2010).
50. F. Sansoz, H. Huang, D.H. Warner, *JOM* **60**, 79 (2008).
51. C.J. Shute, B.D. Myers, S. Xie, T.W. Barbee Jr, A.M. Hodge, J.R. Weertman, *Scripta Mater.* **60**, 1073 (2009).
52. A. Misra, R.G. Hoagland, H. Kung, *Philos. Mag.* **84**, 1021 (2004).
53. N.A. Mara, D. Bhattacharyya, P. Dickerson, R.G. Hoagland, A. Misra, *Appl. Phys. Lett.*, **92**, 231901 (2008).
54. D.L. Porter, F.A. Garner, *J. Nucl. Mater.* **159**, 114 (1988).
55. R.J. Kurtz, F. Gao, H.L. Heinisch, B.D. Wirth, G.R. Odette, T. Yamamoto, *JOM* **56**, 263 (2004).
56. A. Misra, M.J. Demkowicz, X. Zhang, R.G. Hoagland, *JOM* **59**, 62 (2007).
57. X. Zhang, N. Li, O. Anderoglu, H. Wang, J.G. Swadener, T. Hochbauer, A. Misra, R.G. Hoagland, *Nucl. Instrum. Methods Phys. Res., Sect. B* **261** (1–2), 1129 (2007).
58. T. Hochbauer, A. Misra, K. Hattar, R.G. Hoagland, *J. Appl. Phys.* **98**, 123516 (2005).
59. K. Hattar, M.J. Demkowicz, A. Misra, I.M. Robertson, R.G. Hoagland, *Scripta Mater.* **58**, 541 (2008).
60. B.N. Singh, *Philos. Mag.* **28**, 1409 (1973).
61. N. Nita, R. Schaeublin, M. Victoria, R.Z. Valiev, *Philos. Mag.* **85**, 723 (2005).
62. M. Rose, A.G. Balogh, H. Hahn, *Nucl. Instrum. Methods Phys. Res., Sect. B* **127/128**, 119 (1997).
63. M. Samaras, P.M. Derlet, H. van Swygenhoven, M. Victoria, *Phys. Rev. Lett.* **88**, 125505 (2002).
64. H.L. Hienisch, F. Gao, R.J. Kurtz, *J. Nucl. Mater.* **329–333**, 924 (2004).
65. X.M. Bai, A.F. Voter, R.G. Hoagland, M. Nastasi, B.P. Uberuaga, *Science* **327**, 1631 (2010).
66. A. Misra, J.P. Hirth, R.G. Hoagland, J.D. Embury, H. Kung, *Acta Mater.* **52**, 2387 (2004).
67. F. Cao, I.J. Beyerlein, F.L. Addessio, B.H. Sencer, C.P. Trujillo, E.K. Cerreta, G.T. Gray III, *Acta Mater.* **58**, 549 (2010).
68. G.R. Odette, D.T. Hoelzer, *JOM*, September, 84 (2010).
69. G.R. Odette, M.J. Alinger, B.D. Wirth, *Annual Review of Materials Research*, **38**, 471 (2008).
70. G.S. Was, S.J. Zinkle, Y. Guérin, *MRS Bull.* **34** (1), 10 (2009).
71. H. Huang, H. Van Swygenhoven, *MRS Bull.* **34** (3), 160 (2009).
72. I.M. Robertson, P.J. Ferreira, G. Dehm, R. Hull, E.A. Stach, *MRS Bull.* **33** (2), 122 (2008).
73. M. Legros, D.S. Gianola, C. Motz, *MRS Bull.* **35** (5), 354 (2010).
74. D.H. Kalantar, G.W. Collins, J.D. Colvin, J.H. Eggert, J. Hawrelak, H.E. Lorenzana, M.A. Meyers, R.W. Minich, K. Rosolankova, M.S. Schneider, J.S. Stölken, J.S. Wark, *Int. J. Impact Eng.* **33**, 343 (2006).
75. SLAC National Accelerator Laboratory, https://slacportal.slac.stanford.edu/sites/clc_public/instruments/mec/Pages/default.aspx.
76. P.G. Evans, S.J.L. Billinge, *MRS Bull.* **35** (6), 495 (2010). □

JANIS


Liquid Nitrogen Cooled Cryostats

- Top loading models offer rapid sample change, 65 K – 300 K
- Cold finger models from 65 K – 800 K
- Variable temperature operation
- Many models in stock for quick delivery




Sample in Vapor
Sample in Vacuum

Janis Research Company
 2 Jewel Drive Wilmington, MA 01887 USA
 TEL +1 978 657-8750 FAX +1 978 658-0349 sales@janis.com
 Visit our website at www.janis.com



Kids' Science Challenge



WHO	Students in grades 3-6
WHAT	A science competition! Kids submit ideas and experiments for scientists to solve. TOPICS —Super Stuff for Sports, Magical Microbes and Sensational Sounds Winning students work with scientists to bring their ideas to life PLUS other fun prizes.
WHERE	www.kidsciencechallenge.com
WHEN	Entry deadline: February 28, 2011

**Amit Misra**

Guest Editor for this issue of *MRS Bulletin*

Center for Integrated Nanotechnologies,
Materials Physics and Applications Division,
Los Alamos National Laboratory, New
Mexico, USA; e-mail amisra@lanl.gov.

Misra is the co-director of the Center for Materials at Irradiation and Mechanical Extremes, an Energy Frontier Research Center (EFRC) of the U.S. Department of Energy, Office of Basic Energy Sciences. He joined Los Alamos National Laboratory (LANL) as a postdoctoral researcher in November 1996 and was promoted to a staff scientist in August 1998. Misra earned his MS and PhD degrees in materials science and engineering from the University of Michigan and his bachelor's degree in metallurgy from the Institute of Technology, Banaras Hindu University, India. He has co-authored more than 200 peer-reviewed articles in archival journals, conference proceedings, and book chapters. He served as a 2009 volume organizer for *MRS Bulletin*, has co-organized five symposia at the Materials Research Society, and was recently appointed a meeting chair for the 2012 MRS Fall Meeting. Misra also received the 2008 LANL Fellows Prize for outstanding research in nanomechanics.

**Ludovic Thilly**

Guest Editor for this issue of *MRS Bulletin*

Department of Physics and Mechanics of
Materials, P-prime Institute, CNRS-University
of Poitiers, SP2MI, Ave. Marie et Pierre Curie,
86962 Futuroscope, France; tel. 33-5-4949-6831;
and e-mail ludovic.thilly@univ-poitiers.fr.

Thilly has been an associate professor at the University of Poitiers, France, since 2001, where he is involved in the processing and mechanical characterization of complex materials (nanostructured and nanocomposite metals, semiconductors, MAX phases), with an emphasis on the experimental assessment of elementary deformation mechanisms (dislocations, micro- and macro-plasticity). He obtained an engineering diploma in materials science from the National Institute for Applied Sciences, Toulouse, France, in 1997, concurrent to receiving his MS degree in physics of condensed matter at the University of Toulouse. Thilly received his PhD degree from the National Institute for Applied Sciences of Toulouse, France, in 2000, after working on high-strength and high-conductivity nanocomposite metallic wires for high field magnets. He received the Jean Rist Medal (2009) from the French Materials Research Society (SF2M), for his work on the characterization of size effects in the plasticity mechanisms of nanocomposite metals with *in situ* techniques under neutrons or high-energy x-rays.

**Pascal Bellon**

University of Illinois at Urbana-Champaign,
Department of Materials Science and
Engineering, Urbana, IL 61801, USA; tel. 217-
265-0284; and e-mail bellon@illinois.edu.

Bellon is a professor at the University of Illinois at Urbana-Champaign. He received an engineering degree (1984) from Ecole Supérieure d'Electricité, in Gif-sur-Yvette, France, and a PhD degree in materials science (1989) from Université Pierre et Marie Curie, in Paris, France. His research focuses on materials driven into non-equilibrium states and microstructures during their processing or while in service. He particularly investigates self-organization in alloys subjected to irradiation and plastic deformation, and the use of nano-scale self-organization for tailoring performance of materials.

**Nigel D. Browning**

Department of Chemical Engineering and
Materials Science, University of California–Davis,
One Shields Ave., Davis, CA 95616, USA; tel. 530-
754-5563; and e-mail nbrowning@ucdavis.edu.

Browning holds appointments as professor in the Departments of Chemical Engineering and Materials Science and Molecular and Cellular Biology at the University of California, Davis (UC Davis) and is a senior scientist in the Physical and Life Sciences Directorate at Lawrence Livermore National Laboratory (LLNL). At UC Davis, he directs the Interdisciplinary Center for Electron Microscopy, and at LLNL, he leads the dynamic transmission electron microscope (DTEM) project. Browning earned his PhD degree in physics from Cambridge University in 1992. Since that time, he has authored more than 200 peer-reviewed publications on the development and application of advanced techniques in electron microscopy with high spatial, temporal, and energy resolution. He has received the Burton Award from the Microscopy Society of America (2002), the Coble Award from the American Ceramic Society (2003), and was a co-recipient of R&D 100 and Nano 50 awards in 2008 for the development of the DTEM.

**Geoffrey H. Campbell**

Condensed Matter and Materials Division of the
Physical and Life Sciences Directorate at Lawrence
Livermore National Laboratory, MS L-356, PO
Box 808, Livermore, CA 94550, USA; tel. 925-
423-8276; and e-mail ghcampbell@llnl.gov.

Campbell is group leader for the Ultrafast Materials Science Group in the Physical and Life Sciences Directorate at Lawrence Livermore National Laboratory (LLNL). He earned his PhD degree in materials from the University of California, Santa Barbara, in 1990. He was awarded an Alexander von Humboldt Foundation scholarship to perform postdoctoral work at the Max Planck Institute for Metals Research, Institute for Materials Sciences in Stuttgart, Germany. In 1991, Campbell took a postdoctoral position at LLNL and was converted to staff in 1993. Since 2007, he has been the Scientific Capability Leader for Ultrafast Materials Science. Campbell has published more than 90 peer-reviewed papers in the open literature and was co-recipient of an R&D 100 award and a Nano 50 award in 2008 for the development of the dynamic transmission electron microscope.

**Pyuck-Pa Choi**

Max-Planck-Institut für Eisenforschung in
Düsseldorf, Germany; and e-mail p.choi@mpie.de.

Choi has been the head of the Atom Probe Tomography group at the Max-Planck-Institut für Eisenforschung in Düsseldorf since 2009. He received his PhD degree in physics in 2003 from the University of Göttingen, Germany. Afterward, he moved to South Korea where he worked at the University of Ulsan and the Korea Institute of Science and Technology. Choi's research interests include the characterization of nanostructured materials by atom probe tomography and transmission electron microscopy, mechanically driven alloying processes, mechanical and thermal stability of thin film hard coatings, and the characterization of solar cells.



Michael Demkowicz

Department of Materials Science and Engineering, Massachusetts Institute of Technology, Cambridge, MA 02139, USA; e-mail demkowicz@mit.edu.

Demkowicz is the John C. Chipman assistant professor at the Massachusetts Institute of Technology (MIT). He obtained undergraduate degrees in physics, aerospace engineering, and humanities (Plan II Program) from the University of Texas at Austin. He received his MS and PhD degrees in mechanical engineering from MIT, studying under Ali Argon, and went on to

become a director's postdoctoral fellow and then a staff scientist at Los Alamos National Laboratory. In his research, Demkowicz focuses on applying atomistic modeling to materials subjected to irradiation, mechanical loading, and environmental degradation.



John David Embury

McMaster University, Hamilton, Canada; tel. 905-525-9140; and e-mail emburyd@univmail.cis.mcmaster.ca.

Embury is Professor Emeritus at McMaster University. He received his bachelor's degree in metallurgy at the University of Manchester, UK, and his PhD degree in metallurgy at Cambridge University, UK, in 1963. He worked as a research scientist for U.S. Steel, at the University of Newcastle, and as a professor at the Department of Materials Science and Engineering at McMaster University, Canada. As visiting

professor, Embury worked at a number of places such as in Brazil at Aluminum Pechiney, at Cambridge University, Los Alamos National Laboratory, and the Catholic University in Louvain, Belgium. His main interests lie in the microstructure and mechanical behavior of steels and aluminum alloys, in composites, formability, damage, and the behavior of ultrahigh strength materials.



Tim Germann

Theoretical Division, Los Alamos National Laboratory, Los Alamos, NM 87545, USA; tel. 505-665-9772; and e-mail tcg@lanl.gov.

Germann is in the Physics and Chemistry of Materials Group at Los Alamos National Laboratory, where he has been a staff scientist since 2000. He received dual BS degrees in chemistry and computer science from the University of Illinois, and a PhD degree in chemical physics from Harvard University. His research interests include the use of high-performance computing to study high strain-rate material dynamics

and the role of interfaces on material behavior. Among his awards, Germann has received a 1998 IEEE Gordon Bell Prize and a 2006 LANL Fellows Prize for research.



James A. Hawreliak

Condensed Matter and Materials Division, Lawrence Livermore National Laboratory, PO Box 808 L-286, Livermore, CA 94550, USA; tel. 925-424-2905; and e-mail hawreliak1@llnl.gov.

Hawreliak is a research scientist at Lawrence Livermore National Laboratory where he works on developing *in situ* x-ray diagnostics for the Shock Physics group in the Condensed Matter and Materials Division. He earned his PhD degree in atomic and laser physics at the University of Oxford, studying non-local heat transport in laser-produced plasmas. His work

mainly focuses on high-power laser systems, which can simultaneously generate the drive and x-ray backlighter. Currently, Hawreliak is working on bringing *in situ* probing techniques onto the NIF for ultrahigh pressure studies.



Kazuhiro Hono

National Institute for Materials Science in Sengen, Tsukuba, Japan; and e-mail kazuhiro.hono@nims.go.jp.

Hono is managing director of the Magnetic Materials Center and a professor with the Institute for Materials Science at the University of Tsukuba, Japan. He received his master's degree in materials science at Tohoku University, Japan, and his PhD degree in 1988 in materials science at the Pennsylvania State University. As a postdoctoral researcher and senior scientist, Hono worked at the Department of Metallurgical

Engineering and Materials Science at Carnegie Mellon University, at the Institute for Materials Research at Tohoku University, Japan, and at the National Research Institute for Metals (NRIM), Japan. He also is a fellow of the National Institute for Materials Science (NIMS). Hono's primary fields of interest are nanostructured metallic materials, magnetic materials, spintronics materials, atom probe field ion microscopy, and transmission electron microscopy.



Reiner Kirchheim

Materials Physics Institute at the University of Göttingen; and e-mail rkirch@ump.gwdg.de.

Kirchheim is a professor of Lower Saxony at the University of Göttingen and external member of the Max-Planck-Institut für Eisenforschung in Düsseldorf in Germany. He worked at the Max-Planck-Institut für Metals Research from 1971 to 1993 and received his PhD degree in physics from the University of Stuttgart in 1973. From 1993 to 2008, Kirchheim was the director of the Institute for Materials Physics at the University of Göttingen. He works on thermodynamics and

kinetics of materials. He also is a member of the Göttingen Academie of Science and the National Academy of Technical Sciences. Kirchheim's honors include the Carl Wagner Prize (1990), the Honda Memorial Award (2003), the Heyn Memorial Medal (2005), the Lee Hsun Lecture Award (2007), and the Staudinger-Durrer Lecture (2009).



Marquis A. Kirk

Materials Science Division, Argonne National Laboratory, 9700 S. Cass Ave., Argonne, IL 60439, USA; tel. 630-252-4998 and 630-252-5222; and e-mail kirk@anl.gov.

Kirk is director of the IVEM-Tandem user facility at Argonne National Laboratory. He received his PhD degree from Northwestern University in 1972. He has authored more than 200 publications on irradiation effects in metals, semiconductors, and superconductor materials.



Aleksander Kostka

Max-Planck-Institut für Eisenforschung in Düsseldorf, Germany; and e-mail a.kostka@mpie.de.

Kostka is the head of the High Temperature Materials Group at the Max-Planck Institut in Düsseldorf. He received his MS and PhD degrees at the University of Silesia in Poland under the guidance of Professor Henryk Morawiec. Kostka's research focuses on the investigation of metallurgical processes governing formation and evolution of interfacial microstructures of advanced engineering alloys

during processing, creep and welding, and correlation of the microstructure with mechanical properties of these materials.



Terence G. Langdon

Department of Aerospace and Mechanical Engineering, University of Southern California, Los Angeles, CA 90089-1453, USA; tel. 213-740-0491; and e-mail at langdon@usc.edu. Langdon is the William E. Leonhard Professor of Engineering at the University of Southern California in Los Angeles and a research professor of materials science at the University of Southampton in the UK. He holds BSc and DSc degrees from the University of Bristol and a PhD degree from Imperial College, University of London. His research interests are in

high-temperature creep, superplasticity, and the processing and properties of ultrafine-grained materials.



Florence Lecouturier

Laboratoire National des Champs Magnétiques Intenses at CNRS, Toulouse, France; and e-mail florence.lecouturier@lncmi.cnrs.fr.

Lecouturier works on the development of high strength conductors at the French National High Magnetic Field Laboratory (Toulouse and Grenoble). She received her PhD degree in materials science in 1995 from the National Institute for Applied Sciences in Toulouse, France. Lecouturier is primarily active in processing by severe plastic deformation, mechanical and physical properties, and mod-

eling of copper/stainless steel macrocomposites and Cu/X (with BCC/FCC combination as CuNb, CuTa) nanocomposite wires for high magnetic field applications.



Yujiao Li

Max-Planck-Institut für Eisenforschung in Düsseldorf, Germany; and e-mail y.li@mpie.de.

Li is a postdoctoral researcher at the Institute for Materials Physics, University of Göttingen. Currently she works as a visiting scientist at the Max-Planck-Institut für Eisenforschung. Li received her bachelor's degree in 1993 and her master's degree in 1996 in metal working from Xi'an University of Architecture and Technology, China. Afterward, she worked there as a lecturer for six years. In 2006, Li received her PhD degree in materials science from the University

of Erlangen-Nuremberg, Germany, where she studied deformation kinetics of nanostructured metals and creep behavior of Mg alloys. Her current research is focused on the decomposition mechanism of cementite in heavily cold drawn pearlitic steel by using atom probe tomography.



Ke Lu

Institute of Metal Research, Chinese Academy of Sciences, 72 Wenhua Rd., Shenyang 110016, China; tel. 86-24-2390-6826; and e-mail lu@imr.ac.cn.

Lu is a professor and director of the Shenyang National Laboratory for Materials Science in the Institute of Metal Research of the Chinese Academy of Sciences (CAS). His research interests include synthesis, structure, phase transformation, and mechanical properties of nanostructured metals and alloys. He is a Materials Research Society

fellow, a member of CAS, and a member of the German National Academy of Science (Leopoldina).



Reinhard Pippan

Erich Schmid Institute in Leoben, Austria; and e-mail reinhard.pippan@oeaw.ac.at.

Pippan is a professor at the University of Leoben, Austria, and also vice director of the Erich Schmid Institute and head of the Christian Doppler Laboratory for local analysis of deformation and fracture. He studied physics at the Technical University Graz and passed his doctoral studies and the Habilitation degree in solid-state physics at the University of Leoben. His main activities are focused on mechanical properties of metals, alloys, and composites.



Dierk Raabe

Max-Planck-Institut für Eisenforschung in Düsseldorf, Germany; and e-mail d.raabe@mpie.de.

Raabe has been director at the Max-Planck-Institut für Eisenforschung since 1999 and a professor at Rheinisch-Westfälische Technische Hochschule (RWTH) Aachen, Germany. He studied music, metallurgy, and metal physics. In 1992, Raabe earned his PhD degree, and then received his Habilitation degree at RWTH Aachen in physical metallurgy and metal physics in 1997. Between 1997 and 1999, he worked

at the Materials Science and Engineering Department at Carnegie Mellon University in Pittsburgh, USA, and at the National High Magnetic Field Laboratory in Tallahassee, FL, USA. Raabe is mainly active in computational materials science, crystal plasticity, alloy design, and biomaterials.



Bruce A. Remington

Inertial Confinement Fusion Program, NIF Directorate, Lawrence Livermore National Laboratory, L-481, Livermore, CA 94550, USA; tel. 925-423-2712; and e-mail remington2@llnl.gov.

Remington has been a staff physicist at Lawrence Livermore National Laboratory in the Inertial Confinement Fusion Program since 1988, working on laser-driven, high energy density (HED) fluid instabilities, HED laboratory astrophysics, and solid-state dynamics at high pressures and rates. He received his BS degree from Northern Michigan University in

1975 and his PhD degree in nuclear physics from Michigan State University in 1986. Remington is a recipient of the American Physical Society (APS) Division of Plasma Physics Excellence in Plasma Physics award for his work on ablation-front Rayleigh-Taylor instability, and is a fellow of the APS.



Robert E. Rudd

Condensed Matter and Materials Division, Lawrence Livermore National Laboratory, L-045, Livermore, CA 94550, USA; tel. 925-422-4292; and e-mail robert.rudd@llnl.gov.

Rudd has been a staff physicist at Lawrence Livermore National Laboratory since 2000, using atomistic and multiscale computer simulation to study mechanics at the nanoscale with an emphasis on plasticity, fracture, surface growth, and fluid instabilities. He received his BS degree from the University of Virginia in 1987 and his PhD degree from Princeton University in 1992. Rudd invented

the concurrent multiscale modeling technique, Coarse-Grained Molecular Dynamics. He is an editor of the book series, *Oxford Series on Materials Modelling*. In addition, he received the Gordon Bell Prize in Supercomputing in 2007.



Xavier Sauvage

Institut de Physique at the University of Rouen, France; and e-mail xavier.sauvage@univ-rouen.fr. Sauvage is at the French National Center for Scientific Research (CNRS), Institut de Physique in the Groupe de Physique des Matériaux at the University of Rouen. He studied at the Ecole Normale Supérieure de Cachan, France, earned his master's degree in physics of materials in 1998, and his PhD degree in 2001 at the University of Rouen, France, under the supervision of professor D. Blavette. In 2002, he was a postdoctoral researcher at the Max Planck Institute

of Stuttgart, Germany. His primary research is in the fields of severe plastic deformation (SPD) of metallic alloys, stability of metallic nanostructures, phase transformation induced by SPD, and deformation mechanisms in nanostructured materials.



Nobuhiro Tsuji

Department of Materials Science and Engineering, Graduate School of Engineering, Kyoto University, Yoshida Honmachi, Sakyo-ku, Kyoto, 606-8502, Japan; tel. 81-75-753-5462; e-mail nobuhiro.tsuji@ky5.ecs.kyoto-u.ac.jp; and www.tsujilab.mtl.kyoto-u.ac.jp.

Nobuhiro Tsuji is a professor in the Department of Materials Science and Engineering at Kyoto University (KU), Japan. He received his PhD from the Department of Materials Science and Engineering at KU in 1994. He worked as an assistant professor and then as an associate

professor at Osaka University from 1994 to 2009, during which time he developed the accumulative roll bonding (ARB) process with his colleagues. Tsuji has studied bulk nanostructured metals energetically and has been working as a professor of physical metallurgy in the Department of Materials Science and Engineering at KU since March 2009.



Ruslan Valiev

Institute of Physics of Advanced Materials, Ufa State Aviation Technical University, 12K. Marx St. Ufa 450000, Russia; tel. 7(347) 273 34 22; e-mail rvaliev@mail.ru.

Valiev is professor, founder, and director of the Institute of Physics of Advanced Materials, Ufa State Aviation Technical University since 1995. He is the chairman of the International Steering Committee on Severe Plastic Deformation (SPD) and a member of several international professional committees. He has published numerous publications and books and holds

more than 35 patents related to SPD nanomaterials.



Justin S. Wark

Department of Physics, Clarendon Laboratory, University of Oxford, Parks Rd., Oxford, OX1 3PU, UK; tel. 44-1865-272251; and e-mail Justin.wark@physics.ox.ac.uk.

Wark has been a faculty member at the University of Oxford since 1988, where he is a professor of physics. He received his undergraduate degree in physics from Oxford in 1982 and his PhD degree from Imperial College, London, in 1985. Wark's research interests are in using ultra-fast x-ray pulses to diagnose shock compressed matter, the creation and diagnosis of

warm dense matter, and the exploitation of fourth generation light sources for high energy density physics research.

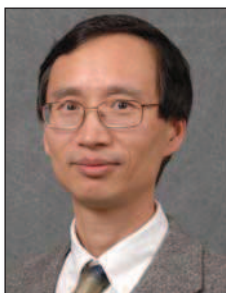


Brian Wirth

Department of Nuclear Engineering, University of Tennessee, Knoxville, TN 37996, USA; tel. (865) 974-2554; and e-mail bdwirth@utk.edu.

Wirth is a professor and Governor's Chair of Computational Nuclear Engineering in the Department of Nuclear Engineering at the University of Tennessee, Knoxville, which he joined in July 2010. He received a BS degree in nuclear engineering from the Georgia Institute of Technology in 1992 and a PhD degree in mechanical engineering from the University of California, Santa Barbara, in 1998, where he was a Department of Energy Nuclear Engineering graduate fellow. Following several years

in the High Performance Computational Materials Science Group at Lawrence Livermore National Laboratory, Wirth joined the faculty at the University of California, Berkeley, as an assistant professor of nuclear engineering in 2002. He was promoted to associate professor in 2006. His research interests involve the combination of multiscale modeling and advanced microstructural characterization to develop improved understanding and models of microstructure-property relationships and microstructural evolution during processing and service in hostile environments, with an emphasis on irradiation effects. He has received a number of awards, including the 2007 Fusion Power Associates David J. Rose Excellence in Fusion Engineering Award and the 2003 Presidential Early Career Award for Scientists and Engineers.

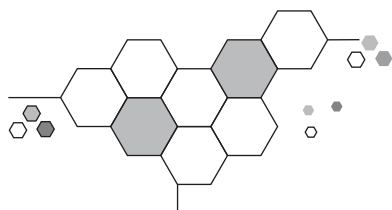


Yuntian Zhu

College of Engineering, Materials Science and Engineering Department, North Carolina State University, Raleigh, NC 27695, USA; tel. 919-513-0559; and e-mail ytzhu@ncsu.edu and www.mse.ncsu.edu/zhu.

Zhu is a professor at the North Carolina State University (NCSSU). He was a team leader at Los Alamos National Laboratory before joining NCSSU in 2007. His research interests include metals and alloys with nano/ultrafine-grain structures, and carbon nanotube composites. Zhu recently received the 2010 The Minerals

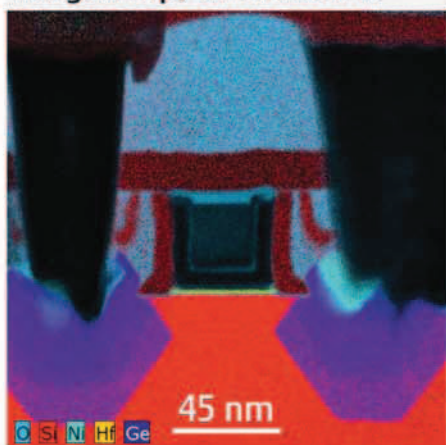
Metals and Materials Society's Materials Processing and Manufacturing Division Distinguished Scientist/Engineer Award, the NCSSU Alumni Distinguished Research Award, and the American Society for Metals (ASM) fellow award.



ChemiSTEM™ technology

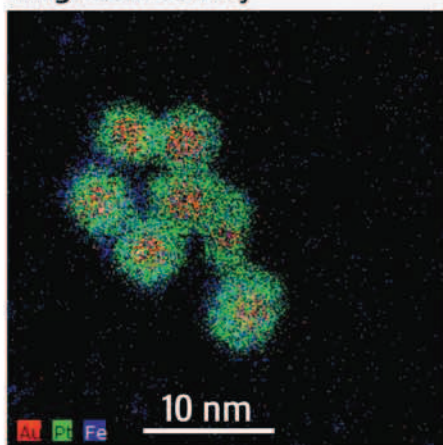
A revolution in EDX analytics

Large map, all elements



45 nm PMOS structure
600 x 600 pixels
Drift correction applied

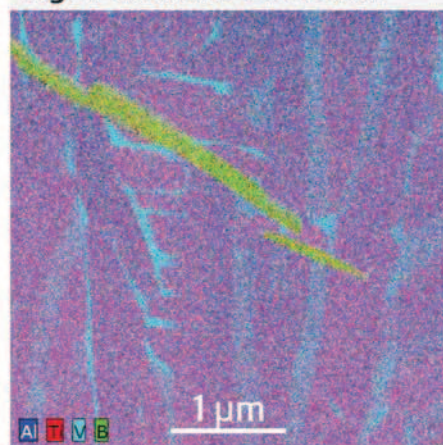
High sensitivity



Au/Pt(Fe) core/shell particles < 5 nm
300 x 300 pixels recorded in < 4 min

Sample courtesy of C. Wang, V. Stamenkovic,
N. Markovic and N.J. Zaluzec, Argonne
National Laboratory

Light element detection



Boron distribution in TiB/TiAl
512 x 512 pixels recorded in < 5 min
100 μsec dwell time; multiple frames

Sample courtesy of
Ohio State University



Tecnai Osiris™

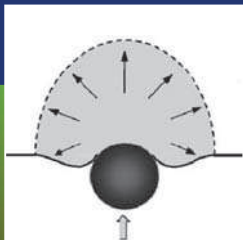
ChemiSTEM™ technology, higher beam current
and revolutionary X-ray detection capability:

- Largest solid angle for EDX detection: 0.9 sr
- Ultimate speed: elemental maps in minutes
- Highest sensitivity for light elements and low concentrations

Learn more at FEI.com/research

© 2010. We are constantly improving the performance of our products, so all specifications are subject to change without notice.





Processing of nanostructured metals and alloys via plastic deformation

Yuntian Zhu, Ruslan Z. Valiev, Terence G. Langdon, Nobuhiro Tsuji, and Ke Lu

Plastic deformation can effectively produce nanostructured metals and alloys in bulk or surface-layer forms that are suitable for practical structural or functional applications. Such nanostructured materials are porosity-free and contamination-free, and therefore they are ideal for studying fundamental mechanisms and mechanical properties. In this article, we first give an overview of the principles of grain refinement by plastic deformation and an introduction to the reported processing techniques. Then the four most-developed and promising techniques will be described in detail: equal-channel angular pressing, high-pressure torsion, accumulative roll bonding for bulk nanostructured metals, and surface mechanical attrition treatment for nanostructured surface layers.

Introduction

Nanostructured materials are defined as solids with grain, subgrain, twin, or dislocation cells with sizes below 100 nm.¹⁻⁴ Such materials usually have superior mechanical and physical properties, including high strength,¹⁻⁴ improved corrosion resistance,⁵ and higher wear resistance.⁶ Two complementary approaches have been developed for synthesizing nanostructured solids. The first is the “bottom-up” approach, in which nanostructured materials are assembled from individual atoms or from nanoscale building blocks such as nanoparticles.⁷ The second is the “top-down” approach, in which existing coarse-grained materials are processed to produce substantial grain refinement and nanostructure. The most successful top-down approaches involve the application of large plastic deformation, in which materials are subjected to plastic strains typically larger than 4–6.

Plastic deformation refines grains by a combination of several mechanisms, including dislocation glide, accumulation, interaction, annihilation, tangling, and spatial rearrangement.⁸⁻¹⁰ For materials with medium or low stacking fault energies, deformation twinning could also play a significant role, especially in the nanocrystalline grain size range.¹⁰ Detailed microstructural evolution may vary with the nature of materials as well as deformation mode, strain rate, and temperature. Hansen and co-workers have done extensive work on the grain refinement

mechanism during rolling with strains less than 100%.⁸ Their general observations also apply to other deformation modes.⁹ In coarse-grained fcc materials, each grain is divided into many subgrains during plastic deformation.⁸ Each subgrain deforms under fewer than five slip systems, but a group of adjacent subgrains acts collectively to fulfill the Taylor criterion for maintaining uniform deformation.¹¹ Each subgrain is usually subdivided into dislocation cells. With increasing strain, large subgrains may further divide into smaller subgrains, and the misorientations between subgrains may increase to form low-angle and high-angle ($>15^\circ$) grain boundaries.

Under rapid dynamic strain rates, the grains may be further refined to form ultrafine grains and nanostructures.¹⁻³ Lu et al. systematically studied the formation of nanostructures under surface mechanical attrition treatment (SMAT).^{10,12} They found that the subgrains become elongated, and their widths become smaller with increasing plastic strain. Finally, the subgrain width equals the dislocation-cell size, forming lamellar subgrains containing a string of dislocation cells. The misorientations across cell boundaries increase with further plastic strain, transforming dislocation cells into subgrains. The equiaxed subgrains further divide into smaller dislocation cells, which, in turn, convert into smaller subgrains as well as nanometer-sized grains with increasing strain. Grain rotation may play a significant role in the formation of the nanometer-sized grains with high-angle

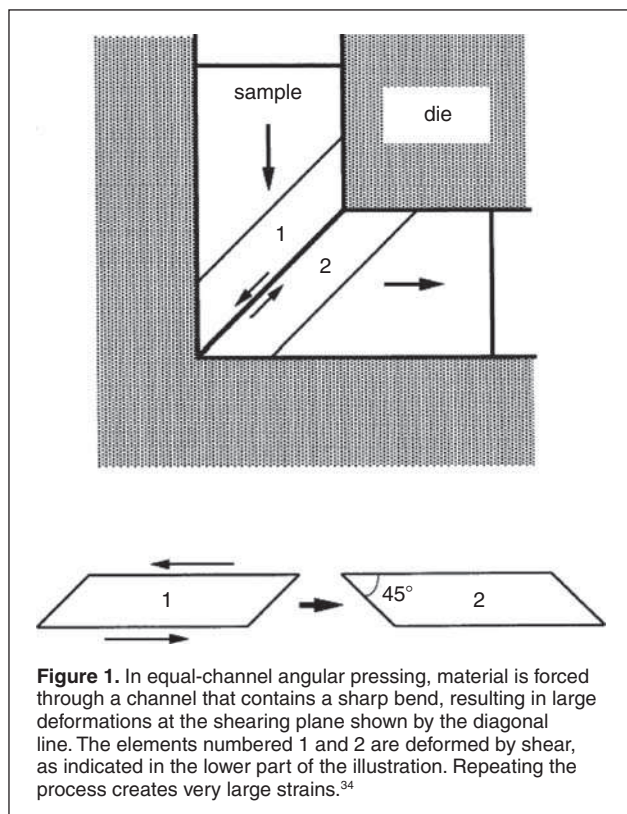
Yuntian Zhu, North Carolina State University, Raleigh, NC 27695, USA; ytzhu@ncsu.edu
Ruslan Z. Valiev, Institute of Physics of Advanced Materials, 12K.Marx St. Ufa 450000, Russia; e-mail rzvaliev@mail.ru
Terence G. Langdon, University of Southern California, Los Angeles, CA 90089, USA; langdon@usc.edu
Nobuhiro Tsuji, Kyoto University, Yoshida Honmachi, Sakyo-ku, Kyoto, 606-8502, Japan; nobuhiro.tsuji@ky5.ecs.kyoto-u.ac.jp
Ke Lu, Institute of Metal Research, Chinese Academy of Sciences, 72 Wenhua Rd., Shenyang 110016, China; lu@imr.ac.cn

boundaries. More details on the formation of nanostructures can be found in papers from Lu's group.^{10,13–15}

Various plastic-deformation techniques have been developed to produce nanostructured materials over the last two decades.¹⁶ The earliest plastic-deformation technique developed for synthesizing nanostructured materials was ball milling.^{17,18} Ball-milled powders need to be consolidated to form bulk nanostructured materials. Techniques developed later do not need the consolidation step to produce nanostructured materials in bulk or surface-layer form. The most developed and significant among these techniques are equal-channel angular pressing (ECAP),¹⁹ high-pressure torsion (HPT),²⁰ accumulative roll bonding (ARB),²¹ and SMAT.¹⁰ The principles, advantages, and limitations of these four techniques will be described in the following sections. Other variants of plastic deformation techniques include repetitive corrugation and straightening,^{9,22} co-shearing process,²³ continuous confined strip shearing,²⁴ ECAP-conform,²⁵ twist extrusion,²⁶ high-pressure tube twisting,²⁷ asymmetric rolling,^{28,29} and accumulative drawing and bonding.^{30–32} Readers can go to the respective references for more details on these techniques.

Equal-channel angular pressing

ECAP, also known as equal-channel angular extrusion, is a technique to process a metallic billet by simple shear.³³ The imposed deformation occurs as the sample passes through the die, as shown schematically in **Figure 1**. The die angle in **Figure 1** is 90°, which is the most used configuration. The theoretical shear



plane is the intersection of the two channels. Two elements adjacent to the shear plane, numbered 1 and 2, are deformed by shear, as depicted in the lower part of the figure.³⁴ The typical ECAP process concentrates intense simple shear on the shear plane. Each pass imposes the equivalent strain of $\epsilon \approx 1$ for the 90° die.^{35,36} Since the cross-sectional area of the sample remains unchanged, the same sample can be processed repeatedly to attain exceptionally high strain.

In practice, different slip systems may be introduced by rotating the billet about its longitudinal axis between each pass, and this leads to several processing routes: route A—no rotation, B_A—rotations by 90° in alternate directions, B_C—rotations by 90° in the same direction, and C—rotations by 180°.

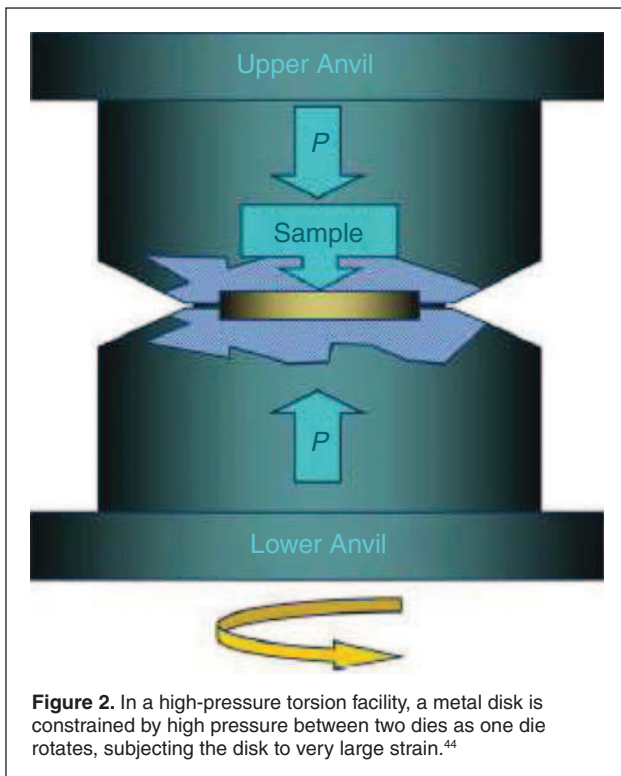
In the early 1990s, ECAP was developed and used for the first time to produce ultrafine-grained metals and alloys,^{37,38} and soon afterward to obtain bulk nanostructured materials with submicrometer-sized grains, subgrain structures, nanoparticles, or other nano-sized structural features.¹ Grain refinement during ECAP is associated with some dislocation substructural characteristics (cells, subgrains, microbands) that are established during the first one or two passes^{39,40} and their transformation to ultrafine grains during further straining.^{19,41,42} At present, ECAP is the most popular severe-plastic-deformation processing technique, and has been used for grain refinement in various metals and alloys, including commercial ones. However, the final grain size, grain shape, and the fraction of high-angle grain boundaries strongly depend on the processing routes and parameters as well as the material properties.

Typically the ECAP process requires the insertion and removal of the billets manually from the die. Recent developments include the incorporation of back-pressure, the development of continuous ECAP processing, and other modifications.¹⁹ This progress moves ECAP processing closer to industrial applications.

High-pressure torsion

The processing of metals by HPT has a long history dating back to the classic work by Nobel Laureate P.W. Bridgman at Harvard University in the 1930s.⁴³ Nevertheless, it is only within the last two decades that HPT has become a major research tool because of the ability to achieve extremely high applied pressures and the consequent production of exceptional grain refinement. Typically, the grain sizes produced in HPT are within the nanoscale range of ~50–100 nm.

Figure 2 provides a schematic illustration of the principle of HPT.⁴⁴ The sample is usually in the form of a relatively thin disk with a diameter of typically ~10 or 20 mm and a thickness of ~0.8 mm. This disk is placed between two massive anvils, and it is held in place within a depression machined into the face of each anvil. During operation, the sample is subjected to a high applied pressure, P , and concurrent torsional straining through rotation of the lower anvil. This type of processing is designated quasi-constrained HPT because there is some limited outward flow of the material around the periphery of the disk during the processing operation.²⁰ Early experiments in HPT were often



conducted under unconstrained conditions where the material flowed out freely under the applied pressure.

It is reasonable to anticipate there may be an important limitation in HPT, because it imposes a strain that is directly proportional to the radial distance from the rotation axis; therefore, there should be a significant strain inhomogeneity across the disk. In practice, however, early HPT experiments demonstrated that the microstructure gradually evolves with increasing strain so that, ultimately, the structure becomes reasonably homogeneous throughout the disk.⁴⁵ This development of homogeneity has been successfully modeled using strain gradient plasticity and incorporating a microstructure-related constitutive description of the material behavior.⁴⁶ Recent experiments have revealed unusual shearing patterns within disks processed by HPT. For example, in a two-phase eutectoid alloy, it was shown that agglomerates of grains were formed, lying parallel to the flow direction around the peripheries of the disks.⁴⁷ In a duplex stainless steel, there was evidence of significant turbulence, including complex swirls and vortices that are analogous to the Kelvin-Helmholtz instability, which is a well-established physical phenomenon in fluid flow.⁴⁸ These observations suggest the occurrence of local shear velocity gradients between adjacent positions within the HPT disks.

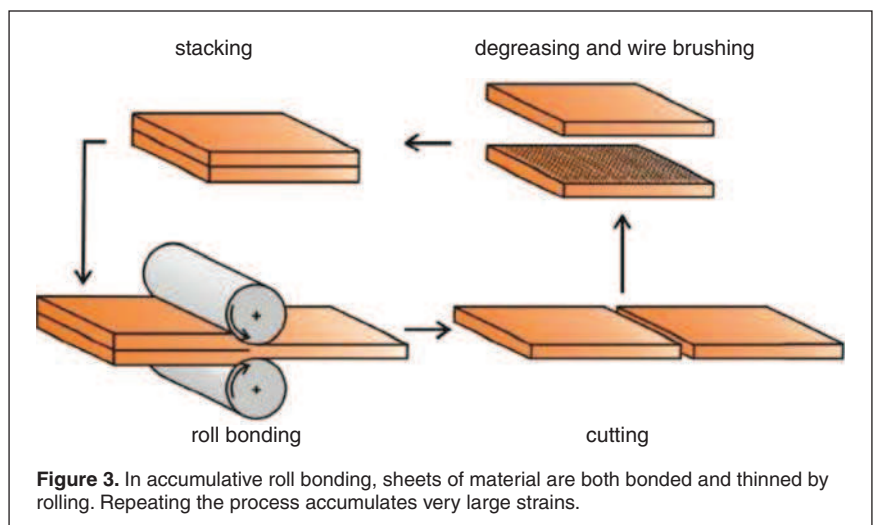
Processing by HPT has been used successfully for cold consolidation,⁴⁹ for inducing phase transformations,⁵⁰ and for producing

partial crystalline-to-amorphous transformations.⁵¹ A potential limitation is that it uses relatively thin disks, but attempts are under way to expand the applicability of HPT processing to cylindrical samples.⁵²

Accumulative roll bonding

ARB is one of the deformation processes that can realize ultrahigh plastic strains in sheet materials for producing nanostructures. **Figure 3** illustrates the principle of the ARB process, which was developed by Saito, Tsuji et al. in 1998.^{21,53–55} ARB uses rolling deformation. It is nearly impossible to realize ultrahigh plastic strain above an equivalent strain of ~ 4 – 5 in conventional rolling because the dimension of the materials (e.g., the thickness) decreases with increasing total rolling strain. In the ARB process, a sheet is rolled by 50% reduction in thickness. The rolled sheet is cut into two pieces, stacked to reform the initial dimensions, and rolled again. In order to obtain one-body solid material, the rolling in the ARB process is also a bonding process, which is known as roll bonding used for the production of clad sheets. To achieve good bonding, the contact surfaces of the sheets are typically treated by degreasing and wire brushing. Roll bonding is sometimes carried out at elevated temperatures, below the recrystallization temperature of the material in order to make the bonding better and to reduce the rolling force. By repeating the procedure, one can apply ultrahigh plastic strain to the sheet material without changing the dimensions.

The von Mises equivalent strain (ϵ_{eq}) after n cycles of ARB can be estimated as $\epsilon_{eq} = 0.8n$ when 50% reduction per cycle is used. An equivalent strain of 4 can be achieved by five ARB cycles in this case. A similar process was performed previously for bulk mechanical alloying of different metals or for fabricating multilayered materials.^{56,57} However, roll bonding was not used in such attempts. Instead, diffusion bonding at elevated temperature, which cannot produce nanostructures through accumulating plastic strain, was carried out between each pressing or rolling. Bulk mechanical alloying by the ARB process is possible, and non-equilibrium structures, including



an amorphous phase, have been produced.⁵⁸ The processing details and the mechanism of ultrafine grain formation in the ARB process are discussed by Huang et al.⁵⁹

The most advantageous feature of the ARB process is its applicability to continuous production of bulky sheet materials. Although ARB has not yet been adopted into large-scale production, such as in the steel industry where huge rolling facilities are used, thin strips (~0.1 mm thick, 300 mm wide, and 3,000 m long) of ultrafine-grained stainless steels already have been produced in a relatively small-scale facility in Japan using the principle of ARB.⁶⁰ ARB is also useful for fundamental studies in laboratories, as it can provide relatively large sheet samples with nanostructures. This enables systematic studies of the mechanical properties of the ultrafine-grained metals,^{61,62} and several unique properties of nanostructured metals, such as “hardening by annealing and softening by deformation”⁶³ and yield-point phenomena in pure Al⁶¹ have been found.

Surface mechanical attrition treatment

The basic principle of SMAT is to impose plastic deformation onto surface layers of bulk metals with large strains and strain rates.^{12,64} As shown in **Figure 4**, spherical steel (or ceramic) balls, a few millimeters in diameter with smooth surfaces, are placed in the bottom of a chamber that is vibrated (usually with a frequency of ~50 Hz–20 kHz). When the balls are agitated, the sample surface is impacted by a large number of flying balls over a short period of time. Each impact of a flying ball (with a velocity of ~1–20 m/s) induces plastic deformation at a high strain rate in the surface layer. Repeated multidirectional impacts result in repeated plastic deformation in the top surface layer that induces grain refinement progressively down to the nanometer regime. Major differences between SMAT and conventional shot peening include (1) much larger energy inputs to material surface (by several orders of magnitude) in

SMAT, and (2) much larger balls with smooth surfaces that are used in SMAT to minimize wearing and damaging the formed nanostructured surface layers.

In SMAT samples, a gradient in grain-size distribution is generated along the depth from the treated surface, from a few nanometers to micrometers, owing to the gradients in strain and strain rate. In the topmost layer, very high strain rates up to $\sim 10^3 \text{ s}^{-1}$ can be imposed, inducing extremely fine nano-sized grains distinct from those in the conventional plastic deformation of bulk metals. Finer grains can be induced at higher strain rates,⁶⁵ owing to an increased dislocation density and/or nanoscale twinning at high strain rates.¹⁰

Nanostructured surface layers have been synthesized in a number of materials, including pure metals (e.g., Cu, Fe, Ti) and alloys.^{13,14,64,66–68} Nanostructured surface layers can be ~50 μm thick, underneath which is an ultrafine-grained layer (>100 μm thick). Thicknesses of the nanostructured surface (and the ultrafine-grained) layer depend upon the nature of materials treated and the processing parameters, such as ball size and vibration frequency. The nanostructured surface layer exhibits higher hardness, strength, wear resistance, fatigue strength, atomic diffusivity, and chemical reactivity than that of the coarse-grained matrix.⁶⁴

SMAT is a low-cost process with a unique flexibility to realize a nanostructured surface layer in localized areas on bulk materials or components without shape change. The gradient grain size distribution eliminates the problem of delamination of the nanostructured layers from their matrix. Recently, SMAT has been successfully applied at BaoSteel Co. (Shanghai, China) for processing cold-rolling rollers, elevating their service life-time by a factor of three.

The depth of the nanostructured layers produced by SMAT is limited by the energy applied onto the materials surface, which also affects surface roughness and contaminations of the surface layer from processing media. The development of new SMAT techniques is in progress to thicken the nanostructured layers with a better control of surface roughness and contaminations (e.g., surface mechanical grinding treatment).⁶⁹

Conclusions

The significance of a processing technique for producing nanostructured materials can be evaluated by two criteria: (1) The capability of producing unique nanostructures for fundamental studies, and (2) the possibility of scaling up for economical industrial applications. The former criterion requires the production of nanostructured materials that are porosity- and contamination-free, while the latter requires continuous production of nanostructured materials in an industrial facility. The four techniques presented in this article meet one or both of the above criteria. High-pressure torsion can

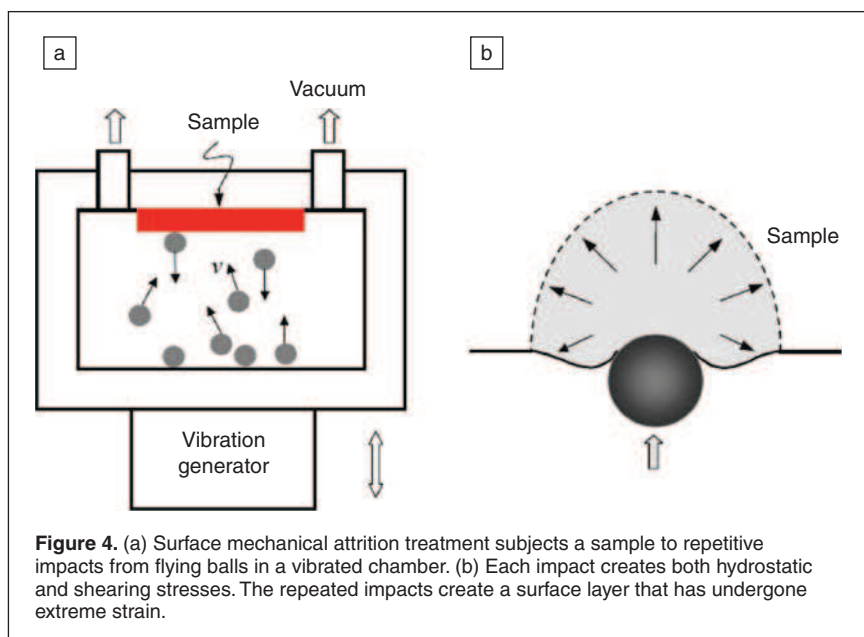


Figure 4. (a) Surface mechanical attrition treatment subjects a sample to repetitive impacts from flying balls in a vibrated chamber. (b) Each impact creates both hydrostatic and shearing stresses. The repeated impacts create a surface layer that has undergone extreme strain.

produce relatively small samples for scientific study and can consolidate powders without applying heating. Continuous equal-channel angular pressing (ECAP) is now on the verge of commercialization for producing nanostructured materials for medical and other applications. Accumulative roll bonding (ARB) has been used to produce long coils of nanostructured/ultrafine-grained stainless steels. Surface mechanical attrition treatment (SMAT) is already in use in a large steel company. Continuous ECAP, ARB, and SMAT are currently being scaled up for industrial productions.

References

1. R.Z. Valiev, R. Islamgaliev, I.V. Alexandrov, *Prog. Mater. Sci.* **45**, 103 (2000).
2. R.Z. Valiev, Y. Estrin, Z. Horita, T.G. Langdon, M.J. Zehetbauer, Y.T. Zhu, *JOM* **58** (4), 33 (2006).
3. Y.T. Zhu, X.Z. Liao, *Nat. Mater.* **3**, 351 (2004).
4. H. Gleiter, *Acta Mater.* **48**, 1 (2000).
5. A. Balyanov, J. Kutnyakova, N.A. Amirkhanova, V.V. Stolyarov, R.Z. Valiev, X.Z. Liao, Y.H. Zhao, Y.B. Jiang, H.F. Xu, T.C. Lowe, Y.T. Zhu, *Scripta Mater.* **51**, 225 (2004).
6. P.Q. La, J.Q. Ma, Y.T. Zhu, J. Yang, W.M. Lu, Q.J. Xue, R.Z. Valiev, *Acta Mater.* **53**, 5167 (2005).
7. H. Gleiter, *Prog. Mater. Sci.* **33**, 223 (1989).
8. B. Bay, N. Hansen, D.A. Hughes, D. Kuhlmannwilsdorf, *Acta Metall. Mater.* **40**, 205 (1992).
9. J.Y. Huang, Y.T. Zhu, H. Jiang, T.C. Lowe, *Acta Mater.* **49**, 1497 (2001).
10. K. Lu, N. Hansen, *Scripta Mater.* **60**, 1033 (2009).
11. G.I. Taylor, *J. Inst. Met.* **62**, 307 (1938).
12. K. Lu, J. Lu, *J. Mater. Sci. Technol.* **15**, 193 (1999).
13. X. Wu, N. Tao, Y. Hong, B. Xu, J. Lu, K. Lu, *Acta Mater.* **50**, 2075 (2002).
14. H.W. Zhang, Z.K. Hei, G. Liu, J. Lu, K. Lu, *Acta Mater.* **51**, 1871 (2003).
15. N.R. Tao, Z.B. Wang, W.P. Tong, M.L. Sui, J. Lu, K. Lu, *Acta Mater.* **50**, 4603 (2002).
16. Y.T. Zhu, D.P. Butt, in *Encyclopedia of Nanoscience and Nanotechnology*, H.S. Nalwa, Ed. (American Scientific Publishers, Stevenson Ranch, CA, 2003), Vol. 6, p. 853.
17. C.C. Koch, *Nanostruct. Mater.* **9**, 13 (1997).
18. R.J. Perez, H.G. Jiang, C.P. Dogan, E.J. Laverna, *Metall. Mater. Trans. A* **29**, 2469 (1998).
19. R.Z. Valiev, T.G. Langdon, *Prog. Mater. Sci.* **51**, 881 (2006).
20. A.P. Zhilyaev, T.G. Langdon, *Prog. Mater. Sci.* **53**, 893 (2008).
21. Y. Saito, H. Utsunomiya, N. Tsuji, T. Sakai, *Acta Mater.* **47**, 579 (1999).
22. Y.T. Zhu, H.G. Jiang, J.Y. Huang, T.C. Lowe, *Metall. Mater. Trans. A* **32**, 1559 (2001).
23. Y. Saito, H. Utsunomiya, H. Suzuki, A. Sakai, *Scripta Mater.* **42**, 1139 (2000).
24. J.C. Lee, H.K. Seok, J.Y. Suh, *Acta Mater.* **50**, 4005 (2002).
25. G.J. Raab, R.Z. Valiev, T.C. Lowe, Y.T. Zhu, *Mater. Sci. Eng. A* **382**, 30 (2004).
26. D. Orlov, Y. Beygelzimer, S. Synkov, V. Varyukhin, Z. Horita, *Mater. Trans.* **49**, 2 (2008).
27. L.S. Toth, M. Arzaghi, J.J. Fundenberger, B. Beausir, O. Bouaziz, R. Arruffat-Massion, *Scripta Mater.* **60**, 175 (2009).
28. J.H. Jiang, Y. Ding, F.Q. Zuo, A.D. Shan, *Scripta Mater.* **60**, 905 (2009).
29. Y.H. Ji, J.J. Park, *Mater. Sci. Eng. A* **499**, 14 (2009).
30. V. Vidal, L. Thilly, F. Lecouturier, P.O. Renault, *Acta Mater.* **54**, 1063 (2006).
31. F. Dupouy, S. Askenazy, J.P. Peyrade, D. Legat, *Phys. B* **211**, 43 (1995).
32. K. Han, J.D. Embury, J.R. Sims, L.J. Campbell, H.J. Schneider-Muntau, V.I. Pantsyrnyi, A. Shikov, A. Nikulin, A. Vorobieva, *Mater. Sci. Eng. A* **267**, 99 (1999).
33. V.M. Segal, V.I. Reznikov, A.E. Drobyshevskiy, V.I. Kopylov, *Russ. Metall.* **99** (1981).
34. K. Nakashima, Z. Horita, M. Nemoto, T.G. Langdon, *Mater. Sci. Eng. A* **281**, 82 (2000).
35. Y. Iwahashi, J.T. Wang, Z. Horita, M. Nemoto, T.G. Langdon, *Scripta Mater.* **35**, 143 (1996).
36. F.Z. Utyashev, F.U. Enikeev, V.V. Latysh, *Ann. Chim. Sci. Mat.* **21**, 379 (1996).
37. R.Z. Valiev, N.A. Krasilnikov, N.K. Tsenev, *Mater. Sci. Eng. A* **137**, 35 (1991).
38. R.Z. Valiev, A.V. Korznikov, R.R. Mulyukov, *Mater. Sci. Eng. A* **168**, 141 (1993).
39. S.C. Baik, R.J. Hellmig, Y. Estrin, H.S. Kim, *Z. Metallkd.* **94**, 754 (2003).
40. Q. Xue, I.J. Beyerlein, D.J. Alexander, G.T. Gray, *Acta Mater.* **55**, 655 (2007).
41. A. Vinogradov, T. Suzuki, S. Hashimoto, K. Kitagawa, A. Kuznetsov, S. Dobatkin, *Mater. Sci. Forum* **503–504**, 971 (2006).
42. Y. Iwahashi, Z. Horita, M. Nemoto, T.G. Langdon, *Acta Mater.* **45**, 4733 (1997).
43. P.W. Bridgman, *Phys. Rev.* **48**, 825 (1935).
44. C. Xu, Z. Horita, T.G. Langdon, *Acta Mater.* **56**, 5168 (2008).
45. A.P. Zhilyaev, G.V. Nurislamova, B.K. Kim, M.D. Baro, J.A. Szpunar, T.G. Langdon, *Acta Mater.* **51**, 753 (2003).
46. Y. Estrin, A. Molotnikov, C.H.J. Davies, R. Lapovok, *J. Mech. Phys. Solids* **56**, 1186 (2008).
47. M. Kawasaki, B. Ahn, T.G. Langdon, *Acta Mater.* **58**, 919 (2010).
48. Y. Cao, Y.B. Wang, S.N. Alhajeri, X.Z. Liao, W.L. Zheng, S.P. Ringer, T.G. Langdon, Y.T. Zhu, *J. Mater. Sci.* **45**, 765 (2010).
49. A.P. Zhilyaev, A.A. Gimazov, G.I. Raab, T.G. Langdon, *Mater. Sci. Eng. A* **486**, 123 (2008).
50. M.T. Perez-Prado, A.P. Zhilyaev, *Phys. Rev. Lett.* **102**, 175504 (2009).
51. J.Y. Huang, Y.T. Zhu, X.Z. Liao, R.Z. Valiev, *Philos. Mag. Lett.* **84**, 183 (2004).
52. G. Sakai, K. Nakamura, Z. Horita, T.G. Langdon, *Mater. Sci. Eng. A* **406**, 268 (2005).
53. Y. Saito, N. Tsuji, H. Utsunomiya, T. Sakai, R.G. Hong, *Scripta Mater.* **39**, 1221 (1998).
54. N. Tsuji, Y. Saito, S.H. Lee, Y. Minamino, *Adv. Eng. Mater.* **5**, 338 (2003).
55. N. Tsuji, *Production of Bulk Nanostructured Metals by Accumulative Roll Bonding (ARB) Process* (Nova Scientific Publishers, CA, 2006).
56. M. Atzmon, K.M. Unruh, W.L. Johnson, *J. Appl. Phys.* **58**, 3865 (1985).
57. K. Yasuna, M. Terauchi, A. Otsuki, K.N. Ishihara, P.H. Shingu, *J. Appl. Phys.* **82**, 2435 (1997).
58. S. Ohsaki, S. Kato, N. Tsuji, T. Ohkubo, K. Hono, *Acta Mater.* **55**, 2885 (2007).
59. X. Huang, N. Tsuji, N. Hansen, Y. Minamino, *Mater. Sci. Eng. A* **340**, 265 (2003).
60. N. Tsuji, *Adv. Eng. Mater.* **12**, 701 (2010).
61. N. Tsuji, Y. Ito, Y. Saito, Y. Minamino, *Scripta Mater.* **47**, 893 (2002).
62. N. Tsuji, S. Okuno, Y. Koizumi, Y. Minamino, *Mater. Trans.* **45**, 2272 (2004).
63. X.X. Huang, N. Hansen, N. Tsuji, *Science* **312**, 249 (2006).
64. K. Lu, J. Lu, *Mater. Sci. Eng. A* **375–377**, 38 (2004).
65. Y.S. Li, Y. Zhang, N.R. Tao, K. Lu, *Acta Mater.* **57**, 761 (2009).
66. K. Wang, N.R. Tao, G. Liu, J. Lu, K. Lu, *Acta Mater.* **54**, 5281 (2006).
67. K.Y. Zhu, A. Vassel, F. Brisset, K. Lu, J. Lu, *Acta Mater.* **52**, 4101 (2004).
68. L. Zhou, G. Liu, X.L. Ma, K. Lu, *Acta Mater.* **56**, 78 (2008).
69. W.L. Li, N.R. Tao, K. Lu, *Scripta Mater.* **59**, 546 (2008).

□

Need to Connect with the Materials Research Society?

Click



www.mrs.org

Call



724.779.3003

Fax



724.779.8313

Write



info@mrs.org



®

Ce	Pr	Nd	Pm	Sm	Eu	Gd	Tb	Dy	Ho	Er	Tm	Yb	Lu
Th	Pa	U	Np	Pu	Am	Cm	Bk	Cf	Es	Fm	Md	No	Lr

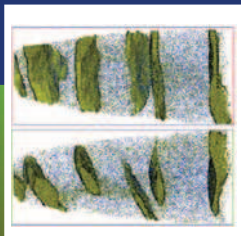
Semiconductors & Laser Crystals

Deposition & Evaporation Source Materials

Foil, Targets, Wire, Tubing, Powders & Pellets

Isotopes & Functionalized Organic Compounds

www.americanelements.com



Metallic composites processed via extreme deformation: Toward the limits of strength in bulk materials

Dierk Raabe, Pyuck-Pa Choi, Yujiao Li, Aleksander Kostka, Xavier Sauvage, Florence Lecouturier, Kazuhiro Hono, Reiner Kirchheim, Reinhard Pippan, and David Embury

We review microstructures and properties of metal matrix composites produced by severe plastic deformation of multiphase alloys. Typical processings are wire drawing, ball milling, roll bonding, equal-channel angular extrusion, and high-pressure torsion of multiphase materials. Similar phenomena occur between solids in frictional contact such as in tribology, friction stir welding, and explosive joining. The resulting compounds are characterized by very high interface and dislocation density, chemical mixing, and atomic-scale structural transitions at heterointerfaces. Upon straining, the phases form into nanoscaled filaments. This leads to enormous strengthening combined with good ductility, as in damascene steels or pearlitic wires, which are among the strongest nanostructured bulk materials available today (tensile strength above 6 GPa). Similar materials are Cu-Nb and Cu-Ag composites, which also have good electrical conductivity that qualifies them for use in high-field magnets. Beyond the engineering opportunities, there are also exciting fundamental questions. They relate to the nature of the complex dislocation, amorphization, and mechanical alloying mechanisms upon straining and their relationship to the enormous strength. Studying these mechanisms is enabled by mature atomic-scale characterization and simulation methods. A better understanding of the extreme strength in these materials also provides insight into modern alloy design based on complex solid solution phenomena.

Introduction

Metal matrix composites with high interface density are produced via severe plastic co-deformation of multiphase alloys.^{1–15} Corresponding compounds are first prepared by liquid or powder metallurgy^{3–12} or through restacking solids of different composition.² Subsequent extreme straining, to promote intense microstructure refinement, proceeds by wire drawing, ball milling, accumulative roll bonding, damascene forging, equal channel angular extrusion, friction, or high-pressure torsion.⁷

Corresponding material systems can be grouped according to a microstructural or chemical classification scheme: From a microstructural perspective, multiphase systems can be classified as either particle-like alloys after primary syn-

thesis or as lamellar or filament-type micro- or nanostructured materials. Often there is a transition between the two, for example, from a second phase with particulate initial shape into a deformation-induced lamellar and nanograined filament composite structure, such as in Cu-Nb, Cu-W, Cu-V, or Cu-Cr.^{2–20} In other cases, the architecture is not changed during deformation, as in the case of pearlite,^{1,21–28} where basic topological changes such as fiber curling occur only at very high strains.

From a chemical perspective, these alloy systems can be classified as immiscible pure-metal–metal-matrix compounds, intermetallic–metal-matrix compounds, or carbide–metal-matrix composites. In pure metal–metal-matrix composites, we observe the formation of supersaturated solid solutions¹⁴

Dierk Raabe, Max-Planck-Institut für Eisenforschung in Düsseldorf, Germany; d.raabe@mpie.de
Pyuck-Pa Choi, Max-Planck-Institut für Eisenforschung in Düsseldorf, Germany; p.choi@mpie.de
Yujiao Li, Max-Planck-Institut für Eisenforschung in Düsseldorf, Germany; y.li@mpie.de
Aleksander Kostka, Max-Planck-Institut für Eisenforschung in Düsseldorf, Germany; a.kostka@mpie.de
Xavier Sauvage, Institut de Physique at the University of Rouen, France; xavier.sauvage@univ-rouen.fr
Florence Lecouturier, Laboratoire National des Champs Magnétiques Intenses at CNRS, Toulouse, France; florence.lecouturier@lncmi.cnrs.fr
Kazuhiro Hono, National Institute for Materials Science in Sengen, Tsukuba, Japan; kazuhiro.hono@nims.go.jp
Reiner Kirchheim, Materials Physics Institute at the University of Göttingen; rkirch@ump.gwdg.de
Reinhard Pippan, Erich Schmid Institute in Leoben, Austria; reinhard.pippan@oeaw.ac.at
David Embury, McMaster University, Hamilton, Canada; emburyd@univmail.cis.mcmaster.ca

and sometimes small amorphous zones.¹⁹ In the case of composites consisting of intermetallics or carbides dispersed in a metallic matrix, one can additionally observe phase changes (from an ordered to a disordered phase or from crystalline to amorphous).^{27–32}

Mechanical alloying to non-equilibrium solid solutions and deformation-driven as well as solid-solution-driven solid-state amorphization phenomena occur preferentially at heterophase interfaces. In cases where extreme strains are imposed, such as in ball milling, initially separate phases can nearly entirely dissolve into the matrix so that the multiphase character is lost.^{14–34} In addition, severe wire drawing of multiphase alloys can lead to complex curling, where the minority phase forms into flat filaments that are bent about their longitudinal axis.

In general, different processes and alloy variants may lead to differences in nanostructure, amorphization, and mechanical alloying. The most essential criteria to identify whether a certain process and material combination tends to undergo preferential deformation-induced amorphization and/or mechanical alloying are the maximum attainable strain, the mutual solubility of the elements in each phase, the mixing energies of the elements stemming from the abutting phases, and the size difference of the solute atoms that enter the other phase during mechanical alloying.

Originally, the main interest in such heavily co-deformed compounds was to design materials with enormous interface-related strengthening combined with good ductility. For instance, multiply re-stacked damascene steels or heavily strained pearlite, such as that used in steel cord and piano wires, are among the strongest nanostructured bulk materials available today, with more than 6 GPa tensile strength (Figures 1–3). Wire-drawn Cu-20 wt% Nb alloys reveal up to 1.8 GPa strength combined with good electrical conductivity.^{7,9}

Beyond the engineering opportunities (such as shown in Figure 1), a number of fundamental questions arise when driving composites toward the limits of strength through extreme deformation. These questions relate to the nature of the complex dislocation, amorphization, and mechanical alloying mechanisms that occur upon straining.^{25–55} Studying these mechanisms has been recently enabled through matured atomic-scale characterization (e.g., atom probe tomography and high-resolution transmission electron microscopy) and simulation methods (e.g., molecular dynamics with improved potentials).

In this article, we give an overview of deformation microstructures and the resulting mechanical properties

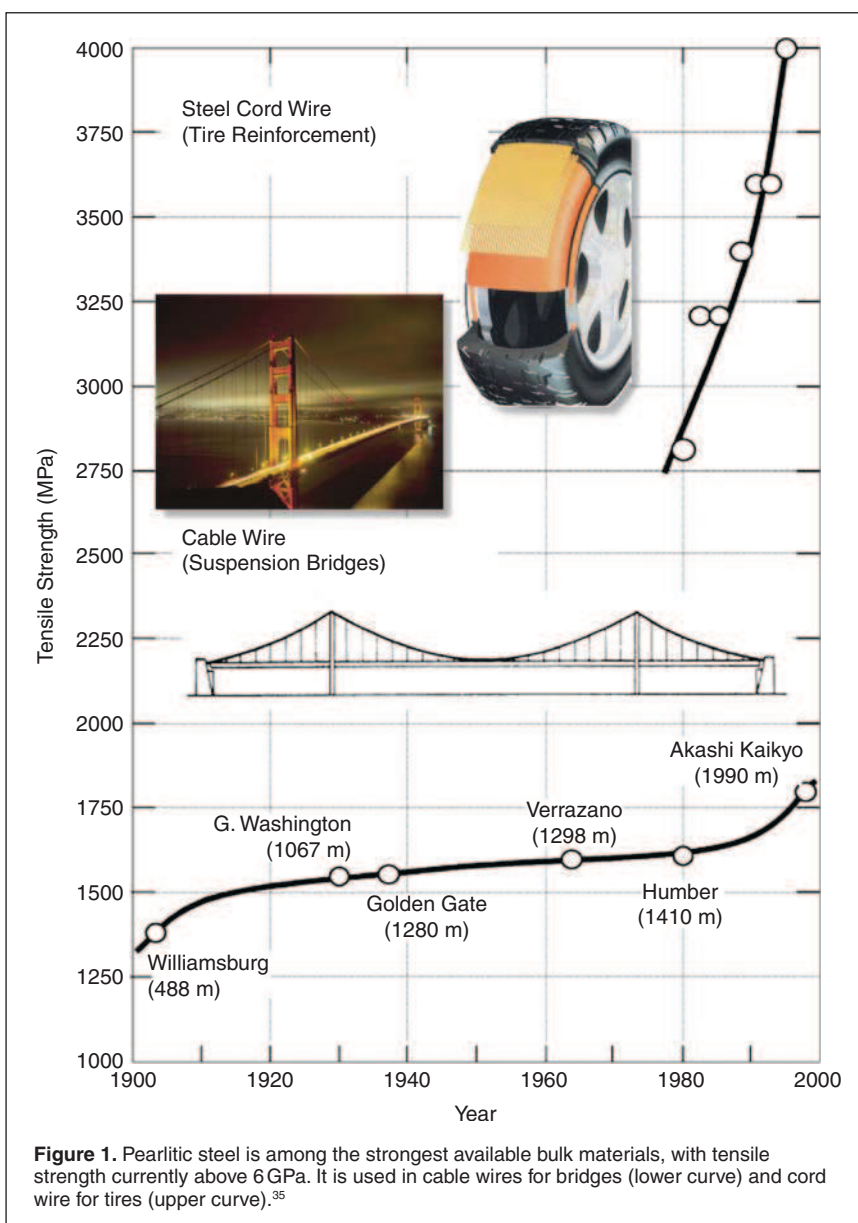
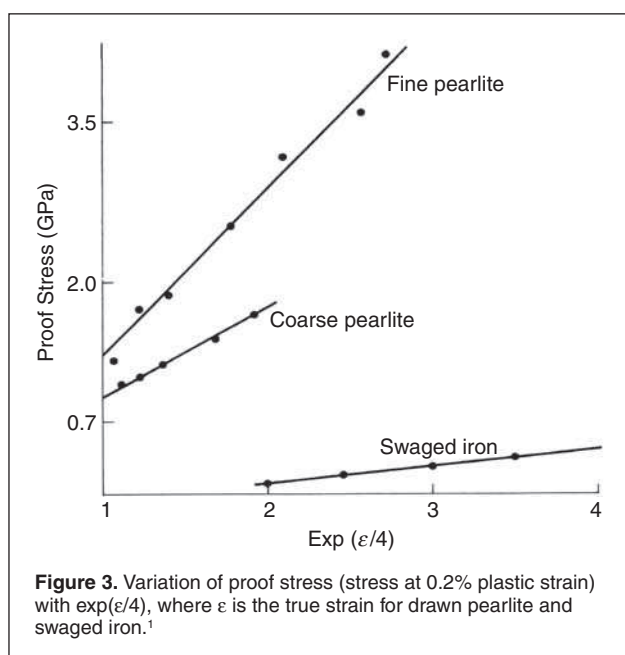
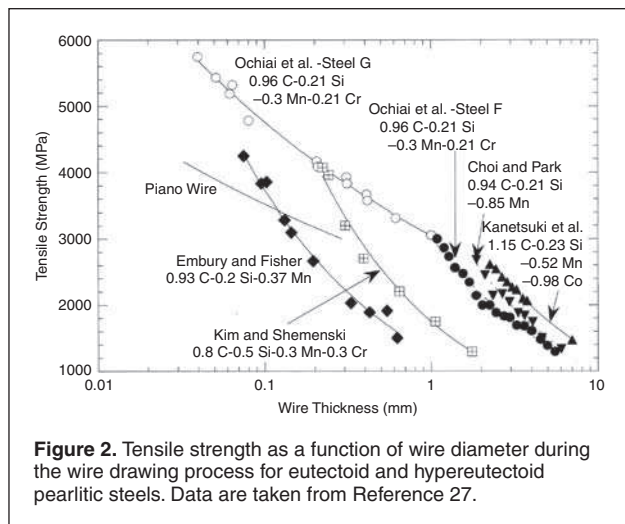


Figure 1. Pearlitic steel is among the strongest available bulk materials, with tensile strength currently above 6 GPa. It is used in cable wires for bridges (lower curve) and cord wire for tires (upper curve).³⁵

obtained by extreme straining (true strains of 3–6, in some cases even up to 10). The aim is to identify microstructure features that are common to a number of different material combinations and processing conditions, including not only extreme bulk co-deformation but also nanotribology and frictional joining, as they reveal similar degrees of heavy local co-deformation. The main similarity among these different systems is that extremely strained heterophase interface areas are involved in all cases. In these regions, profound similarities can be observed in terms of the active mechanisms that may finally lead to interface-related plasticity, structural transitions (e.g., amorphization), atomic-scale mechanical alloying, phase formation, and phase decomposition.

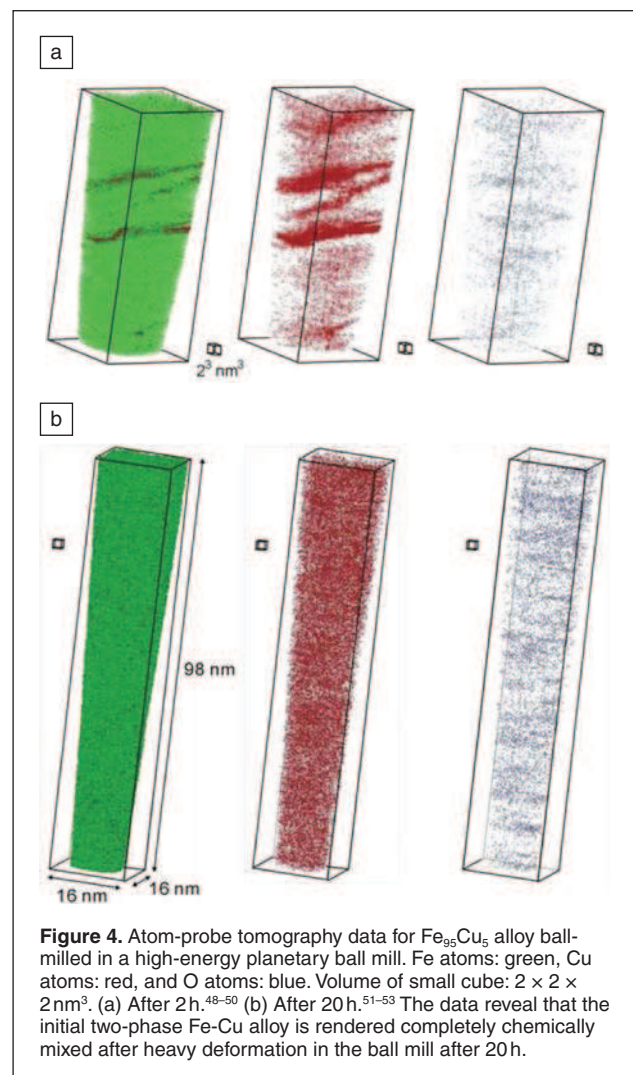
Characteristic to all of these processes is that they lead to a certain degree of deformation-driven microstructure

hierarchy. This means that upon increasing co-deformation, a sequence in the microstructure evolution and also in the corresponding microstructure-property relations appears. The sequence of mechanisms generally does not follow the same strain dependence. However, as a rule, at low strains (micrometer spacing of interfaces), dislocation-based Orowan loop expansion and Hall-Petch mechanisms at the interfaces prevail, while at large strains (nanometer spacing of interfaces), dislocation-assisted atomic-scale processes through the interfaces determine the evolution of microstructure and strength. More specifically, in the nanoscopic regime, a number of mechanisms play a role, including structural decomposition, dislocation source size limitation, interface dislocation reactions, internal stresses, mechanically driven alloying across heterophase boundaries, and phase decomposition.



As an example, **Figure 4** shows results from atom probe tomography, where in a two-phase Fe-5 at.% Cu alloy with a large miscibility gap, the individual phases gradually start to dissolve under intense deformation obtained via ball milling.^{51–53} The initial two-phase sample, analyzed after two hours, has not yet been completely mixed at an atomic scale (Figure 4a). Besides regions in which Cu atoms are dissolved in the Fe matrix, some Cu-rich fragments still exist. These fragments are formed by repeated fracture and cold-welding processes of powder particles trapped between colliding balls. After 20 h ball milling, no Cu-rich fragments appear (Figure 4b). The Cu atoms are nearly homogeneously distributed in the Fe matrix.

Of particular interest in this context is the question why extremely co-deformed composites still reveal very high and further increasing strength, although, in most cases, the interfaces are gradually dissolved and hence lose their separating function between the initial phases. This aspect will be discussed in the final section. This article is structured following the microstructure hierarchy, placing attention first on the extreme co-deformation of metal matrix composites



and subsequently on similar heterophase interface phenomena that play a role in the field of tribology and friction-dominated joining.

Hardening mechanisms of co-deformed composites: The micrometer scale

Metallic composites exposed to severe co-deformation go through a sequence of complex microstructure refinement phenomena. At low and average strains, the coexisting phases undergo a shape reduction that is related to the externally imposed strain, although usually not at a one-to-one relation, as the harder phases deform less than the matrix. Exceptions apply when the material undergoes necking and shear banding, where the harder phase can also be severely strained. This mesoscopic refinement reduces the average phase spacing. The interphase distance and the phase thickness determine the mean free path of the lattice dislocations at these scales, which governs the Hall-Petch hardening that is mainly responsible for the compound strength in this regime.

A simple microstructure-property relationship for the strength of wire-drawn pearlite can be formulated through a geometric model, where we assume by similitude that the strain-induced phase boundary spacing, d , and the external wire diameter, D , are proportional:

$$\frac{d_0}{d(\epsilon)} = \frac{D_0}{D(\epsilon)}, \quad (1)$$

where the “0” subscript indicates the initial value and the true strain ϵ is defined by

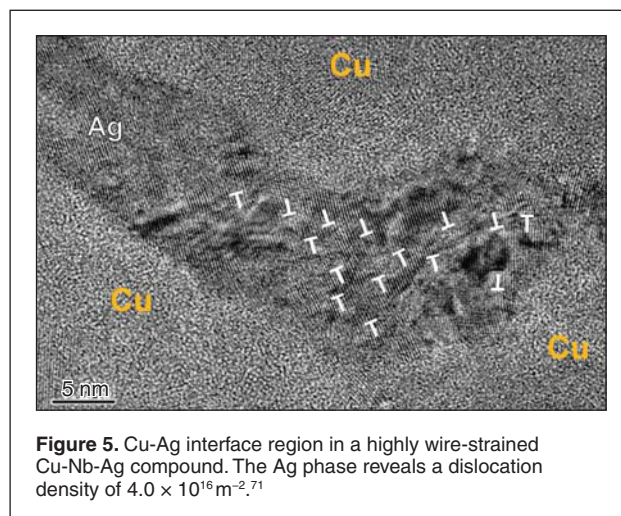
$$\epsilon = 2 \ln(D_0 / D(\epsilon)). \quad (2)$$

Thus, if we assume a Hall-Petch scaling law, the stress σ is given by

$$\sigma(\epsilon) = \sigma_0 + \frac{k}{\sqrt{d_0}} \exp\left(\frac{\epsilon}{4}\right), \quad (3)$$

with a material-dependent strengthening coefficient k . Experimental results confirm the proportionality of proof stress (stress at 0.2% plastic strain) to the quantity $\exp(\epsilon/4)$ for drawn pearlite and for swaged iron (Figure 3).

Upon further reduction in the interphase spacing, conventional bulk plasticity becomes less relevant for further increase in strength. This means that dislocation-dislocation interactions within the constituent phases and the Hall-Petch effect are gradually replaced by three effects, namely, limitations in activating dislocation sources, dislocation reactions at the heterointerfaces, and Orowan expansion of dislocations within the lamellae. Also, it was observed by many researchers^{9,14,16,23,29,30,36,42} that very high dislocation and vacancy densities can be stored in this regime, **Figure 5**. For Cu-Nb nanocomposites, these mechanisms were studied in detail by a number of groups.^{6–17,20,54} The dominating plastic deformation



mechanism in this material is the nucleation of single dislocation loops expanding in closely spaced parallel planes (Orowan mechanism) between Nb fibers, which behave as whiskers with an elevated elastic limit. Postmortem studies identified the dislocations involved in the process and revealed their role as associated defects at the complex Cu/Nb interfaces. As deformation proceeds, the number of loops increases, thus decreasing the distance between the loops on parallel planes.⁵⁴ When the number of dislocations at the interface is sufficient to accommodate the misfit between Cu and Nb, the mechanism stops. Pearlitic steels often start to deform plastically via the Orowan mechanism at low strains, since their starting microstructure is already very fine, with a typical interlamellar spacing of about 100 to 200 nm.^{7,9,17,44,55}

Upon further microstructure refinement, dislocation penetration effects start to occur through heterointerfaces (even among non-coherent phases). Such heterophase slip transfer effects probably occur not only in the form of single-slip transition effects but also in the form of localization effects across interfaces by micro- or shear bands.^{28–32}

Heterophase interface mechanics: Slip transmission and internal stresses

When the microstructure refinement reaches a level where intra-phase dislocation multiplication and motion become geometrically impeded, slip transmission across the heterointerfaces starts to gain momentum. Embury⁵⁶ and Bieler⁵⁷ suggested criteria that promote slip transfer across interfaces. First, the resolved shear stress of the dislocations at the interface should be highest on the activated system. Second, the misorientation between the active slip planes on either side of the interface should be at a minimum at the boundary. Third, the configuration at the interface should be one of minimum energy. Another criterion is the ability for co-deformation of the abutting phases. In this context, the yield stress difference and ductility of both phases are important. Moreover, size effects could play a role, such as in the Fe-C system, where coarse pearlite cannot be

easily drawn because cementite is brittle, while fine pearlite can be well co-deformed, such as in steel cord^{1,21–28} (Figures 1, 2, and 3).

In Cu-based alloys such as Cu-Ag or Cu-bcc (bcc: Nb, W, V, Mo, Cr, Fe), the criteria outlined previously are often fulfilled for the co-deformation of the two fcc phases Cu and Ag, as both materials form similar textures,^{7,9} promoting a higher degree of orientation coherency (i.e., the orientations of the highly stressed slip systems match). Further examples of through-interphase slip transfer exist for Cu-Zr, α - β brass, and Ni-W. The bcc materials such as Nb or V often form textures that reveal Kurdjumov–Sachs coincidence between the leading slip systems in the bcc material and the corresponding systems in the fcc Cu.^{7,9,17}

Dislocation slip across heterophase interfaces becomes active at high flow stresses and nanoscale fiber diameters because fibers with a micrometer-scale diameter can be deformed by regular dislocation multiplication and glide mechanisms. Slip transmission across the interface will create residual interface dislocations that may rearrange by glide or climb. Wang et al.^{49,50} published atomistic and elasticity predictions that suggest that inbound lattice dislocations may preferably enter the interface rather than penetrating through it.

These simulations and experimental hints imply three important points regarding the consequences of interphase slip transfer: First, dislocation slip across an interface does not only represent an elementary unit of shear that is carried into the neighboring phase, but it represents an elementary step in chemical mixing across a heterophase-interface. Second, the fact that misfit dislocation debris may remain inside the interface initiates a structural rearrangement of the interface structure. Third, such mechanisms can lead to substantial internal stresses.^{35,58} In Cu alloys with small Cr filaments, Embury and Sinclair showed that during the flux of dislocations across the interface between Cu and Cr, each slip transfer event leaves a residual misfit amount of shear and, hence, an unbalanced plastic transphase strain rate.^{47,56,57} This effect leads to the buildup of an unrelaxed elastic strain and an additional hardening rate that is proportional to the shear transmission, the volume fraction, and the elastic modulus of the Cr phase. At large plastic strains, the internal strains developed in the two phases^{34,58} result in an extended elastic-plastic transition and dimensional instability (**Figure 6**).^{59,60}

These three aspects show that large straining of polyphase metallic alloys with slip transfer among co-deforming phases profoundly changes the chemistry, the crystallography, and the internal atomistic structure of heterointerfaces, when the interlamellar spacing becomes so small that intraphase dislocation motion and multiplication is impeded.

Mechanical alloying at heterophase interfaces: The atomic scale

One observation that is common to all heavily co-deformed metallic multiphase alloys (composites, tribology, frictional joints) is the phenomenon of mechanical alloying.^{14,22,28,51–53}

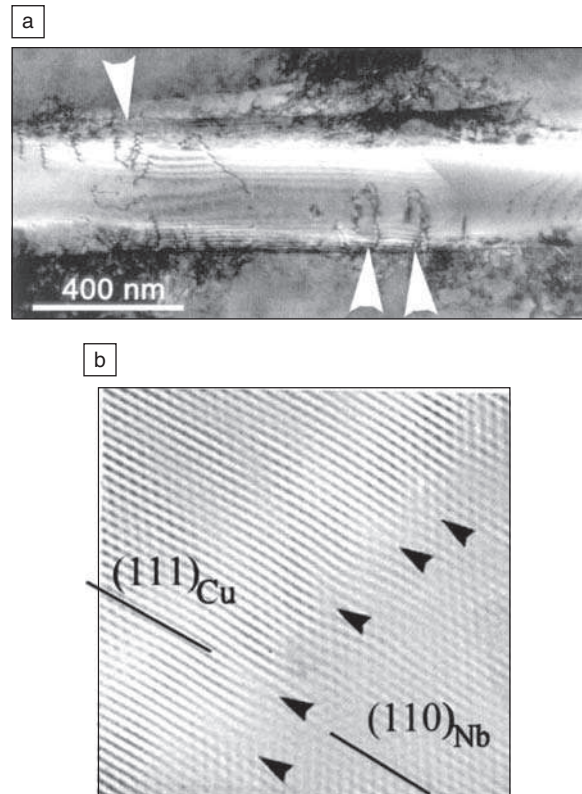


Figure 6. (a) Heavily wire-strained Cu-Cr composite. The transmission electron microscopy image reveals a flux of dislocations across the heterophase interface, where each event leaves a residual unbalanced plastic strain at the interfaces, which gives a buildup of unrelaxed elastic strain.⁶⁰ (b) Details of a Cu/Nb interface by high-resolution electron microscopy after deformation, showing an array of dislocations, indicated by arrows, at the interface. This dislocation structure reveals that the Cu-Nb interfaces in nanofilamentary composite wires can be semi-coherent.⁶⁰

This means that multiphase materials with limited mutual solid-state solubility undergo plasticity-stimulated chemical mixing to levels far beyond equilibrium solubility. In many cases, this phenomenon leads to the complete dissolution of the minority phase into the matrix phase (Figure 4).

Mechanical alloying was observed in pearlite^{24,25,27} and in various Cu-alloys after heavy straining (e.g., milling, drawing, rolling, torsion).^{14,22,28,51–53,61–64} These observations raise two important issues. The first one is why massive mixing across heterointerfaces occurs among materials that usually reveal much smaller equilibrium mutual solubility. The second one is whether strengthening in such alloys at higher strains is based on phase boundaries or only on zones of local high strength (e.g., through layers of strong directional bonding). The latter question is particularly relevant, as some systems, such as pearlite wire, reveal the highest tensile stresses at large wire deformations, where the cementite phase has been nearly dissolved (i.e., where the original phases and sharp interfaces no longer exist).^{22,28,61} Instead, the former interface regions are rendered into diffuse, chemically graded mechanically alloyed

zones, where strengthening more likely results from these solute effects rather than from sharp-interface mechanics (**Figure 7**).⁶⁴ For instance, for drawn pearlite, it is usually sufficient to impose true strains of 3, 4, or 5 to achieve a nanoscaled structure, cementite decomposition, and high strength. When drawing further, the strength increases, although the cementite has—to some extent—already dissolved, so that sharp interfaces can no longer play a dominant role for the strength.

In the following section, we discuss mechanically induced mixing in more detail. Various explanations were suggested to understand forced chemical mixing during co-deformation of phases consisting of non-soluble elements. The first one assumes a purely diffusion-driven mechanism.^{65,66} The second one assumes defect-enhanced diffusion (dislocations, vacancies).^{67,68} The third one is mainly built on interface roughening and plasticity-driven mechanical mixing (followed by subsequent short-range diffusion) via shear transfer (dislocations, shear bands) across heterophase interfaces.^{67–72} The latter mechanism is also referred to as dislocation shuffling.⁷¹

A purely diffusion-driven approach can be ruled out for explaining forced chemical mixing among multiphase alloys, with small mutual solubility owing to the absence of thermodynamic driving forces. Even under consideration of enhanced vacancy densities, capillary pressure (Gibbs–Thomson effect), and internal stresses, no negative mixing enthalpy among most of the Cu- and Fe-based systems studied so far is obtained. The absence of a sufficient driving force for spontaneous interdiffusion and phase dissolution is also evident from annealing experiments, which show that wire-drawn and mechanically alloyed metal-matrix composites undergo immediate de-mixing and coarsening rather than further diffusion-driven alloying.

The second group of approaches for explaining mechanical mixing is based on plasticity-assisted short-range diffusion.

This mechanism attributes accelerated diffusion in binary systems to a deformation-induced increase in the non-equilibrium vacancy density. These additional diffusion carriers lead to chemical mixing across the interface. Although this effect is possible, one argument stands against it for explaining spontaneous alloying. All phases in a mechanically mixed alloy are plastically strained, though not to the same extent (i.e., an increased vacancy concentration is present in all phases). However, the excess vacancy concentration and their mobility do not have to be the same in all phases, so this could give rise to asymmetric diffusion gradients.

Hence, we conclude that deformation-stimulated increased diffusion is possible within the phases and also across the heterophase interfaces, but the net flux in either direction depends on the asymmetry in the defect densities and mobilities. Also, although diffusion across the interfaces is likely, it still cannot explain the massive non-symmetric interphase mixing observed,⁷¹ because there are not sufficiently high thermodynamic driving forces.

A related mechanism of mechanical mixing is conceivable, though, in cases where the density of dislocations is so high that they attract larger quantities of solute atoms from the neighboring phase, owing to their high solubility. This effect is well known in the Fe-C system, where tertiary carbides dissolve as the C has a higher binding energy at the dislocation than within the carbide. Such an effect might also be responsible for the phenomenon that in heavily wire-drawn pearlite, strain aging after deformation leads to an increase in strength and loss in ductility. This mechanism is, however, not based on pipe diffusion or higher vacancy densities but on the higher solubility of dislocations for solutes.

In contrast to these mechanisms that are more driven by diffusion and enhanced defect solubility, it is also conceivable that

transphase dislocation-assisted carrier mechanisms assist mechanically induced chemical mixing. This phenomenon is described by the dislocation-shuffle mechanism.⁷¹ While elementary single-slip heterophase transmission effects, as described previously, can explain local structural changes of the interfaces and the buildup of internal stresses, corresponding multislip shear transfer (shear on more than one slip system) across heterointerfaces can lead to massive chemical mixing (**Figure 8**). Dislocation shuffling describes transphase plastic deformation on more than one slip system. Such shearing and interface roughening can create small embedded particles consisting of atoms from one phase in the other. Such tiny material portions can be further cut by dislocations running through them, thereby increasing their energy through the Gibbs–Thomson effect so that they finally dissolve.⁷¹

In a corresponding experiment with a thin multilayered starting microstructure consisting

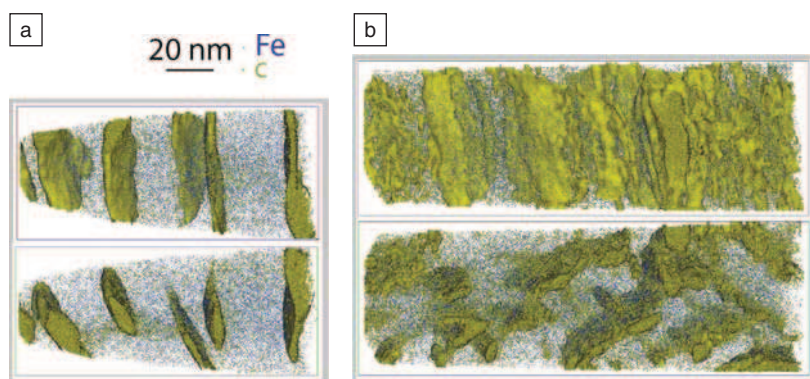
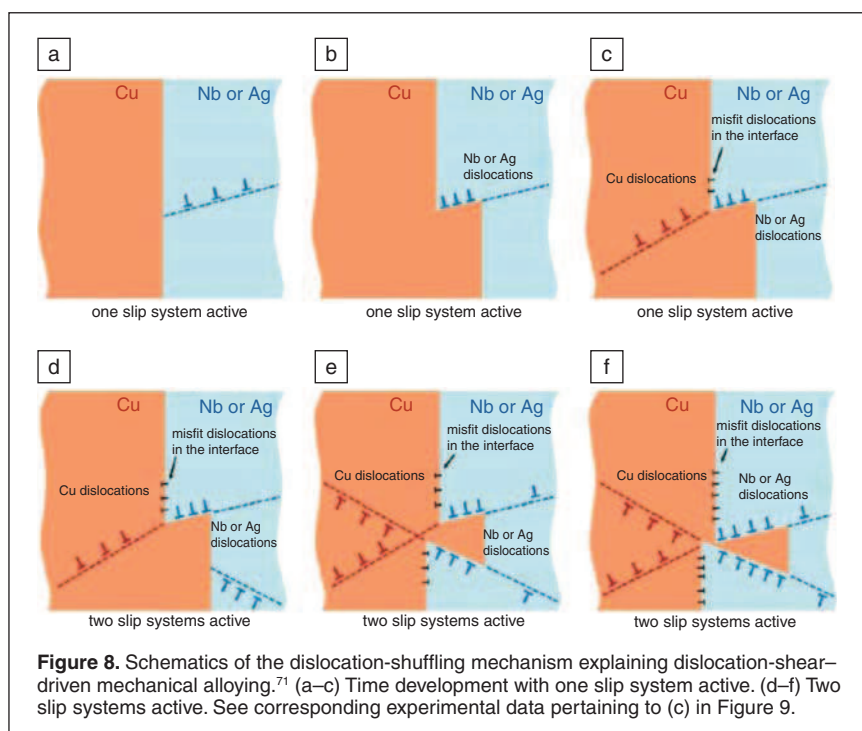


Figure 7. (a) Front view (top) and top view (bottom) of 3D atom probe tomography of cold drawn pearlitic steel wire (Fe-0.81C-0.2Si-0.49Mn wt% or Fe-3.66C-0.39Si-0.48Mn at.%) at a true wire strain $\epsilon = 2$. The reconstructed volume is $54 \times 52 \times 122 \text{ nm}^3$ containing 6.8 million atoms. Only 20% of the carbon atoms (large green dots) and 0.5% of the iron atoms (small blue dots) are displayed for clarity. An isoconcentration surface (green) drawn at 7 at.% C is shown to visualize the cementite lamellae. (b) As (a) for $\epsilon = 5.40$, the reconstructed volume is $60 \times 60 \times 180 \text{ nm}^3$ containing 20 millions atoms.⁶⁴ Although the interfaces between phases are no longer well defined, the strength of this material continues to increase with increasing strain.



of parallel Cu and V filaments, Sauvage⁷² observed such an elementary shear event across the Cu/V interface (**Figure 9a**) (note that Figure 9a shows an unpublished analysis from a data set measured for Reference 72.) Similar effects were observed in Cu-Nb nanocomposites⁷¹ and pearlite (**Figure 9b**).¹⁴

Deformation-driven amorphization

Extreme co-deformation of multiphase alloys or of bulk heterophases in frictional contact reveal, in some cases, deformation-driven amorphization phenomena. Two situations have been observed. First, some systems undergo amorphization without substantial non-equilibrium chemical mixing among the phases. In the field of multiphase co-deformation, this occurs for the Ni-Ti system, which undergoes amorphization if subjected to severe plastic deformation, but without substantial local composition change. This first group of systems obviously can be thermodynamically de-stabilized by a sufficiently high defect density without the contribution of compositional changes.

The second group comprises systems where solid-state amorphization is connected to the preceding formation of non-equilibrium solid solutions during deformation. This effect seems to occur particularly in composites with negative enthalpy of mixing. Typically, the pure bulk elements of the compounds addressed in this overview, such as Fe, Cu, Ag, and Nb, do not become amorphous when exposed to heavy straining as single phase bulk materials. This observation indicates that a relationship exists between mechanical alloying, the enthalpy of mixing of the newly formed compounds, and amorphization. This argument is also supported by the fact that the abutting phases in Fe and Cu compos-

ites frequently reveal very high dislocation densities, **Figure 5**. The relationship between mechanical mixing and amorphization seems to apply, in particular, to the Cu-matrix in Cu-Nb- or Cu-Zr-based composites and to the ferritic phase in pearlite. These matrix phases become amorphous only when mechanically alloyed. Deformation-induced amorphization of Cu during wire drawing was reported in Cu-Nb, Cu-Nb-Ag (**Figure 8b**), and Cu-Zr (**Figure 10**).^{9,15,71,74–77} In all cases, at least one pair of the constituent elements reveal a negative enthalpy of mixing. Similar observations were reported on pearlitic wire at relatively low true strains as low as 1, although these observations are, in part, under debate.

For instance, according to the Gibbs free energy versus concentration diagram, amorphous Cu-Nb could be stable at 25°C, relative to the bcc and fcc solid solutions that could be formed by forced mixing, for Cu concentrations between 35 at.% and 80 at.%.^{71,72} Most of the published Cu-Nb alloys where amorphization

occurred fall in this regime. Similar results were observed in Cu-Zr, **Figure 10**.⁷¹

Another way to explain amorphization in severely deformed multiphase alloys is to consider the increase in the free energy due to dislocations.^{66–71} If the stored deformation energy increases upon straining, it is conceivable that transformation into the amorphous regime is energetically favorable, **Figure 5**. This argument, however, is not fully convincing, because dislocations can be absorbed, in part, in the interfaces rather than being stored within the phases.^{50,51,71}

Owing to these considerations, we suggest that amorphization takes place in co-deformed metallic composites in a two-step mechanism that consists of first, a dislocation-shuffling or shear-band-related transphase plastic deformation and chemical mixing process,^{71,72} and second, a gradual amorphization in regions where both heavy mixing and high dislocation densities exist. The transition seems to be particularly likely in systems that fulfill at least some of the classical glass-forming rules. In systems that reveal amorphization without substantial chemical mixing, the effect is attributed to the large accumulated dislocation densities.

Microstructures and properties during frictional contact of heterointerfaces

Similar intense deformation conditions and metallurgical effects, as discussed for heavily co-deformed multiphase alloys, also occur at heterointerfaces between bodies that are brought in frictional contact such as encountered in tribology, friction stir welding, and explosive joining.^{78–80} In these cases, the extreme deformation is localized at the interface regions (i.e., these materials do not undergo bulk deformation). However, at the interfaces that are in frictional contact, similar

Why do co-deformed composites have high strength after phase dissolution?

Takahashi discussed the upper limits of possible strengthening mechanisms that may theoretically determine the strength of severely strained composites.^{22,24} The reasoning behind such estimates is the somewhat counter-intuitive observation that the strength of co-deformed compounds increases further with ongoing straining, even in cases where the original phases were dissolved via mechanical alloying. This means that the originally chemically sharp heterointerfaces are blurred and even gradually lost. Hence, in such cases, conventional strengthening based on a sharp and (mostly) incoherent interface cannot be responsible for the strength increase with further straining. Instead, real microstructures of severely deformed multiphase alloys are characterized by graded rather than sharp interfaces, and, in extreme cases, can even reveal entirely dissolved phases. In such cases, the matrix seems to be mainly hardened by high non-equilibrium fractions of solute atoms in the form of a mechanically driven solid solution and its effect on the Peierls potential and a high stored-dislocation content.

According to Takahashi, when considering eutectoid pearlite, the upper-bound strength that can be achieved by dislocation strengthening amounts to about 5 GPa. This value is given by the upper limit to the dislocation density that can be stored in the material. The upper limit of Hall-Petch and Orowan hardening through grain refinement is about 2 GPa. The upper strength limit given by a maximum amount of mechanically driven solid solution is about 0.5 GPa. This estimate seems to be a bit low, though, as it is based on the assumption of pure solid-solution hardening, and the high internal stresses created by an excess amount of interstitials is neglected in this balance. Finally, second-phase hardening gives an upper bound of 4 GPa. According to Takahashi, linear summation of these contributions would result in an upper bound of the strength of about 11.5 GPa. We do not suggest that this approach of describing the upper bound value for pearlite proof strength is exact, as the second phases gradually dissolve as just stated. Also, the contribution of

the solid-solution strengthening could be higher owing to the fact that the cementite becomes strongly dissolved, providing a higher C content. Finally, the materials build up large internal stresses during severe deformation, which provides an additional source of strengthening. Irrespective of these points,

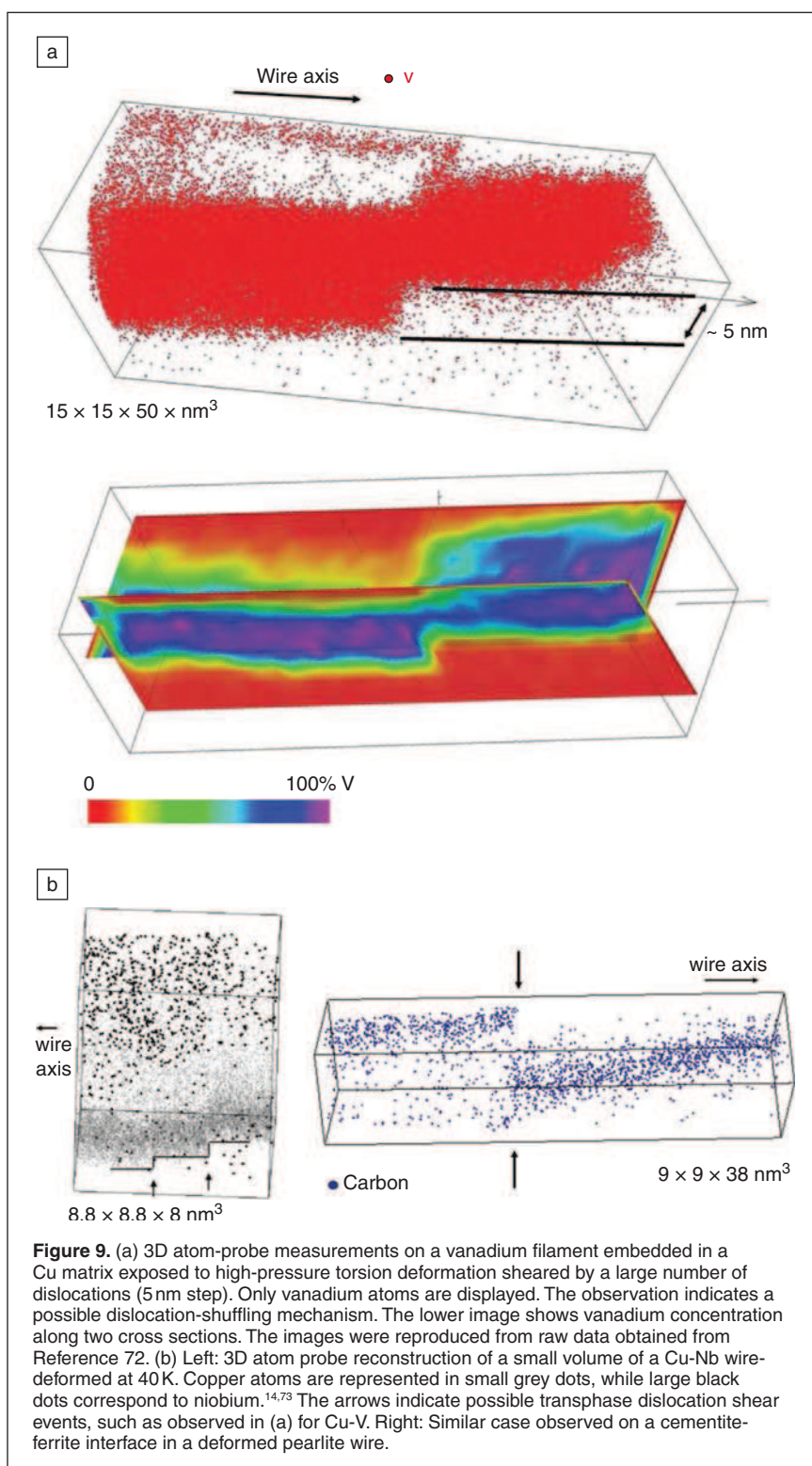
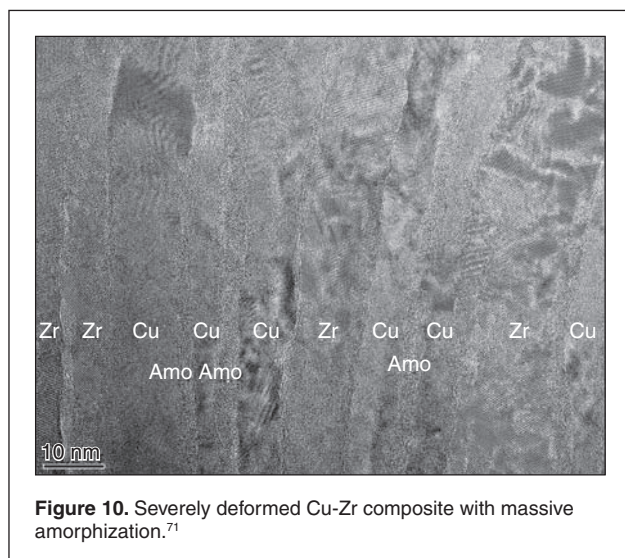


Figure 9. (a) 3D atom-probe measurements on a vanadium filament embedded in a Cu matrix exposed to high-pressure torsion deformation sheared by a large number of dislocations (5 nm step). Only vanadium atoms are displayed. The observation indicates a possible dislocation-shuffling mechanism. The lower image shows vanadium concentration along two cross sections. The images were reproduced from raw data obtained from Reference 72. (b) Left: 3D atom probe reconstruction of a small volume of a Cu-Nb wire-deformed at 40 K. Copper atoms are represented in small grey dots, while large black dots correspond to niobium.^{14,73} The arrows indicate possible transphase dislocation shear events, such as observed in (a) for Cu-V. Right: Similar case observed on a cementite-ferrite interface in a deformed pearlite wire.

phenomena occur as in co-deformed composites, namely deformation-driven chemical mixing, amorphization, and very high accumulated dislocation densities. Hence, the interface regions of bulk co-deformed systems and tribological systems reveal phenomena of high similarity.



the simple estimate reveals that several mechanisms other than the Hall-Petch effect can contribute to substantial strength in severely co-deformed composites.

Summary

Multiphase alloys can be rendered into ultrahigh strength bulk compounds by severe plastic co-deformation, which transforms the phases into nanoscaled filaments. At moderate and intermediate deformation, the microstructure is characterized by a high interface density. Strengthening in this regime is mainly due to Orowan and Hall-Petch effects. At high deformation, strengthening is determined by interface dislocation reactions, heterophase dislocation penetration, and high dislocation density. In this strain regime, intense deformation-driven chemical mixing (mechanical alloying) and atomic-scale structural transitions (e.g., amorphization) occur. For deformation-driven mixed systems with glass-forming characteristics (negative enthalpy of mixing), mechanical alloying and amorphization are considered to be associated phenomena. In mechanically mixed systems without the typical glass-forming tendency, structural transitions are attributed to the reduction of the high stored dislocation densities by amorphization. Among the various mechanisms that can lead to massive mechanical alloying, we suggest a dominant role for transphase dislocation shuffling or shear-band mechanisms, in which lattice dislocations penetrate the interfaces between abutting phases acting as carriers of deformation-driven chemical mixing. Heavily co-deformed multiphase materials offer an enormous potential for advanced alloy design. These materials today represent the largest class of ultrahigh strength nanostructured bulk materials.

References

1. J.D. Embury, R.M. Fisher, *Acta Metall.* **14**, 47 (1966).
2. F.P. Levi, *J. Appl. Phys.* **31**, 1469 (1960).
3. G. Frommeyer, G. Wassermann, *Acta Metall.* **23**, 1353 (1975).
4. J. Bevk, J.P. Harbison, I.L. Bell, *J. Appl. Phys.* **49**, 6031 (1978).
5. P.D. Funkenbusch, T.H. Courtney, *Acta Metall.* **33**, 913 (1985).
6. W.A. Spitzig, A.R. Pelton, F.C. Laabs, *Acta Metall.* **35**, 2427 (1987).

7. A.M. Russell, L.S. Chumbley, Y. Tian, *Adv. Eng. Mater.* **2**, 11 (2000).
8. M.H. Hong, W.T. Reynolds, Jr., T. Tarui, K. Hono, *Metall. Mater. Trans. A* **30**, 717 (1999).
9. D. Raabe, F. Heringhaus, U. Hangen, G. Gottstein, *Z. Metallkd.* **86**, 405 (1995).
10. D. Raabe, K. Miyake, H. Takahara, *Mater. Sci. Eng. A* **291**, 186 (2000).
11. F. Dupouy, S. Askénazy, J.P. Peyrade, D. Legat, *Phys. B* **211**, 43 (1995).
12. J.T. Wood, J.D. Embury, M. Ashby, *Acta Mater.* **45**, 1099 (1997).
13. J.D. Embury, K. Han, *Curr. Opin. Solid State Mater. Sci.* **3**, 304 (1998).
14. X. Sauvage, L. Thilly, F. Lecouturier, A. Guillet, D. Blavette, *Nanostruct. Mater.* **11**, 1031 (1999).
15. X. Sauvage, L. Renaud, B. Deconihout, D. Blavette, D.H. Ping, K. Hono, *Acta Mater.* **49**, 389 (2001).
16. L. Thilly, F. Lecouturier, J. von Stebut, *Acta Mater.* **50**, 5049 (2002).
17. F. Heringhaus, D. Raabe, G. Gottstein, *Acta Metall.* **43**, 1467 (1995).
18. Y. Sakai, K. Inoue, H. Maeda, *Acta Metall.* **43**, 1517 (1995).
19. Y. Sakai, H.J. Schneider-Muntau, *Acta Metall.* **45**, 1017 (1997).
20. F. Heringhaus, H.J. Schneider-Muntau, G. Gottstein, *Mater. Sci. Eng.* **347**, 9 (2003).
21. G. Langford, *Metall. Trans.* **8A**, 861 (1977).
22. T. Tarui, N. Maruyama, J. Takahashi, S. Nishida, H. Tashiro, *Nippon Steel Techn. Rep.* **91**, 56 (2005).
23. S. Goto, R. Kirchheim, T. Al-Kassab, C. Borchers, *Trans. Nonferrous Met. Soc. China* **17**, 1129 (2007).
24. J. Takahashi, T. Tarui, K. Kawakami, *Ultramicroscopy* **109**, 193 (2009).
25. A. Taniyama, T. Takayama, M. Arai, T. Hamada, *Scripta Mater.* **51**, 53 (2004).
26. K. Oh-ishi, H.W. Zhang, T. Ohkubo, K. Hono, *Mater. Sci. Eng. A* **456**, 20 (2006).
27. D.R. Lesuer, C.K. Syn, O.D. Sherby, D.K. Kim, in *Metallurgy, Processing and Applications of Metal Wires*, H.G. Paris, D.K. Kim, Eds. (TMS, Warrendale, PA, 1996).
28. K. Hono, M. Ohnuma, M. Murayama, S. Nishida, A. Yoshie, T. Takahashi, *Scripta Mater.* **44**, 977 (2001).
29. S. Ohsaki, K. Yamazaki, K. Hono, *Scripta Mater.* **48**, 1569 (2003).
30. S. Ohsaki, K. Hono, H. Hidaka, S. Takaki, *Scripta Mater.* **52**, 271 (2005).
31. H.W. Zhang, S. Ohsaki, S. Mitao, M. Ohnuma, K. Hono, *Mater. Sci. Eng. A* **421**, 191 (2006).
32. S. Ohsaki, S. Kato, N. Tsuji, T. Ohkubo, K. Hono, *Acta Mater.* **55**, 2885 (2007).
33. H.R. Gong, B.X. Liu, *J. Appl. Phys.* **96**, 3020 (2004).
34. J.D. Embury, M.A. Hill, W.A. Spitzig, Y. Sakai, *MRS Bull.* **8**, 57 (1993).
35. M. Elices, *J. Mater. Sci.* **39**, 3889 (2004).
36. K. Spencer, F. Lecouturier, L. Thilly, J.D. Embury, *Adv. Eng. Mater.* **6**, 290 (2004).
37. E. Botcharova, J. Freudenberger, A. Gaganov, K. Khlopov, L. Schultz, *Mater. Sci. Eng. A* **416**, 261 (2006).
38. G. Langford, *Metall. Trans.* **1**, 465 (1970).
39. C. Trybus, W.A. Spitzig, *Acta Metall.* **37**, 1971 (1989).
40. J.G. Sevillano, *J. Phys. III* **6**, 967 (1990).
41. U. Hangen, D. Raabe, *Acta Metall.* **43**, 4075 (1995).
42. D. Raabe, D. Mattissen, *Acta Mater.* **46**, 5973 (1998).
43. D. Raabe, D. Mattissen, *Acta Mater.* **47**, 769 (1999).
44. D. Raabe, U. Hangen, *Acta Metall.* **44**, 953 (1996).
45. A. Misra, J.P. Hirth, R.G. Hoagland, *Acta Mater.* **53**, 4817 (2005).
46. J.D. Embury, J.P. Hirth, *Acta Metall.* **42**, 2051 (1994).
47. J.D. Embury, C.W. Sinclair, *Mater. Sci. Eng. A* **319**, 37 (2001).
48. J.D. Embury, *Scripta Metall. Mater.* **27**, 981 (1992).
49. J. Wang, R.G. Hoagland, J.P. Hirth, A. Misra, *Acta Mater.* **56**, 5685 (2008).
50. J. Wang, R.G. Hoagland, J.P. Hirth, A. Misra, *Acta Mater.* **56**, 3109 (2008).
51. C. Wille, T. Al-Kassab, P.P. Choi, Y.S. Kwon, *Ultramicroscopy* **109**, 599 (2009).
52. C. Wille, T. Al-Kassab, M. Schmidt, P.P. Choi, Y.S. Kwon, *Int. J. Mater. Res.* **99**, 541 (2008).
53. P.P. Choi, T. Al-Kassab, Y.S. Kwon, J.S. Kim, R. Kirchheim, *Microsc. Microanal.* **13**, 347 (2007).
54. L. Thilly, O. Ludwig, M. Véron, F. Lecouturier, J.P. Peyrade, S. Askénazy, *Philos. Mag. A* **82**, 925 (2002).
55. M. Janecek, F. Louchet, B. Doisneau-Cottignies, Y. Bréchet, N. Guelton, *Philos. Mag. A* **80**, 1605 (2000).
56. C.W. Sinclair, J.D. Embury, G.C. Weatherly, *Mater. Sci. Eng. A* **272**, 90 (1999).
57. T.R. Bieler, P. Eisenlohr, F. Roters, D. Kumar, D.E. Mason, M.A. Crimp, D. Raabe, *Int. J. Plast.* **25**, 1655 (2009).
58. J.M. Atienza, J. Ruiz-Hervias, M.L. Martinez-Perez, F.J. Mompean, M. Garcia-Hernandez, M. Elices, *Scripta Mater.* **52**, 1223 (2005).
59. L. Thilly, S. Van Petegem, P.O. Renault, F. Lecouturier, V. Vidal, B. Schmitt, H. Van Swyghoven, *Acta Mater.* **57**, 3157 (2009).

60. F. Dupouy, E. Snoeck, M.J. Casanove, C. Roucau, J.P. Peyrade, S. Askénazy, *Scripta Mater.* **34**, 1067 (1996).
61. C. Borchers, T. Al-Kassab, S. Goto, R. Kirchheim, *Mater. Sci. Eng. A* **502**, 131 (2009).
62. X. Sauvage, F. Wetscher, P. Pareige, *Acta Mater.* **53**, 2127 (2005).
63. J.Y. Huang, Y.D. Yu, Y.K. Wu, D.X. Li, H.Q. Ye, *Acta Mater.* **45**, 113 (1997).
64. Y.J. Li, P. Choi, C. Borchers, Y.Z. Chen, S. Goto, D. Raabe, R. Kirchheim, *Acta Mater.* (2010), in press.
65. J. Eckert, J.C. Holzer, C.E. Krill III, W.L. Johnson, *J. Appl. Phys.* **73**, 2794 (1993).
66. J. Eckert, J.C. Holzer, C.E. Krill III, W.L. Johnson, *J. Mater. Res.* **1992**, 7 (1980).
67. E. Ma, H.W. Sheng, J.H. He, P.J. Schilling, *Mater. Sci. Eng. A* **286**, 48 (2000).
68. R.B. Schwarz, *Mater. Sci. Forum* **269–272**, 665 (1998).
69. H. Gleiter, *Acta Metall.* **16**, 455 (1968).
70. K. Differt, U. Essmann, H. Mughrabi, *Phys. Status Solidi A* **104**, 95 (1987).
71. D. Raabe, S. Ohsaki, K. Hono, *Acta Mater.* **57**, 5254 (2009).
72. X. Sauvage, C. Genevois, G. Da Costa, V. Pantisyrny, *Scripta Mater.* **61**, 660 (2009).
73. X. Sauvage, A. Guillet, D. Blavette, L. Thilly, F. Lecouturier, *Scripta Mater.* **46**, 459 (2002).
74. D. Raabe, U. Hangen, *Mater. Lett.* **22**, 155 (1995).
75. D. Raabe, U. Hangen, *J. Mater. Res.* **10**, 3050 (1995).
76. T.L. Wang, J.H. Li, K.P. Tai, B.X. Liu, *Scripta Mater.* **57**, 157 (2007).
77. J. Koike, D.M. Parkin, M. Nastasi, *Philos. Mag. Lett.* **62**, 257 (1990).
78. D.A. Rigney, X.Y. Fu, J.E. Hammerberg, B.L. Holian, M.L. Falk, *Scripta Mater.* **49**, 977 (2003).
79. M. Moseler, P. Gumbsch, C. Casiraghi, A. Ferrari, J. Robertson, *Science* **309**, 1545 (2005).
80. H.-J. Kim, A. Emge, R. Winter, P. Keightley, W.-K. Kim, M.L. Falk, D.A. Rigney, *Acta Mater.* **57**, 5270 (2009). □

Handbook of Modern Ion Beam Materials Analysis

Second Edition

EDITORS

Yongqiang Wang
and Michael Nastasi

NOW AVAILABLE

The most comprehensive database on ion beam analysis ever published—revised and updated from the popular handbook released in 1995!



MRS ORDER AT WWW.MRS.ORG/IBH2

4K CRYO COOLERS

Save Power and Money



For over 25 years ULVAC has been producing cryo-coolers for ULVAC cryopumps. Now 4K cryocoolers are available in North America to save you power and money.

Two models to choose from:

0.3W @ 4K or 1.0W @ 4K

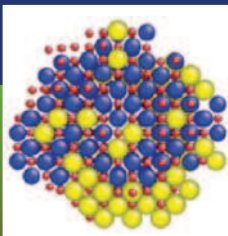
4K models feature:

- 0.3W @ 4K with only 1.7 kW input power
- Low vibration levels
- Excellent thermal stability at 4K
- High reliability – 1000s installed
- Attractive pricing

Contact your new source for 4K cryocoolers, call 800-99ULVAC or email sales@us.ulvac.com

ULVAC

ULVAC Technologies, Inc.
Methuen, MA – Tel.: 978-686-7550
www.ulvac.com



Atomic-scale design of radiation-tolerant nanocomposites

M.J. Demkowicz, P. Bellon, and B.D. Wirth

Recent work indicates that materials with nanoscale architectures, such as nanolayered Cu-Nb composites and nanoscale oxide dispersion-strengthened steels, are both thermally stable and offer improved performance under irradiation. Current understanding of the atomic-level response of such materials to radiation yields insights into how controlling composition, morphology, and interface-defect interactions may further enable atomic-scale design of radiation-tolerant nanostructured composite materials. With greater understanding of irradiation-assisted degradation mechanisms, this bottom-up design approach may pave the way for creating the extreme environment—tolerant structural materials needed to meet the world's clean energy demand by expanding use of advanced fission and future fusion power.

Introduction

Structural materials used in nuclear reactors must withstand some of the harshest conditions met in existing technology. All of the factors limiting their lifetime and performance at high temperatures and in corrosive media, such as creep and stress corrosion cracking, are exacerbated by irradiation.^{1,2} These materials are also subject to degradation by mechanisms distinctive to radiation environments, such as volumetric swelling and anisotropic growth.^{3,4}

Decades of traditional alloy development have yielded incremental enhancements in materials performance under irradiation.⁵ Advanced fission and future fusion reactor designs, however, call for far more dramatic progress, such as materials able to sustain radiation doses up to 10 times higher than in current reactors while withstanding liquid metal corrosion⁶ or being implanted with up to several atomic percent of helium.⁷

The last several decades have also witnessed major advances in our understanding of the atomic-scale origins of material behavior under irradiation^{8,9} thanks to improvements in experimental techniques such as high-resolution transmission electron microscopy and atom probe tomography (APT), as well as computer modeling techniques such as classical potential molecular dynamics (MD) and density functional theory. This knowledge provides a foundation for the emergence of first-principles, atomic-scale design of materials for radiation resistance.

In contrast to purely hit-and-miss materials development, atomic-scale design aims to achieve superior radiation response by purposefully manipulating composition and microstructure to control the behavior of radiation-induced defects. It relies on modeling to determine the impact of these modifications on engineering-level material behavior. Atomic-scale design is being used today to accelerate the improvement of existing materials. In the longer term, however, it seeks to realize unconventional materials that could not have arisen through a series of gradual modifications.

Although only fledgling in the area of structural materials, atomic-scale design has already shown success in other energy-related fields, such as the search for novel battery electrode materials.¹⁰ (See the article by Gerbrand Ceder in the September 2010 issue of the *MRS Bulletin*.) This article illustrates how atomic-scale design for radiation resistance is being pursued in the tailoring of radiation-resistant interfaces, design of stable microstructures, and development of nanostructured ferritic alloys (NFAs). Challenges facing this approach to materials engineering are also discussed.

Atomic-level origin of radiation damage

The topic of radiation effects in structural materials encompasses a vast literature dating from 1942¹¹ and cannot be fully reviewed in this article. It is well understood, however, that the root causes of radiation damage are individual and clustered

M.J. Demkowicz, Massachusetts Institute of Technology, Cambridge, MA 02139, USA; demkowicz@mit.edu
P. Bellon, University of Illinois at Urbana-Champaign, Urbana, IL 61801, USA; bellon@illinois.edu
B.D. Wirth, University of Tennessee, Knoxville, TN 37996, USA; bdwirth@utk.edu

vacancies and self-interstitials produced during cascades of collisions between energetic particles and target atoms.¹² The subsequent diffusion and clustering of these defects, along with the associated transport of impurities, lead to accelerated creep,¹ volumetric swelling,³ segregation of alloying elements,¹³ and embrittlement.¹⁴ Furthermore, the forced atomic mixing taking place in the collision cascades themselves can lead to disordering of chemically ordered phases and to dissolution of precipitates.¹⁵ These processes can severely limit material and component lifetimes in radiation environments.

In addition to clustering and diffusing, radiation-induced vacancies and interstitials also may recombine if they come close enough to each other. Since both defects are annihilated in the process, recombination may be thought of as a “self-healing” mechanism. Thus, enhancing vacancy-interstitial recombination is one of the strategies for improving the radiation resistance of crystalline materials discussed in the examples that follow.

Tailored interfaces

Interfaces are efficient sinks and recombination sites for radiation-induced point defects,¹⁶ so it may be possible to improve the radiation resistance of many materials by increasing their interface area per unit volume, for instance, by refining their grain size using severe plastic deformation. (See the Zhu et al. and Raabe et al. articles in this issue.) Interfaces with differing atomic structures, however, may exhibit disparate sink strengths,^{17,18} diffusivities,¹⁹ mechanical properties,²⁰ and susceptibilities to embrittlement.²¹ Moreover, interfaces also increase the free energy of a material and, in some cases, may be its weakest microstructural link, limiting its overall lifetime.²² For enhanced performance under irradiation, it is therefore not sufficient for a material to contain a large number of interfaces; they must also be of the right kind.

Interface structure and properties are functions of crystallographic misorientation, habit-plane direction, properties of the adjacent materials such as crystal structure, cohesive energy, elastic constants, and many other factors. Atomic-scale design of interfaces is the judicious selection of these parameters to obtain interfaces with desired properties. Since the design space afforded by these parameters is infinite, a hit-and-miss approach can never exhaust it. Design of interfaces for radiation resistance therefore requires an understanding of the connection between their structure and the mechanisms of their interaction with point defects. Recent work on fcc-bcc heterophase interfaces in Cu-Nb multilayer composites affords an example of how modeling and experiments can describe this connection and how it may be applied for atomic-scale design.

Cu-Nb multilayer composites can be synthesized as thin films by magnetron sputtering

with individual layer thicknesses from hundreds of nanometers to as thin as 1 nm. Thanks, in part, to the limited solubility of Cu and Nb (see following section), these composites are thermally stable up to 800°C.²³ Their response to radiation has been studied between room temperature and 1200°C using He-ion bombardment at energies between 33 keV and 150 keV and fluences up to 1.5×10^{17} ions/cm².²⁴ Some of these experiments produced in excess of 10 displacements per atom (dpa). (At 1 dpa, every atom in the material has been displaced once, on average, by a collision with a high-energy particle.²⁵)

The Cu-Nb multilayers remain morphologically stable under these conditions, with no mixing or amorphization detected.^{26,27} Their radiation-induced defect concentrations are far below those of pure fcc Cu and bcc Nb subjected to similar dpa levels, as shown in **Figure 1**, and decrease with decreasing thickness of the individual layers, that is with increasing interface area per unit volume. Thus, radiation resistance of these materials can be unambiguously attributed to interfaces. Thanks to the distinctive microstructure of magnetron-sputtered Cu-Nb multilayers, all the heterophase interfaces found in them are nearly identical,²⁸ a fact that makes them an ideal model system for investigating interface–point defect interactions. An atomic model of a Cu-Nb bilayer containing one interface constructed according to the experimentally observed crystallography is shown in **Figure 2a**.

MD modeling using a specially constructed Cu-Nb-embedded-atom-method potential has shown that the number of point defects created in collision cascades near Cu-Nb interfaces is about 50–70% smaller than in pure Cu or Nb,²⁹ confirming that these interfaces are excellent point-defect sinks. The remaining defects may subsequently diffuse to interfaces and become trapped as well. Under steady-state irradiation in the absence of other defect sinks, equal numbers of vacancies and interstitials arrive at the interfaces and undergo accelerated recombination, effectively healing radiation damage.

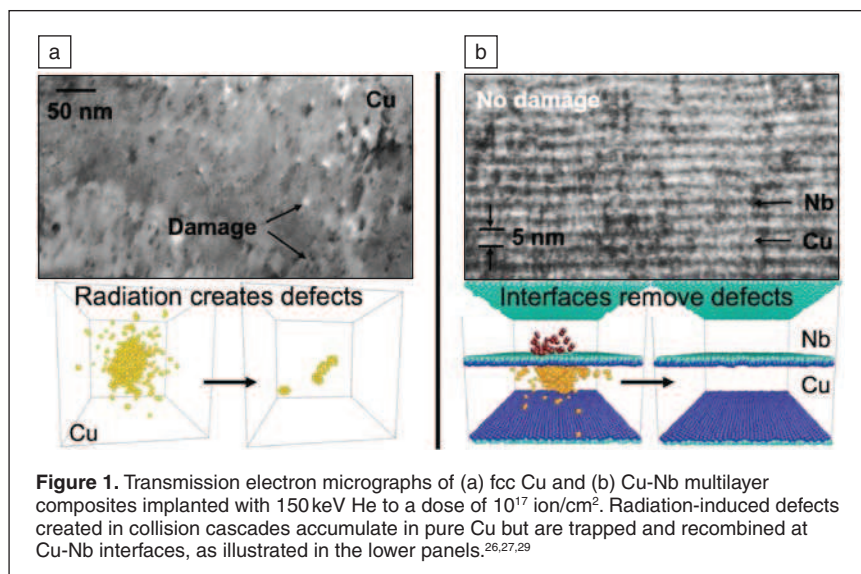


Figure 1. Transmission electron micrographs of (a) fcc Cu and (b) Cu-Nb multilayer composites implanted with 150 keV He to a dose of 10^{17} ion/cm². Radiation-induced defects created in collision cascades accumulate in pure Cu but are trapped and recombined at Cu-Nb interfaces, as illustrated in the lower panels.^{26,27,29}

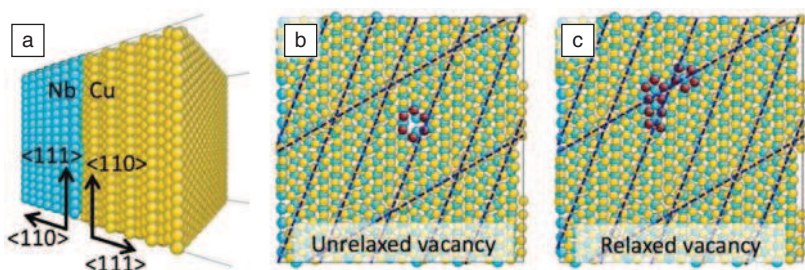


Figure 2. (a) Simulated Cu-Nb bilayer with the same crystallography as observed experimentally in multilayer composites.²⁸ (b) An unrelaxed vacancy (red atoms) in the Cu interface plane (c) migrates to the nearest intersection between misfit dislocations (dashed lines) and causes a local interface reconstruction (red atoms).^{30,31}

Investigation of the atomic structure of Cu-Nb interfaces reveals the reason for their high efficiency in trapping point defects. Figure 2b shows a plane view of the interfacial Cu and Nb. While this interface has no strict periodicity, it nevertheless contains a quasi-periodic pattern of low coordination sites where a Cu atom and a Nb atom are situated nearly one on top of the other. This quasi-periodicity arises from the presence of two sets of parallel interface misfit dislocations.^{30,31} The low coordination sites occur at the intersections between misfit dislocations.

Figure 2b shows a vacancy created in the interfacial Cu plane by removing an atom. Before relaxation, this defect is compact, like vacancies found in perfect crystals. Annealing for 10 ps at 300 K, followed by conjugate gradient energy minimization, however, leads to the interface reconstruction shown in Figure 2c. In it, the vacancy migrates to the nearest misfit dislocation intersection and delocalizes over an area of about 2 nm². Its formation energy drops by about 1.6 eV in the process. Introduction of interstitials into a Cu-Nb interface leads to the same kind of interface reconstruction.^{30,31} If both a vacancy and an interstitial are formed in the vicinity of the same misfit dislocation intersection, they undergo spontaneous recombination as they relax.

Misfit-dislocation intersections are therefore both trapping sites and recombination centers for radiation-induced defects absorbed at Cu-Nb interfaces. This insight suggests that interfaces could be tailored for radiation resistance, for example by maximizing the number of misfit-dislocation intersections in them. The areal density of these intersections can be obtained through analytical investigation of the Frank-Bilby equation^{31,32}

$$\bar{\mathbf{b}} = (\mathbf{I} - \mathbf{F}^{-1}) \hat{\mathbf{p}}, \quad (1)$$

which specifies the average Burgers vector content per unit length $\bar{\mathbf{b}}$ along a unit vector $\hat{\mathbf{p}}$ in the plane of an interface. Here, \mathbf{F} is the deformation gradient that characterizes the misorientation and misfit between the two crystals that meet at the interface, and \mathbf{I} is the identity tensor. The number of trapping sites in an interface is therefore primarily a function of interface

crystallography, which may be controlled by appropriate synthesis techniques.

Considerations besides interface geometry, such as misfit dislocation core width or the elastic properties of the materials that meet at the interface, are likely to enter into this atomic-scale design strategy as studies on more interfaces are conducted. Under some conditions, for example, overlap between dislocation cores may render the misfit-dislocation model inapplicable. This design approach also may be extended to tailoring interface properties other than point defect sink strength, such as diffusivity⁶² or resistance to degradation by implanted helium.⁶³

Stable microstructures

Nanostructured materials may coarsen, either during thermal annealing or when subjected to external forcing such as irradiation or severe plastic deformation. Coarsening during thermal annealing is not surprising since these materials may contain a significant amount of excess free energy, owing to the large volume fraction of interfaces. In the presence of irradiation or other external forcing, however, the microstructural evolution is no longer driven solely by the reduction of excess free energy, and coarsening may be enhanced or suppressed. Under appropriate irradiation conditions, nanostructured states, in fact, can become stable steady states, thus providing for intrinsic resistance against coarsening.

Several strategies can be envisioned to suppress coarsening of nanostructures under thermal annealing by lowering the coarsening driving force and the relevant mobility. The driving force is directly controlled by the interfacial free energy, while the coarsening kinetics is largely controlled either by the mobility of the interfaces or by the long-range transport of alloying elements. A first approach is therefore to use alloying elements that segregate at interface boundaries so as to reduce the interfacial energy. For instance, in the case of nanograin materials, this can be achieved by adding Fe to Y (References 33 and 34), P to Ni (Reference 33), or W to Ni (Reference 34). The resulting nanograin materials are thermodynamically metastable. Recently, the possibility of obtaining thermodynamically stable systems with vanishing grain boundary energy also has been discussed.^{33,35,37}

Secondly, for two-phase materials, metastable nanostructures can be obtained by restricting interfaces to be planar, with zero average curvature. Such planar interfaces can, for instance, be synthesized by physical vapor deposition, as discussed previously for Cu-Nb nanolayers, or by accumulative roll bonding.⁶⁴ Unlike some naturally occurring layered microconstituents such as pearlite, these structures are free from necks connecting coarsening identical layers, thus improving their resistance to coarsening.

Thirdly, dispersion of long-lived nanoscale precipitates can be achieved, as in the nanostructured ferritic steels discussed in

the following section. The very low solubility of the precipitating elements (e.g., Y, Ti, and O) combined with their low diffusivity in the Fe matrix lead to nanostructures that, even though not thermodynamically stable or metastable, are apparently remarkably long-lived even at high temperatures.

Under irradiation, the resistance to coarsening of the previously mentioned nanostructures may be reduced, owing to point defect supersaturation, sustained point defect and chemical fluxes to interfaces, and to the forced mixing produced by energetic displacement cascades. An alternative route to the synthesis of radiation-resistant nanostructures takes advantage of irradiation-induced self-organization reactions at the nanoscale. Examples of these self-organization reactions triggered by irradiation are (1) the stabilization of ordered gamma prime precipitates a few nanometers in diameter in a gamma matrix in Ni-Al alloys;³⁵ (2) the formation of void and bubble lattices in many metals and alloys (see Reference 36 for a review); and (3) the patterning of nanoscale phases in immiscible alloy systems,^{37–41} for instance in Cu-Ag, Cu-Fe, Cu-Co, Cu-Nb, Cu-Mo, and Cu-W.

Self-organization reactions are of particular interest, as they result in a high density of semi-coherent or incoherent interfaces, which may serve as point defect sinks, as discussed in the previous section. In the case of moderately immiscible elements such as Cu-Ag, Cu-Co, and Cu-Fe, the self-organization is rationalized by a dynamic competition between medium-scale chemical mixing forced by displacement cascades and coarsening driven by thermally activated transport.³⁷ Accordingly, the temperature range over which nanoscale patterning takes place can be shifted to a higher temperatures by using slow diffusers. This has been confirmed experimentally in Cu-based binary alloys, see **Figure 3**. The maximum temperature for patterning, however, remains limited for these alloy systems.

Much higher maximum temperatures for patterning are experimentally obtained by using highly immiscible alloy systems, such as Cu-Nb, Cu-Mo, and Cu-W, see **Figure 4**. Precipitate sizes around 3 to 6 nm and Cu grain sizes around 20 to 30 nm are measured during irradiations up to 75 dpa at temperatures up to 600°C for Cu-Nb and 800°C for Cu-W (i.e., 85% of the melting temperature of the Cu matrix). A different rationalization needs to be invoked in these systems, because recoil mixing is highly reduced or negligible since little or no mixing takes place during thermal spikes, owing to the immiscibility of these elements in the liquid state.⁴² Vo et al.⁴⁰ have recently proposed that the observed nanostructuring results from the coagulation of small solute clusters during thermal spikes. At intermediate temperatures, thermal coarsening is suppressed due to the low solubility and low diffusivity of the Nb, Mo, and W solute atoms in Cu. As a result, the maximum precipitate size should be dictated by the cascade size, a prediction that is in good agreement with MD simulation results. Work is in progress to assess the resistance of these nanostructures to creep under irradiation and to swelling in the presence of He atoms.

The identification of the controlling parameters responsible for spontaneous nanoscale patterning of precipitates under irradiation makes it possible to guide the design of

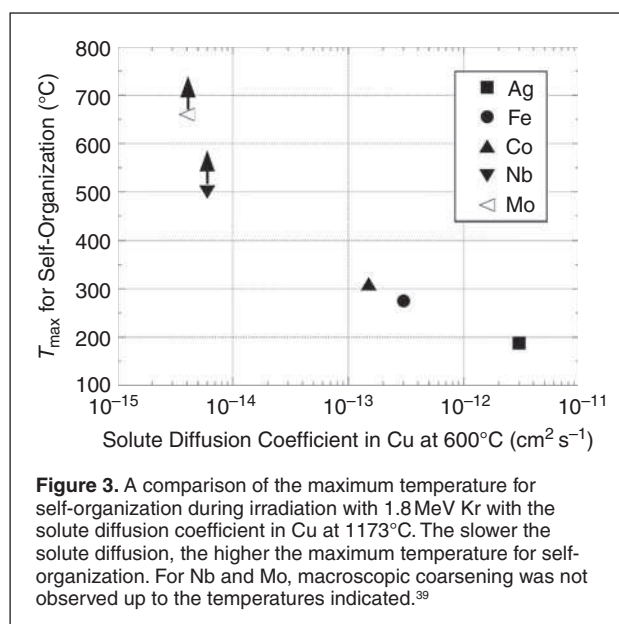


Figure 3. A comparison of the maximum temperature for self-organization during irradiation with 1.8 MeV Kr with the solute diffusion coefficient in Cu at 1173°C. The slower the solute diffusion, the higher the maximum temperature for self-organization. For Nb and Mo, macroscopic coarsening was not observed up to the temperatures indicated.³⁹

radiation-resistant materials. The previously mentioned studies revealed, in particular, the role of solute solubility, solute diffusion, heat of mixing, and mixing and decomposition in displacement cascades on the stabilization of radiation-resistant self-organized nanostructures. There is clearly great interest in extending these studies to the resistance of these nanostructures to swelling and creep.

Nanostructured ferritic alloys

Nanostructured ferritic alloys (NFAs) hold tremendous promise for future fuel cladding and structural materials applications in advanced nuclear fission and fusion reactor concepts. A more comprehensive bibliography on NFAs may be found in the recently published review by Odette et al.⁴³ NFAs are Fe-Cr-based ferritic, or in some cases, ferritic-martensitic,⁴⁴ alloys with an ultrahigh density of nanometer-sized Y-Ti-O-rich precipitate clusters. NFAs are distinguished from more traditional oxide dispersion steels by a higher number density and smaller size of precipitates, which produce much greater interfacial area available for trapping and recombining point defects.^{43,45–48} These alloys have indeed demonstrated outstanding high-temperature properties and remarkable tolerance to irradiation-induced displacement damage.^{43,47–49} Furthermore, NFAs hold tremendous promise for managing high levels of insoluble gases, such as are implanted in fusion energy or spallation neutron irradiation environments.⁴⁷

While NFAs are in the early stages of development, it is increasingly clear that the nanometer Y-Ti-O precipitate clusters are responsible for the outstanding thermal and mechanical properties and good behavior in irradiation environments. As with the earlier examples of planar interfaces and stable, self-organizing nanostructures, the principles of atomic-scale design of interfacial characteristics will be important in optimizing NFAs for nuclear applications. However, detailed understanding of

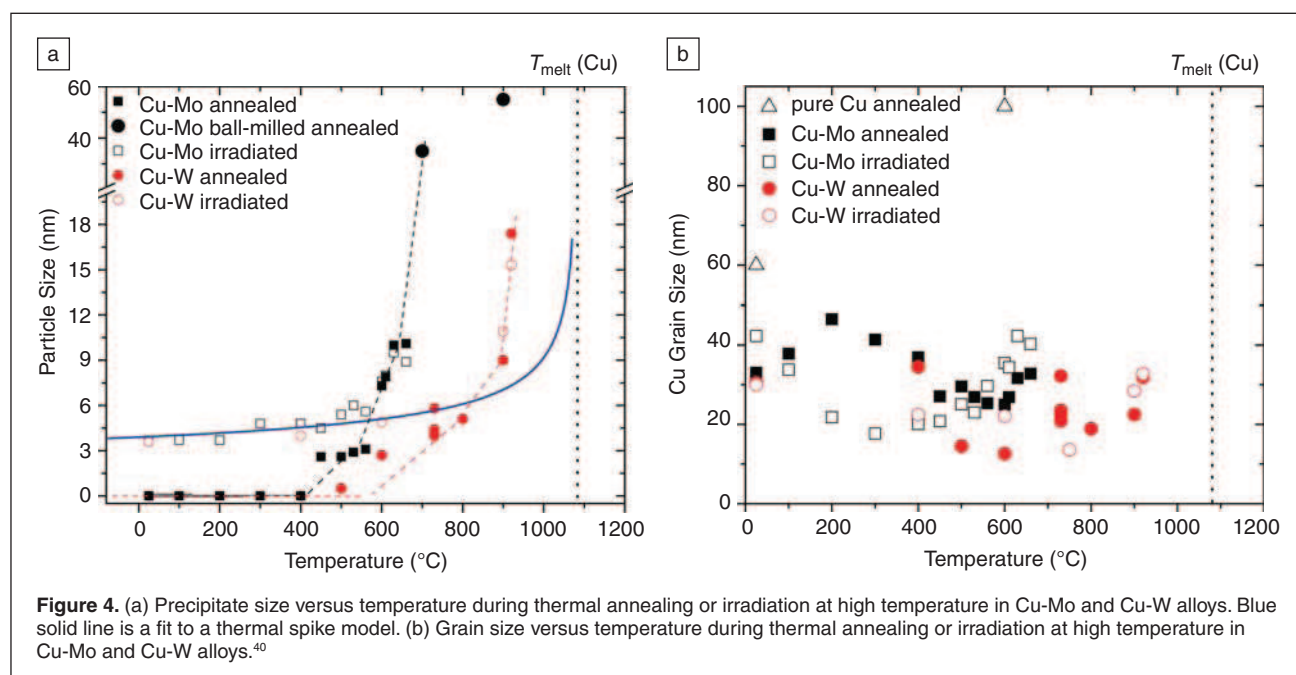


Figure 4. (a) Precipitate size versus temperature during thermal annealing or irradiation at high temperature in Cu-Mo and Cu-W alloys. Blue solid line is a fit to a thermal spike model. (b) Grain size versus temperature during thermal annealing or irradiation at high temperature in Cu-Mo and Cu-W alloys.⁴⁰

the composition and structure of the nanometer-sized Y-Ti-O precipitate clusters, as well as their precipitation and aging (Ostwald ripening) kinetics, is required before atomic-scale design can be fully exploited.

Experimental characterization, predominately by APT, indicates that the Y-Ti-O precipitates have different compositions than stoichiometric oxide phases, which include $\text{Y}_2\text{Ti}_2\text{O}_7$, and orthorhombic Y_2TiO_5 , as well as YTiO_3 and YTi_2O .^{43,50} Figure 5 shows an example of an enlarged atom image of a nanometer-sized Y-Ti-O precipitate cluster in oxide-dispersion-strengthened steel (Figure 5a), along with the elemental maps for Cr, Y, Ti, and O that show Y and Ti association and the high precipitate number density.^{48,51} High-resolution transmission electron microscopy (TEM) studies reveal that larger Y-Ti-O precipitates are semi-coherent, $\text{Y}_2\text{Ti}_2\text{O}_7$ pyrochlore structures,^{52,53} consistent with a picture that the Y-Ti-O-rich nanoscale precipitates are coherent, sub-oxide transition phases.

APT also indicates that some Y-Ti-O precipitate clusters have complex core-shell structures^{51,54,55} in which the cores contain higher Y concentrations, while the shells are enriched in Ti and O. Yet, as noted by Odette et al.,^{43,50} the APT observations are not fully consistent with other characterization techniques, including small-angle neutron scattering, high-resolution TEM, photon spectroscopy, and positron-annihilation spectroscopy.⁵⁶ For example, more recent high-resolution TEM studies have indexed both the pyrochlore and

orthorhombic phases in extraction replicas, but many of the smaller particles are not easily identified as known oxide phases.⁵⁷ Thus, despite a large number of experimental characterization studies, a self-consistent understanding of the character of the nanometer-sized Y-Ti-O precipitate clusters remains lacking, although it is likely that they consist of a range of compositions, and perhaps also interfacial structures.

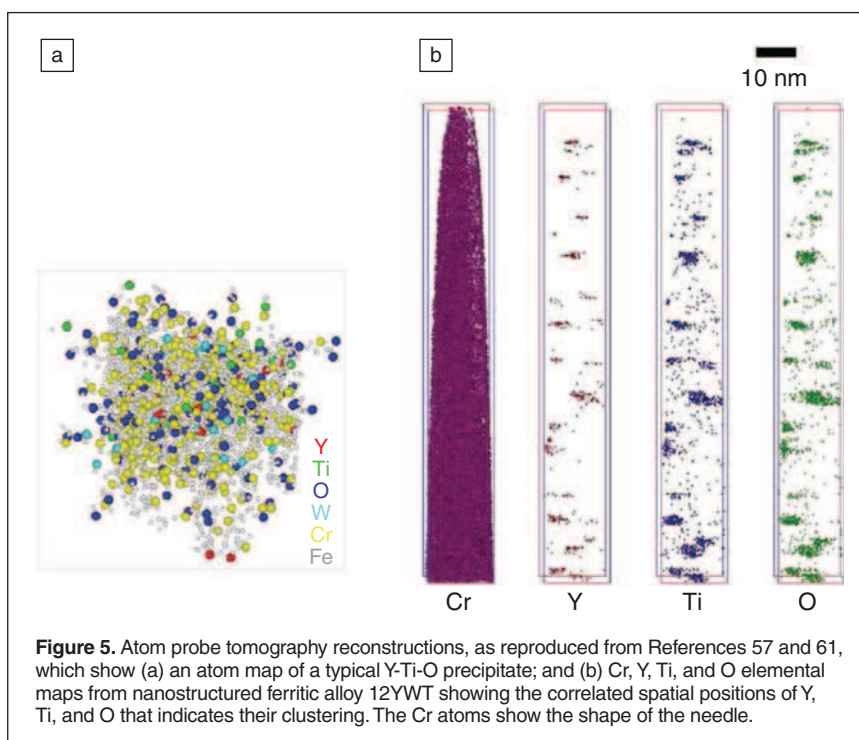


Figure 5. Atom probe tomography reconstructions, as reproduced from References 57 and 61, which show (a) an atom map of a typical Y-Ti-O precipitate; and (b) Cr, Y, Ti, and O elemental maps from nanostructured ferritic alloy 12YWT showing the correlated spatial positions of Y, Ti, and O that indicates their clustering. The Cr atoms show the shape of the needle.

Electronic-structure calculations by Jiang and co-workers have investigated the structure and possible precipitation sequence of very small Y-Ti-O clusters in a magnetic bcc Fe matrix.⁵⁸ Their results indicate that an energetically favorable clustering sequence exists, beginning with the formation of an O-O pair, which is centered on an Fe lattice site, akin to the structure of a split interstitial dumbbell. The energy of the small cluster is further reduced, indicating an energetically bound configuration, through the addition of nearest neighbor Y atoms, followed by nearest neighbor substitutional O and Ti.⁵⁸

Alinger et al. used lattice Monte Carlo (LMC) simulations to explore the composition of nanometer-sized Y-Ti-O phases.⁵⁹ These LMC simulations used a number of simplifying assumptions, including simple pair-bond energies and a simple treatment of lattice strain energy, that remain to be fully assessed. However, the LMC model mapped energetically favorable structures for the Y-Ti-O precipitates, indicative of a strong chemical potential driving force, that are reasonably consistent with the experimental observations. **Figure 6** summarizes the LMC simulation results as a function of effective lattice strain at 0°C (Figure 6a) and as a function of matrix O concentration at 400°C for a fixed lattice strain (Figure 6b).⁵⁹ The simulated nanoclusters are roughly spherical (faceted polyhedral), with segregated regions of Y and Ti, a slight enrichment of Ti at the

interface, and a Ti to Y ratio of about 2:1, reasonably consistent with the APT characterization. Additional effort is focused on refining the Fe-Y-Ti-O interaction potentials and to evaluate the effect of lattice strain energy directly.

It is tempting to conclude that the segregation of Ti to the Y-O-Fe interface, as well as core-shell structures, may be partially responsible for the good thermal stability and strength of NFAs. Another possibility, raised by Fu et al., is that strong binding between oxygen and vacancies in the Y-Ti-O nanoclusters is critical to providing the structure and thermal stability of the precipitates. They found that oxygen prefers the octahedral interstitial position in the bcc Fe matrix as expected, but that the oxygen strongly binds with neighboring vacancies or Ti atoms.⁶⁰ Recent positron-annihilation results, which are very sensitive to vacancies, have reported long-lifetime components in the range of 270–300 ps in NFAs^{56,61} but cannot yet be considered conclusive proof of the role of vacancies in the Y-Ti-O precipitates.

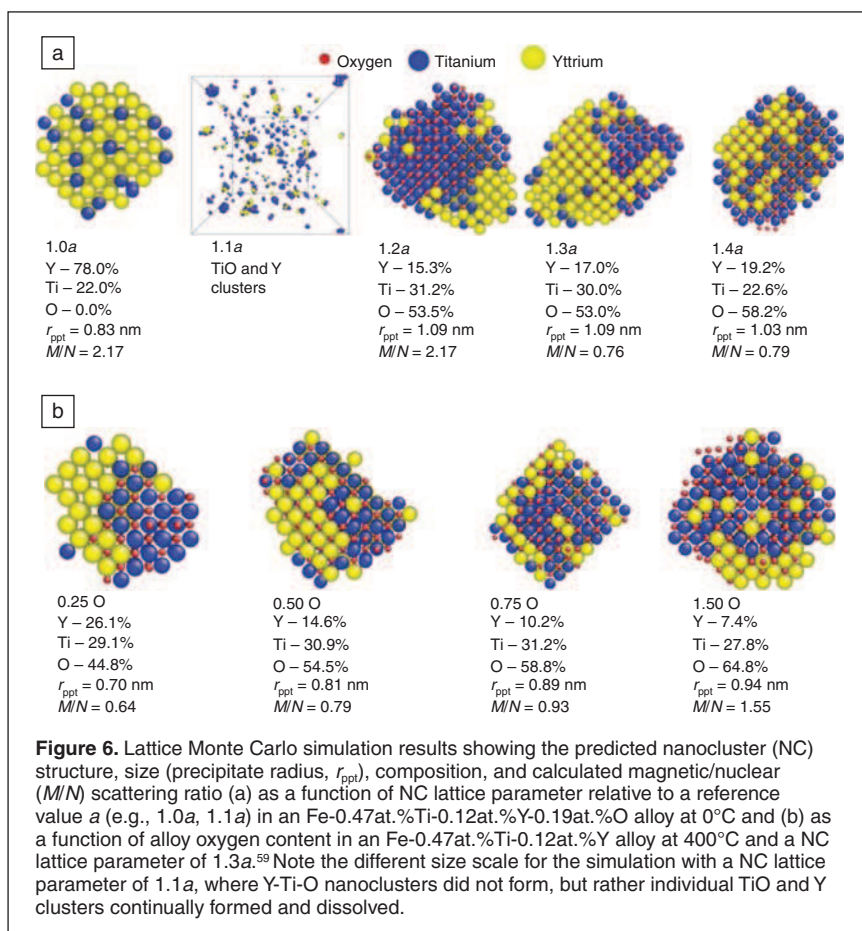
In summary, NFAs produced with a high density of the Y-Ti-O nanoscale precipitate clusters have outstanding mechanical properties, remarkable thermal stability, and quite good radiation tolerance. While, the character of the Y-Ti-O nanoscale precipitate clusters remains to be fully resolved, there are indications that the use of atomic-scale design can provide

insight into the optimal precipitate characteristics involving the segregation of vacancies, Ti, or other alloying elements to reduce interfacial energies and precipitate coarsening kinetics to optimize the radiation resistance of this emerging class of advanced alloys.

Challenges and research directions

The three illustrative examples discussed in this article indicate several challenges to the further development of atomic-scale design of materials for radiation resistance. As was shown in the case of tailoring interface structure, for atomic-scale design to be successful, quantitative structure-property or structure-mechanism relationships for interfaces must be developed and verified. Considerable insight into these relationships has already been gained from previous work, but much of it—being qualitative in nature—is insufficient for atomic-scale design. For example, further work is required to fully understand the structure and mobility of interfaces at elevated temperatures or with segregated impurities and how this structure affects interface interactions with extrinsic point and line defects.

Gaining a quantitative understanding of structure-mechanism interactions in interfaces will require modeling methods with improved accuracy able to access large time and length scales. Such a capability will be especially useful in untangling the physics of complex collective



phenomena, such as thermally activated post-cascade demixing at irradiated heterophase interfaces. Correspondingly, verification of insights gained from modeling requires experimental techniques with greater spatial and temporal resolution.

Finally, applying atomic-scale design to create real, physical materials calls for improvements in the control of synthesis at all length scales, from the atomic composition of oxide precipitates in oxide dispersion strengthened steels, to the crystallography of individual interfaces, and the microstructure of multiphase composites. One approach to achieving such synthesis is to take advantage of the nanoscale compositional patterning that irradiation may trigger in alloy systems composed of immiscible elements, as discussed in this article. While the control parameters responsible for these self-organization reactions have been identified for simple binary alloys, tailoring the properties of interfaces in these structures is likely to require the use of ternary and other multicomponent alloys. These challenges will make atomic-scale design for radiation resistance a field of intense research in the years to come.

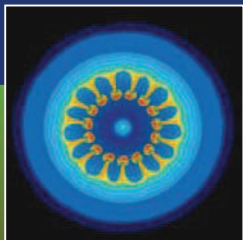
Acknowledgments

M.J.D. acknowledges support from the Los Alamos LDRD program and the U.S. Department of Energy, Office of Science, Office of Basic Energy Sciences under Award No. 2008LANL1026 through the Center for Materials at Irradiation and Mechanical Extremes, an Energy Frontier Research Center. P.B. acknowledges fruitful collaboration with R.S. Averback and support by the U.S. Department of Energy, Office of Basic Energy Sciences under Grant DEFG02-05ER46217 and by the NSF under Grant DMR 08-04615. B.D.W. acknowledges support by the National Science Foundation under contract NSF DMR 0548259 and the U.S. Department of Energy, Office of Fusion Energy Sciences, under grant DE-FG02-04GR54750.

References

1. K. Ehrlich, *J. Nucl. Mater.* **100**, 149 (1981).
2. R.S. Zhou, E.A. West, Z.J. Jiao, G.S. Was, *J. Nucl. Mater.* **395**, 11 (2009).
3. L.K. Mansur, *Nucl. Technol.* **40**, 5 (1978).
4. V. Fidleris, *At. Energy. Rev.* **13**, 51 (1975).
5. T. Allen, H. Burlet, R.K. Nanstad, M. Samaras, S. Ukai, *MRS Bull.* **34**, 20 (2009).
6. Y. Guerin, G.S. Was, S.J. Zinkle, *MRS Bull.* **34**, 10 (2009).
7. S.J. Zinkle, *Phys. Plasmas* **12**, 8 (2005).
8. D.R. Olander, "Fundamental Aspects of Nuclear Reactor Fuel Elements," (Technical Information Center, Office of Public Affairs, Oak Ridge, TN, 1976).
9. G.S. Was, *Fundamentals of Radiation Materials Science: Metals and Alloys* (Springer, Berlin, 2007).
10. K.S. Kang, Y.S. Meng, J. Breger, C.P. Grey, G. Ceder, *Science* **311**, 977 (2006).
11. E.P. Wigner, U.S. Atomic Energy Commission, Physics Division (1942).
12. D.J. Bacon, Y.N. Osetsky, *Int. Mater. Rev.* **47**, 233 (2002).
13. K.C. Russell, *Prog. Mater. Sci.* **28**, 229 (1984).
14. G.R. Odette, G.E. Lucas, *JOM* **53**, 18 (2001).
15. G. Martin, *Phys. Rev. B: Condens. Matter* **30**, 1424 (1984).
16. B.N. Singh, *Philos. Mag.* **29**, 25 (1974).
17. R.W. Siegel, S.M. Chang, R.W. Balluffi, *Acta Metall.* **28**, 249 (1980).
18. M. Dollar, H. Gleiter, *Scripta Metall.* **19**, 481 (1985).
19. K. Inderjeet, Y. Mishin, W. Gust, *Fundamentals of Grain and Interphase Boundary Diffusion* (Wiley, Chichester, NY, 1995).
20. R.G. Hoagland, R.J. Kurtz, *Philos. Mag.* **A 82**, 1073 (2002).
21. Y. Mishin, M. Asta, J. Li, *Acta Mater.* **58**, 1117 (2010).
22. H. Schroeder, W. Kesternich, H. Ullmaier, *Nucl. Eng. Des./Fusion* **2**, 65 (1985).
23. A. Misra, R.G. Hoagland, H. Kung, *Philos. Mag.* **84**, 1021 (2004).
24. A. Misra, M.J. Demkowicz, X. Zhang, R.G. Hoagland, *JOM* **59**, 62 (2007).
25. M.A. Nastasi, J.W. Mayer, J.K. Hirvonen, *Ion-Solid Interactions: Fundamentals and Applications* (Cambridge University Press, Cambridge, NY, 1996).
26. T. Hochbauer, A. Misra, K. Hattar, R.G. Hoagland, *J. Appl. Phys.* **98**, 123516 (2005).
27. X. Zhang, N. Li, O. Anderoglu, H. Wang, J.G. Swadener, T. Hochbauer, A. Misra, R.G. Hoagland, *Nucl. Instrum. Methods Phys. Res., Sect. B* **261**, 1129 (2007).
28. T.E. Mitchell, Y.C. Lu, A.J. Griffin, M. Nastasi, H. Kung, *J. Am. Ceram. Soc.* **80**, 1673 (1997).
29. M.J. Demkowicz, R.G. Hoagland, *Int. J. Appl. Mech.* **1**, 421 (2009).
30. M.J. Demkowicz, R.G. Hoagland, J.P. Hirth, *Phys. Rev. Lett.* **100**, 136102 (2008).
31. M.J. Demkowicz, J. Wang, R.G. Hoagland, in *Dislocations in Solids*, J.P. Hirth, Ed. (Elsevier, Amsterdam, 2008), Vol. 14, pp. 141.
32. K.M. Knowles, *Philos. Mag.* **A 46**, 951 (1982).
33. R. Kirchheim, *Acta Mater.* **50**, 413 (2002).
34. A.J. Detor, C.A. Schuh, *Acta Mater.* **55**, 4221 (2007).
35. R.S. Nelson, J.A. Hudson, D.J. Mazey, *J. Nucl. Mater.* **44**, 318 (1972).
36. W. Jaeger, H. Trinkaus, *J. Nucl. Mater.* **205**, 394 (1993).
37. R.A. Enrique, P. Bellon, *Phys. Rev. Lett.* **84** (2000).
38. R.A. Enrique, K. Nordlund, R.S. Averback, P. Bellon, *J. Appl. Phys.* **93**, 2917 (2003).
39. S.W. Chee, B. Stumph, N.Q. Vo, R.S. Averback, P. Bellon, *Acta Mater.* **58**, 4088 (2010).
40. N.Q. Vo, S.W. Chee, D. Schwen, X. Zhang, P. Bellon, R.S. Averback, *Scripta Mater.* (2010), in press.
41. P. Krasnochtchekov, R.S. Averback, P. Bellon, *Phys. Rev. B: Condens. Matter* **72**, 1 (2005).
42. R.S. Averback, T. Diaz de la Rubia, *Solid State Phys.* **51**, 281 (1998).
43. G.R. Odette, M.J. Alinger, B.D. Wirth, *Annu. Rev. Mater. Res.* **38**, 471 (2008).
44. S. Ukai, T. Okuda, M. Fujiwara, T. Kobayashi, S. Mizuta, H. Nakashima, *J. Nucl. Sci. Technol.* **39**, 872 (2002).
45. D.J. Larson, P.J. Maziasz, I.S. Kim, K. Miyahara, *Scripta Mater.* **44**, 359 (2001).
46. M.J. Alinger, G.R. Odette, D.T. Hoelzer, *J. Nucl. Mater.* **329/333**, 382 (2004).
47. T. Yamamoto, G.R. Odette, P. Miao, D.T. Hoelzer, J. Bentley, N. Hashimoto, H. Tanigawa, R.J. Kurtz, *J. Nucl. Mater.* **367-370**, 399 (2007).
48. D.T. Hoelzer, J. Bentley, M.A. Sokolov, M.K. Miller, G.R. Odette, M.J. Alinger, *J. Nucl. Mater.* **367**, 166 (2007).
49. I.S. Kim, J.D. Hunn, N. Hashimoto, D.L. Larson, P.J. Maziasz, K. Miyahara, E.H. Lee, *J. Nucl. Mater.* **280**, 264 (2000).
50. G.R. Odette, D.T. Hoelzer, *J. Nucl. Mater.* (2010), In press.
51. M.K. Miller, K.F. Russell, D.T. Hoelzer, *J. Nucl. Mater.* **351**, 261 (2006).
52. M. Klimiankou, R. Lindau, A. Moslang, *J. Cryst. Growth* **249**, 381 (2003).
53. M. Klimiankou, R. Lindau, A. Moslang, *Micron* **36**, 1 (2005).
54. E.A. Marquis, *Appl. Phys. Lett.* **93**, 181904 (2008).
55. C.A. Williams, E.A. Marquis, A. Cerezo, G.D.W. Smith, *J. Nucl. Mater.* **400**, 37 (2010).
56. M.J. Alinger, S.C. Glade, B.D. Wirth, G.R. Odette, T. Toyama, Y. Nagai, M. Hasegawa, *Mater. Sci. Eng., A* **518**, 150 (2009).
57. D. Bhattacharyya, P. Dickerson, G.R. Odette (2010), in press.
58. Y. Jiang, J.R. Smith, G.R. Odette, *Phys. Rev. B* **79**, 064103 (2009).
59. M.J. Alinger, B.D. Wirth, H.J. Lee, G.R. Odette, *J. Nucl. Mater.* **367**, 153 (2007).
60. C.L. Fu, M. Krcmar, G.S. Painter, X.Q. Chen, *Phys. Rev. Lett.* **99**, 225502 (2007).
61. J. Xu, C.T. Liu, M.K. Miller, H.M. Chen, *Phys. Rev. B* **79**, 020204(R) (2009).
62. K. Kolluri, M.J. Demkowicz, *Phys. Rev. B* **82**, 193404 (2010).
63. M.J. Demkowicz, D. Bhattacharyya, I. Usov, Y.Q. Wang, M. Nastasi, A. Misra, *Appl. Phys. Lett.* **97**, 161903 (2010).
64. S.C.V. Lim, A.D. Rollett, *Mater. Sci. Eng. A* **520**, 189 (2009). □





Metal deformation and phase transitions at extremely high strain rates

R.E. Rudd, T.C. Germann, B.A. Remington, and J.S. Wark

The powerful lasers being constructed for inertially confined fusion generate enormous pressures extremely rapidly. These extraordinary machines both motivate the need and provide the means to study materials under extreme pressures and loading rates. In this frontier of materials science, an experiment may last for just 10s of nanoseconds. Processes familiar at ambient conditions, such as phase transformations and plastic flow, operate far from equilibrium and show significant kinetic effects. Here we describe recent developments in the science of metal deformation and phase transitions at extreme pressures and strain rates. Ramp loading techniques enable the study of solids at high pressures (100s of GPa) at moderate temperatures. Advanced diagnostics, such as *in situ* x-ray scattering, allow time-resolved material characterization in the short-lived high-pressure state, including crystal structure (phase), elastic compression, the size of microstructural features, and defect densities. Computer simulation, especially molecular dynamics, provides insight into the mechanisms of deformation and phase change.

Introduction

Materials driven at extremely high strain rates constitute an important frontier of materials science. In applications such as laser-driven inertially confined fusion, materials can be driven so fast that many conventional materials concepts must be reconsidered. The high-powered lasers used in this work can compress materials to densities many times their ambient density over a period on the order of 10 nanoseconds. Since the drive is typically uniaxial, at least locally, the high compression rate is accompanied by a high shear strain rate, and the rates affect material behavior both in the kinetics of phase transitions and the mechanisms of plastic deformation. The processes of damage and fracture in the associated rarefaction waves are also affected. In the past, these extraordinary strain rates were associated with shock waves—compressive waves with a front that steepens due to nonlinear material response that causes the wave velocity to increase with pressure. More recently, the high strain rates can be attained in strong ramp compression, in which nonsteady-state waves are tailored to have a rapid rise but not as abrupt as a shock wave at the same pressure. This distinction is important for materials dynamics because shock waves generate a great deal of heat. Shock waves with pressures greater than a few hundred GPa typically melt solids, so the ensuing dynamics are the purview of fluid dynamics. The heat production is a consequence of conservation of mass,

momentum, and energy at the shock front. This heat production follows the Rankine-Hugoniot equations, and it has been known for some time that a pressure reached through two smaller shock waves results in less heat production than if the same pressure were reached in a single shock. Ramp compression can be viewed as the limit in which the pressure increase is broken up into many small shocks and has been called quasi-isentropic. It is not actually isentropic, since plastic work and other sources of dissipation generate heat. Ramp compression opens up new applications; it also facilitates the study of solid materials at extremely high strain rates and high pressures.

From a materials viewpoint, high rates affect the mechanisms of deformation. Some mechanisms are too slow to respond on the time scale of an experiment. Slow processes such as creep are irrelevant to high-rate deformation. Processes such as dislocation motion are sufficiently fast and are understood to play an important role in metal deformation at moderate to high rates. As the rate increases, the dislocations must flow faster, so according to the dislocation-mobility law, the shear stress must be higher. At low stresses, dislocations move from one lattice site to the next through a thermally activated hopping over the lattice hurdle known as the Peierls barrier. If the material is to respond at high rates, however, the shear stress must be high enough that dislocations can glide across the Peierls barrier rapidly without waiting for a thermal fluctuation.

R.E. Rudd, Lawrence Livermore National Laboratory, L-045, Livermore, CA 94550, USA; robert.rudd@llnl.gov

T.C. Germann, Los Alamos National Laboratory, Los Alamos, NM 87545, USA; tcg@lanl.gov

B.A. Remington, Lawrence Livermore National Laboratory, L-481, Livermore, CA 94550, USA; remington2@llnl.gov

J.S. Wark, Clarendon Laboratory, University of Oxford, Parks Rd., Oxford, OX1 3PU, UK; justin.wark@physics.ox.ac.uk

At that point, the dislocation motion is limited by dissipative processes involving phonon emission and scattering: phonon drag. The mechanism may change from dislocation flow to twinning in order to allow the material to deform and relieve the high shear stress on the rapid time scale of the experiment. The material also may undergo a phase transformation under dynamic loading, and the deformation rates affect the resulting microstructure in interesting ways.

The extreme environments of fusion-class lasers

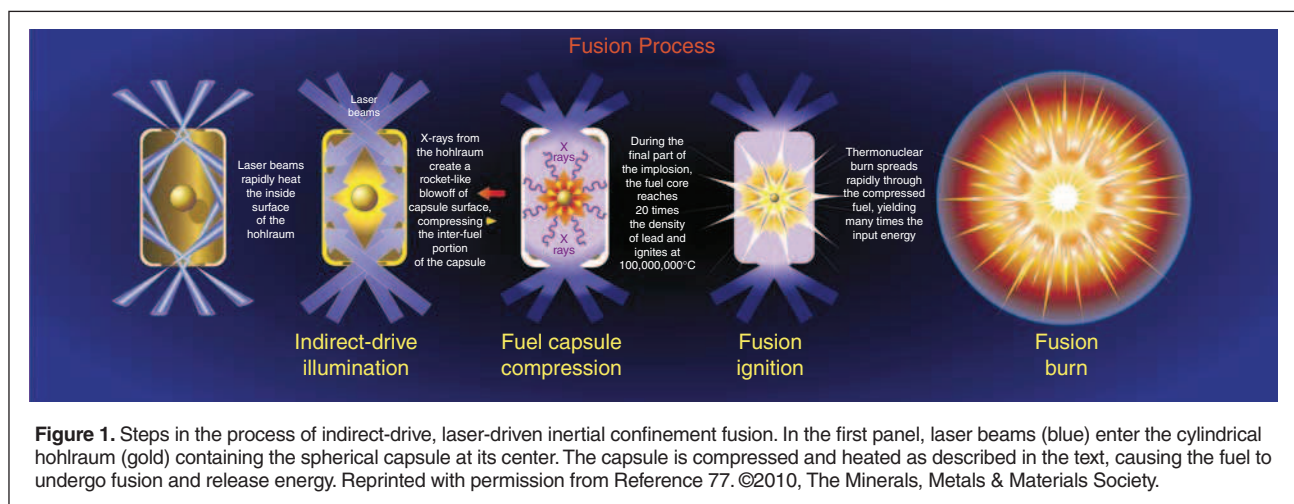
Laser-driven inertially confined fusion (ICF) is a promising path to nuclear fusion energy,¹ a relatively green energy source with an abundant fuel supply. The energy stored in the deuterium in sea water is sufficient to power the Earth at the current rate for billions of years.² Nuclear fusion is the process that powers the sun. Terrestrial nuclear fusion requires producing stellar conditions—high compression and high temperature—in a confined region. The idea of inertially confined fusion is to compress the fuel into this state dynamically, using shock waves³ or shock waves plus another energy source in fast ignition.⁴

Lasers can provide the power to compress and heat the fuel. The National Ignition Facility plans to achieve ignition with 1–2 MJ of laser energy in 192 laser beams directed into a small hollow metal cylinder known as a hohlraum.⁵ Inside, the UV laser light heats the inner surface of the hohlraum generating x-rays. These x-rays uniformly bathe the outer surface of a fuel capsule held in the cavity of the hohlraum, rapidly heating it to over a million degrees. This surface layer rapidly expands radially outward, (ablates) in something like a rocket exhaust, in reaction to which the capsule is driven radially inward (implodes). This all takes place in ~10 nanoseconds, compressing the deuterium-tritium (DT) fuel to a density of ~1000 g/cm³. Successful compression of the fuel to these conditions would produce the high density and high temperature needed for the hydrogen isotopes to fuse, releasing a burst of nuclear energy, as illustrated in **Figure 1**.

Materials science at extremely high rates and pressures

In this article, we focus on material behavior under the conditions associated with fusion-class lasers: the effect of high rate on plasticity, failure, and phase transitions. In the context of ICF, the material in the pusher (the outer shell of the capsule) is driven at very high rates during the laser-induced compression. As it implodes, it is subject to hydrodynamic instabilities that can degrade ICF performance or prevent ignition entirely. The best known of these instabilities is the Rayleigh-Taylor (RT) instability, in which ripples grow at an interface between a dense fluid accelerated by a lighter (less dense) fluid. A layer of water initially suspended above air has the same instability, since the lighter air effectively accelerates the water against the action of gravity to hold it in place. Perturbations on the interface grow until the air bubbles up through the water and spikes of water fall down through the air. The RT instability is not only important in laser ICF applications, but also in explosive metal forming,⁶ in planetary interiors in naturally occurring geophysical flows,⁷ and in other dynamic experiments, including heavy-ion experiments⁸ and pulsed power experiments.^{9,10}

In ICF, the RT instability can occur at two locations on the capsule, as shown in **Figure 2**.¹¹ First, the outer surface is unstable at the ablation front where a low-density plasma from the x-ray-induced ablation pushes on the dense shell. Perturbations from the capsule surface roughness seed the instability at the ablation front, leading to the growth of bubbles and spikes. These perturbations may be transmitted through to the inner surface (feed through), which becomes RT unstable later in the implosion when the fuel is compressed enough to decelerate the pusher (stagnation). The denser pusher material (plastic, beryllium) is decelerated by the less dense, hot DT fuel, and again bubbles and spikes can grow, this time on the inner surface. Spikes of cold, inert pusher material may disrupt the hot spot and the initiation of nuclear burn (ignition).



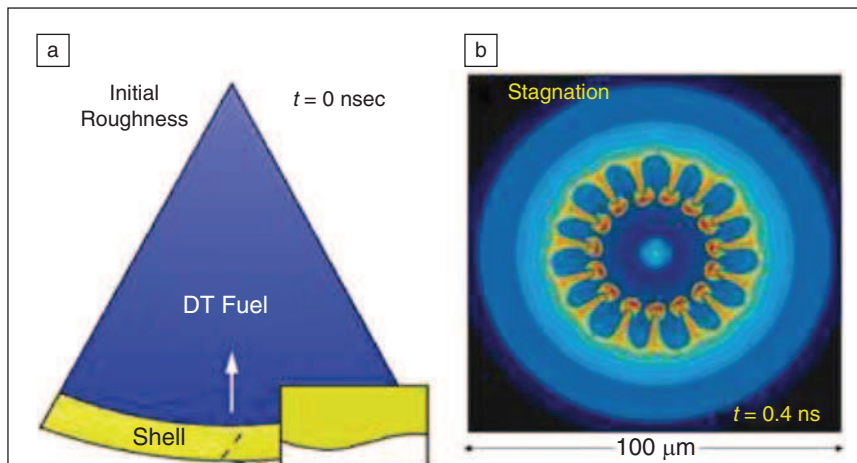


Figure 2. Schematic illustration of processes involving the Rayleigh-Taylor (RT) instability during inertially confined fusion capsule compression. The shell, or pusher, surrounds the deuterium-tritium (DT) fuel. (a) The initial surface roughness of one sector of the spherical capsule is depicted. The surface perturbations seed RT growth at the ablation front, which feeds through to perturb the inner surface of the capsule. (b) The development of RT bubbles and spikes as the capsule shell stagnates against the fuel.⁷⁶

The RT growth can be controlled in several ways, such as improving the initial smoothness of the capsule shell.³ This is a materials-processing challenge. Another approach is to alter the dynamics, either by thickening the shell, which undesirably reduces the ultimate compression,³ or by increasing the strength of the pusher material.¹¹ The RT growth necessarily involves shearing of the material, and strength of the solid material reduces the rate at which the material can shear. In order to predict how RT growth is altered, it is necessary to understand material strength at extremely high strain rates and pressures.

In the following sections of this article, we first consider recent developments in laser-driven material experiments that allow materials to be deformed in a controlled manner at extremely high strain rates using ramp compression to keep the materials solid. The entire experiment lasts but a few 10s of nanoseconds, so it poses numerous challenges to the experimenters, as described in the next section on materials measurements. Then we turn to how computer simulations, especially at the atomic scale, are used to provide further insight into high-rate material-deformation processes. We end with a discussion of phase transformation at high rates.

Laser experiments on materials

A laser-based, experimental platform has been developed to study solid materials' dynamics at ultrahigh strain rates and pressures, relevant to the regimes found in ICF but in planar geometry. An intense laser pulse is focused onto a $\sim 200\text{ }\mu\text{m}$ -thick plastic foil, launching a several-hundred-GPa shock wave. When this shock breaks out the back side of the foil, it unloads across a $\sim 300\text{ }\mu\text{m}$ vacuum gap as a plasma flow. When this plasma stagnates on the far side of the gap, it launches a ramp wave through the sample (Figure 3a). This ramped "plasma drive" allows the sample to be loaded quasi-isentropically, to pressures of many hundreds of GPa, and accelerated. Provided that the ramp wave does not steepen

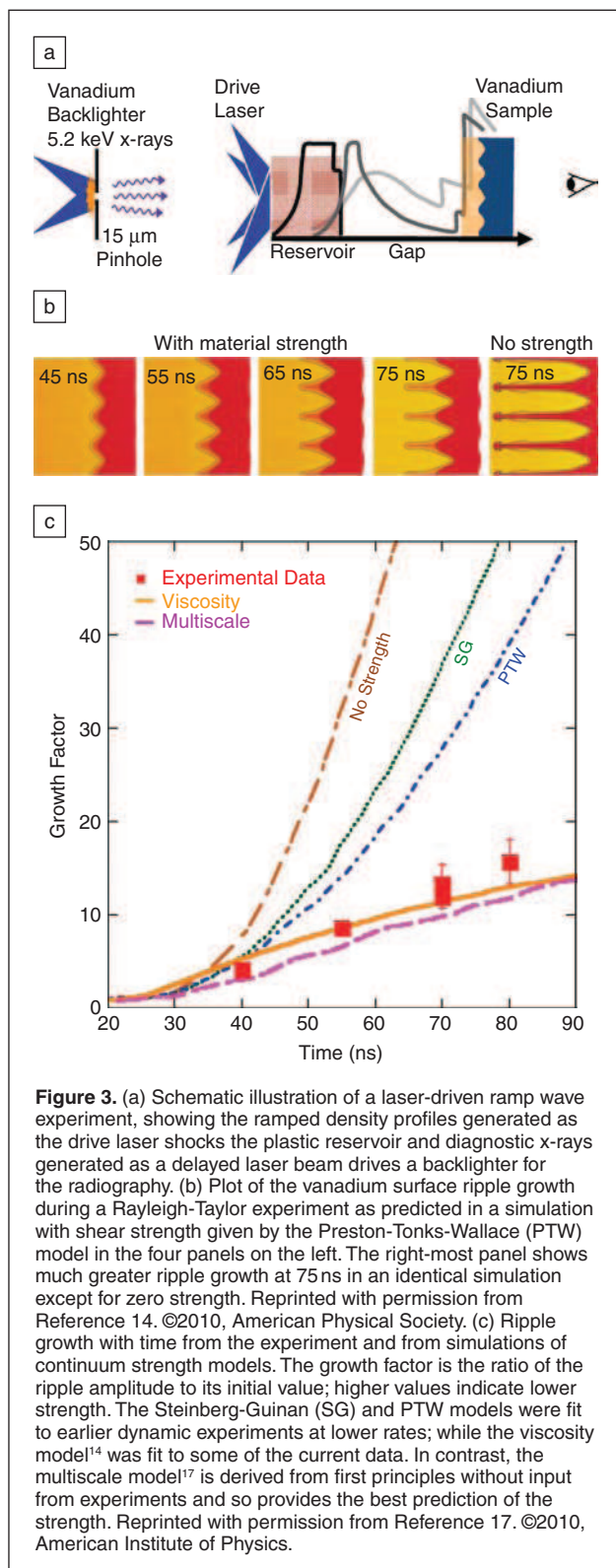
into a shock, the sample temperature does not rise above $\sim 1/3$ of the melt temperature, allowing solid-state materials dynamics to be studied at ultrahigh strain rates and pressures.^{12–16} The strain rates are very high, on the order of 10^7 s^{-1} , corresponding to a characteristic strain of $\sim 10\%$ over a characteristic time scale of $\sim 10\text{ ns}$.

One approach to study material deformation dynamics at ultrahigh strain rates is to imprint the metal foil to be studied with a pre-imposed ripple. The ramped plasma drive accelerates this rippled foil, and the interface (between the stagnating plasma drive and the rippled foil) is subject to the RT instability, as described previously. A recent result uses the plasma drive to load and accelerate a $35\text{ }\mu\text{m}$ -thick vanadium (V) foil at accelerations of $\sim 5 \times 10^{13}\text{ cm/s}^2$ ($0.5\text{ }\mu\text{m/ns}^2$) (i.e., ~ 50 billion gs).¹⁴ The RT instability creates shear stresses that make the ripple amplitude larger, whereas material shear strength resists this plastic flow of material. In the absence of material strength, the ripple amplitude would increase very rapidly, whereas the higher the material strength, the more it resists this plastic flow (see Figure 3b).

The RT-based experiment is distinguished from other recent approaches to measuring strength under dynamic conditions^{18–21} in that the strength is not inferred from a surface velocity measurement, but instead from a measurement of the ripple growth. The growing ripple amplitude is measured with in-flight x-ray radiography by focusing a different subset of lasers onto a "backlighter" foil to generate a burst of $\sim 5\text{ keV}$ He- α diagnostic x-rays. The contrast in the intensity of transmitted backlighter x-rays determines the ripple amplitude. We quantify this as a "growth factor," that is, the ratio of final amplitude to initial amplitude. For a series of experiments in V at maximum pressures of $\sim 100\text{ GPa}$, the growth factor has been measured as a function of time (Figure 3c). This is compared with 2D simulations that include materials-strength models. The data are very sensitive to the strength model, so that data allow strength models to be tested and, if needed, "calibrated." Examples of different strength models are shown in Figure 3c, including a state-of-the-art multiscale model (discussed later in article).

Determining the microscopic material behavior

The determination of microscopic behavior is essential; a fundamental understanding of the way in which materials respond to deformation at ultrahigh strain rates necessitates knowledge of what is occurring at the lattice level. This requirement has led to the development of x-ray diffraction on nanosecond and subnanosecond timescales. Separate but synchronized beams from the same pulsed lasers that are used to launch compression waves into materials can, when focused to even higher intensities, produce extremely hot (10^6 – 10^7 K) plasmas, which are copious sources of diagnostic x-rays intense enough for the recording of single-shot diffraction patterns. Three different



diffraction geometries have been developed, each with a particular application: diverging-beam, white light Laue, and powder (Debye-Scherrer). The best atomic number, Z , for the x-ray source depends on the diffraction technique used.

Diverging-beam—the most developed of the geometries—employs quasi-monochromatic x-radiation emitted by a plasma of a mid-to-low- Z element. The dominant radiation comes from the resonance lines of helium-like ions, close in energy to the more-familiar K-shell radiation used in a conventional x-ray tube.^{22–24} Radiation from the small ($\sim 100 \mu\text{m}$) x-ray source diverges onto the shocked crystal, diffracts when the Bragg condition is met, and is recorded on a large-area detector. The arcs on film correspond to diffraction from planes with differing Miller indices, and compression (or tension) in the crystal can be directly determined from the shift in the arc, as shown in **Figure 4**.

Apart from small shifts due to certain types of defects,²⁵ the shift in the Bragg angle from a particular plane is related to the elastic strain within the crystal. Since most compression experiments operate in a geometry in which the target is subject to uniaxial strain (i.e., the total strain, elastic plus plastic, is zero perpendicular to the shock propagation direction), x-ray diffraction allows a direct determination of both the elastic and plastic components of strain within the sample. The diverging-beam technique has been used to show that single crystals of silicon can sustain very high elastic strains on these nanosecond timescales,²⁶ as well as demonstrating that single crystals of copper, shocked to 100 GPa pressures at high strain rates (close to 10^{10} s^{-1}), deform plastically but still support shear stresses in the GPa regime.²⁷ Furthermore, for single crystals that maintain integrity during a phase transition, the new phase can be determined. For example, nanosecond diffraction has been used to directly monitor the alpha-epsilon transition in shocked single-crystal (001) iron, with the mechanism for rapid transition showing remarkable agreement with molecular dynamics simulations.²⁸

The second geometry that has been developed for nanosecond diffraction is white light Laue, where a “cocktail” of medium- to high- Z elements acts as the x-ray source. Emission from the L-shells of the various ions produces broad-band radiation over a wide energy range (~ 3 to 10 keV). Collimated x-rays from the source are incident on the shocked crystal, which is placed several cm away. In principle, the technique is well-suited to diagnose phase transitions and changes in shape of the unit cell due to deviation from hydrostatic compression. It has also been suggested that it may provide information on the nature and density of defects present during the shock compression.²⁹

The diverging-beam and Laue geometries are ideal for studying the response of single crystals. The study of polycrystalline matter can be performed in Debye-Scherrer geometry, which employs quasi-monochromatic radiation (as in the diverging-beam geometry), but the light again is collimated before incidence upon the shocked target (as in Laue geometry). This technique promises to yield significantly new insight into the response of shocked matter at the lattice level, as it can provide information on how individual grains respond as a function of their orientation relative to the shock propagation direction.³⁰

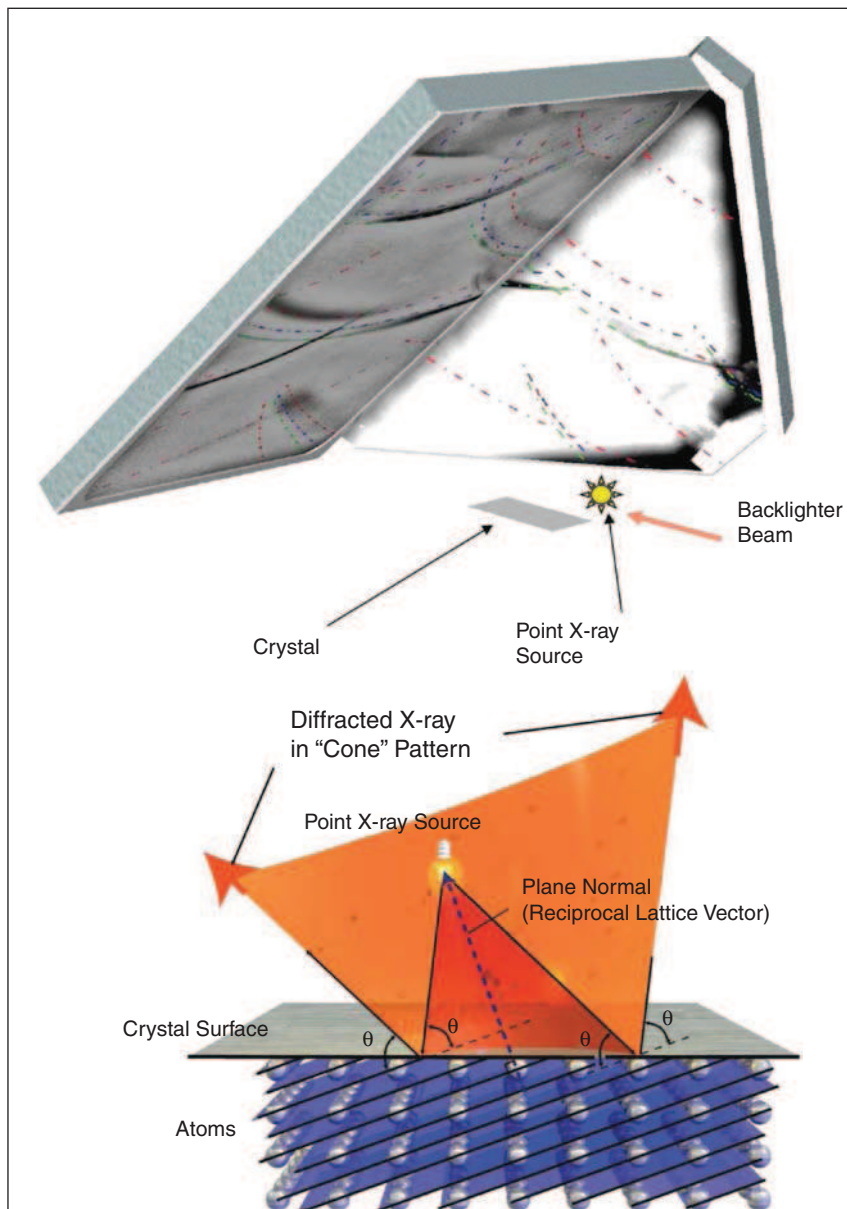


Figure 4. Diverging-beam geometry for nanosecond x-ray diffraction. One of the high-power laser beams is shined on a “backlighter” foil to create a small ($\sim 100\text{ }\mu\text{m}$) hot plasma that emits quasi-monochromatic diagnostic x-rays. These then diverge onto the compressed crystal and diffract when the Bragg condition is met, forming arcs on a large-area detector, as shown at the top. As shown, the Bragg condition is met at the angle θ with respect to a lattice plane (in blue), and the resulting cone of diffracted light (shown in orange) makes the arc on the detector. Shifts in the positions of the arcs allow the lattice spacings to be measured, with components both parallel and perpendicular to the uniaxial strain direction. (See also the article by Browning et al. in this issue of the *MRS Bulletin*.)

Computer modeling of materials dynamics

Computer simulation provides additional insight into the nature of high-rate plastic flow, especially at the microscopic level. Molecular dynamics (MD) simulates the motion of many atoms within a representative region of a material³¹ up to a cubic micron of material for up to a few nanoseconds.^{32,33} It has been used to simulate mechanisms of plasticity at the atomic scale as well as to simulate plastic waves directly.

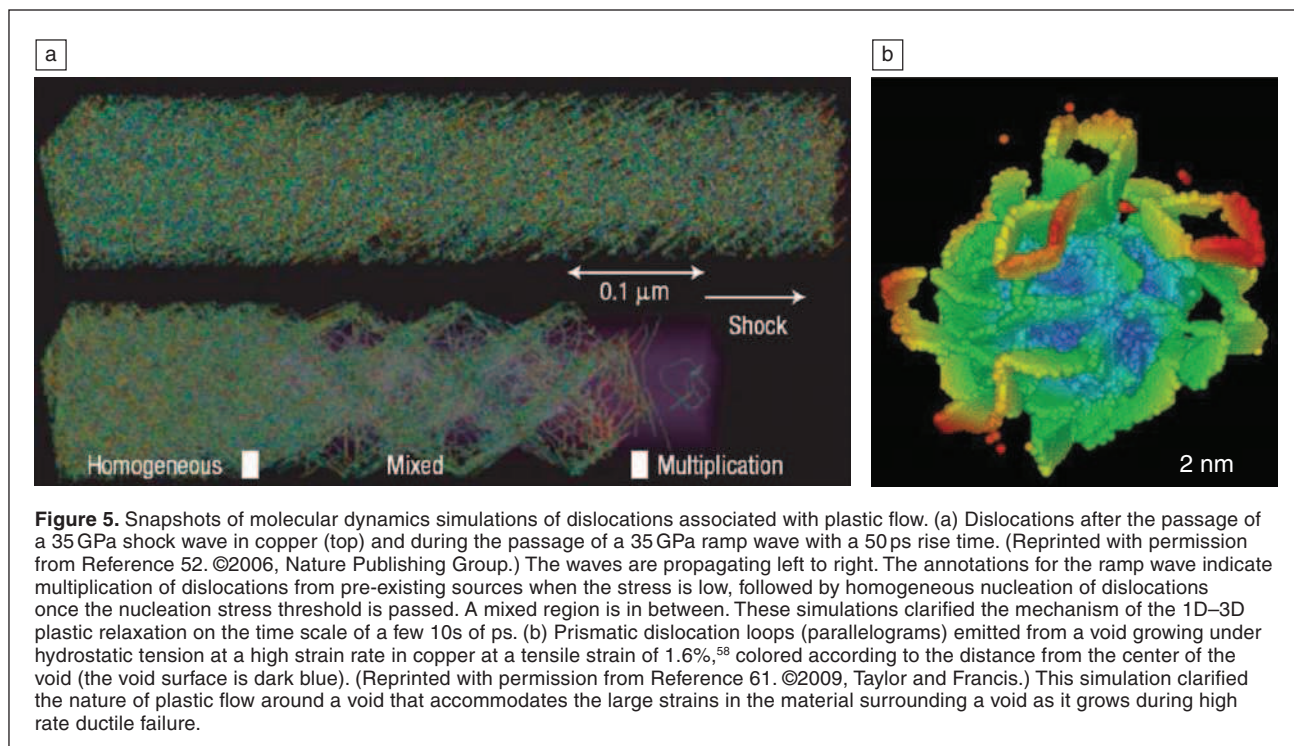
Concurrent multiscale techniques extend MD to larger system volumes.^{34–37} Hierarchical multiscale models start with quantum mechanical calculations and pass information up through a hierarchy of scales to create a continuum-level model of constitutive behavior (e.g., strength).^{38,39}

The dynamics of shock waves can be modeled at the atomic level with MD.^{40,41} Holian and co-workers were the first to conduct sufficiently large MD simulations to study the plasticity behind the shock front in solids.^{42–46} A “piston” such as a momentum mirror drives one surface of the crystal at a steady velocity, u_p , launching a shock wave at a velocity $u_s > u_p$.^{43,47–50} The relationship between u_s and u_p is an important material property called the Hugoniot, the locus of thermodynamic states for shock waves. Using the calculated potential energy difference to locate dislocations, very high dislocation densities were observed to nucleate from the pristine crystal lattice due to the high shear stress of the shocked material^{43,45,46,48,51} (**Figure 5a**).

The transition from 1D to 3D compression due to plasticity in a shock wave²⁶ has been analyzed further with MD using simulated x-ray diffraction and dislocation analysis, including dislocation density ($>10^{14}/\text{cm}^2$) and average dislocation velocities.⁵² In addition to single crystals, the behavior of nanocrystalline materials has been simulated with MD for shock and ramp waves for fcc⁵³ and bcc⁵⁴ systems. Mechanisms of plasticity involving dislocations and twins nucleated at the grain boundaries have been identified.

Continuum-level multiphysics computer simulations play an important role in modeling laser-driven dynamics experiments (see, for example, Reference 55). Recently, Becker and co-workers developed a hierarchical multiscale model of rate-dependent strength. The quantum-based model, without any adjustable parameters, achieved good agreement with the experimental vanadium RT growth rate, indicating plasticity dominated by high-velocity dislocations in the phonon-drag regime.¹⁴

Dynamic fracture also has been simulated using large-scale MD simulations. Such processes can occur in fusion-class lasers just by stray light hitting support structures, launching a compressive wave that creates tension and fracture (spallation) when it bounces off a free surface.⁵⁶ MD simulations have given detailed information about the nucleation,^{57,58} growth,^{59–61} and coalescence^{62–64} of voids associated with dynamic ductile fracture. Rudd and Belak⁵⁹



observed the emission of prismatic loops during void growth in MD simulations (Figure 5b), and related theories have been proposed.^{65,66} Very large-scale direct numerical simulation of spallation also has yielded insight into the collective mechanisms of plasticity at the atomic scale.^{67–70}

Phase transformations

The pressure-induced polymorphic transformation of iron was first detected in shock-loading experiments at Los Alamos more than 50 years ago, inferred from the split multiple-wave structure that developed.^{78,79} A few years later, static high-pressure x-ray diffraction measurements confirmed the transition from a body-centered cubic (bcc) ground state to a hexagonal close-packed (hcp) structure at 13 GPa, a landmark triumph for the nascent shock-physics community.⁸⁰ However, it was only within the past decade that a concerted effort involving the large-scale MD simulations and ultrafast *in situ* x-ray diffraction techniques described earlier was able to conclusively demonstrate that the same bcc-hcp structural transformation seen under static conditions can occur on sub-nanosecond timescales, much faster than previously inferred.²⁸

Multimillion-atom MD simulations of defect-free iron single crystals subjected to shock compression in the $[001]_{\text{bcc}}$ crystallographic direction demonstrated the formation of a split-wave structure above the transition pressure, with the leading wave corresponding to an elastically compressed bcc lattice and the trailing wave corresponding to the direct transformation into the hcp product phase via a simple shuffle mechanism.⁷¹ As the shuffle can proceed in either of two equivalent directions, the product phase is

nucleated in both variants, separated by twin boundaries that evolve via a grain-growth mechanism on timescales up to and beyond the 10s of picoseconds accessible by direct MD. Laser-driven shock experiments on single-crystal Fe foils 10–100 μm thick, loaded in the same direction, demonstrated a remarkable degree of agreement with simulations, including the elastic compression of the bcc lattice up to ~6% followed by a direct shuffle transformation to a twinned hcp product phase.²⁸ Simulated x-ray diffraction patterns, computed directly from the atomic positions of the MD simulations, provide an even more quantitative comparison between simulation and experiment, including the amount of compression and rotation in each phase⁷² and even the product grain size.⁷³

For shock loading in either the $[011]$ or $[111]$ direction, multiple pathways into both hcp and fcc product phases compete, involving larger shear distortions than the more direct $[001]$ mechanism. As a result, MD simulations indicate a much smaller grain size and a larger amount of fcc product. The amount depends strongly on shock pressure and timescale, because it involves a competition between a kinetically favored fcc product and an energetically favored hcp one.⁷⁴ Of course, the response of a bulk polycrystalline sample is determined both by the combined responses of the constituent grains and by the plasticity and/or product phase nucleation and wave scattering at grain boundaries. These effects are seen in **Figure 6**, which vividly illustrates the variety of responses of individual grains, as well as the shock broadening that is beginning to occur as a result of wave scattering and the dispersion of shock velocities.⁷⁵

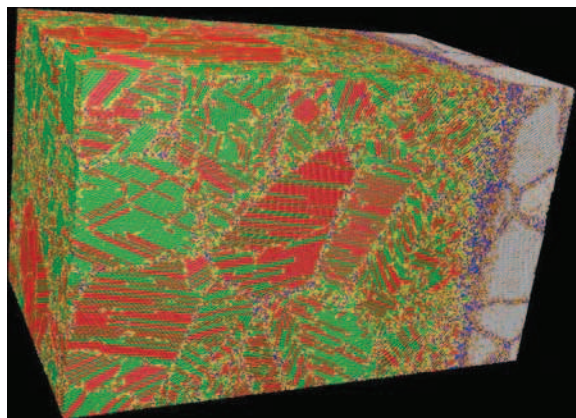


Figure 6. Molecular dynamics simulation of an iron polycrystal with 32.7 nm average grain size and 50 K initial temperature subjected to 39 GPa shock loading (~19% volumetric compression). Atoms are colored by their local structure, with grey, red, and green denoting bcc, hcp, and fcc structures, respectively. The shock wave, traveling from left to right, has nearly reached the end of the 110 nm sample length (~30 million atoms) 14.6 ps after impact. Reprinted with permission from Reference 75. ©2007, American Physical Society.

Conclusion

The next decade promises to be an exciting period in the development of our understanding of metal deformation and phase transitions at extremely high strain rates. Controlled materials experiments under these extreme conditions are possible due to the development of new platforms and techniques, such as the plasma drives on fusion-class lasers reviewed here. Ramped compression, as opposed to shock compression, keeps the materials solid even at ultrahigh pressure. Material properties can be determined even in experiments that only last a few 10s of nanoseconds. We have discussed several examples of keV diagnostic techniques based on bright x-ray backlighters. X-ray radiography is used to determine the Rayleigh-Taylor growth rate of ripples to infer the material shear strength. X-ray diffraction is used to determine phase change and the kinetics of plasticity. The nature of dynamic experiments makes computer modeling important. Molecular dynamics provides a view into the mechanisms of plasticity, failure, and phase change at the atomic scale. Multiscale models are beginning to be able to predict complex macroscopic properties such as plastic flow from first principles. In the coming decade, the laser drives, diagnostic capabilities, and large-scale simulation promise to mature and lift the veil from materials behavior in this extraordinary regime.

Acknowledgments

R.E.R. and B.A.R. wrote parts of this article under the auspices of the U.S. Department of Energy at the Lawrence Livermore National Laboratory under Contract DE-AC52-07NA27344. T.C.G. wrote part of this article under the auspices of the U.S. Department of Energy at Los Alamos National Laboratory under Contract DE-AC52-06NA25396.

References

1. J. Nuckolls, L. Wood, A. Thiessen, G.B. Zimmerman, *Nature* **239**, 129 (1972).
2. R. Post, *Phys. Today* **26**, 30 (1973).
3. J. Lindl, *Phys. Plasmas* **2**, 3933 (1995).
4. M. Tabak, D.S. Clark, S.P. Hatchett, M.H. Key, B.F. Lasinski, R.A. Snavely, S.C. Wilks, R.P.J. Town, R. Stephens, E.M. Campbell, R. Kodama, K. Mima, K.A. Tanaka, S. Atzeni, R. Freeman, *Phys. Plasmas* **12**, 057305 (2005).
5. C.A. Haynam, P.J. Wegner, J.M. Auerbach, M.W. Bowers, S.N. Dixit, G.V. Erbert, G.M. Heestand, M.A. Henesian, M.R. Hermann, K.S. Jancaitis, K.R. Manes, C.D. Marshall, N.C. Mehta, J. Menapace, E. Moses, J.R. Murray, M.C. Nostrand, C.D. Orth, R. Patterson, R.A. Sacks, M.J. Shaw, M. Spaeth, S.B. Sutton, W.H. Williams, C.C. Widmayer, R.K. White, S.T. Yang, B.M. Van Wronterghem, *Appl. Opt.* **46**, 3276 (2007).
6. J.S. Rinehart, J. Pearson, *Explosive Working of Metals* (Pergamon Press, Oxford, 1963).
7. C.P. Conrad, P. Molnar, *Geophys. J. Int.* **129**, 95 (1997).
8. M. Temporal, J.J. López Cela, A.R. Piriz, N. Grandjouan, N.A. Tahir, D.H.H. Hoffmann, *Laser Part. Beams* **23**, 137 (2005).
9. M. Sheppard, W. Atchison, R. Keinigs, J. Stokes, *Proc. IEEE Pulsed Power Conf.* **2**, 892 (1999).
10. S.A. Slutz, M.C. Herrmann, R.A. Vesey, A.B. Sefkow, D.B. Sinars, D.C. Rovang, K.J. Peterson, M.E. Cuneo, *Phys. Plasmas* **17**, 056303 (2010).
11. B.A. Remington, S.V. Weber, M.M. Marinak, W.W. Hsing, N.M. Hoffman, in *Inertial Confinement Fusion Quarterly Report* (UCRL-LR-105821-95-4, 1995), p. 232.
12. J. Edwards, K.T. Lorenz, B.A. Remington, S. Pollaine, J. Colvin, D. Braun, B.F. Lasinski, D. Reisman, J.M. McNaney, J.A. Greenough, R. Wallace, H. Louis, D. Kalantar, *Phys. Rev. Lett.* **92**, 075002 (2004).
13. K.T. Lorenz, M.J. Edwards, S.G. Glendinning, A.F. Jankowski, J. McNaney, S.M. Remington, *High Energy Density Phys.* **2**, 113 (2006).
14. H.-S. Park, K.T. Lorenz, R.M. Cavallo, S.M. Pollaine, S.T. Prisbrey, R.E. Rudd, R.C. Becker, J.V. Bernier, B.A. Remington, *Phys. Rev. Lett.* **104**, 135504 (2010).
15. J.F. Barnes, P.J. Blewett, R.G. McQueen, K.A. Meyer, D. Venable, *J. Appl. Phys.* **45**, 727 (1974).
16. J.F. Barnes, D.H. Janney, R.K. London, K.A. Meyer, D.H. Sharp, *J. Appl. Phys.* **51**, 4678 (1980).
17. H.-S. Park, B.A. Remington, R.C. Becker, J.V. Bernier, R.M. Cavallo, K.T. Lorenz, S.M. Pollaine, S.T. Prisbrey, R.E. Rudd, N.R. Barton, *Phys. Plasmas* **17**, 056314 (2010).
18. J.R. Asay, T. Ao, T.J. Vogler, J.-P. Davis, G.T. Gray III, *J. Appl. Phys.* **106**, 073515 (2009).
19. D.K. Bradley, J.H. Eggert, R.F. Smith, S.T. Prisbrey, D.G. Hicks, D.G. Braun, J. Biener, A.V. Hamza, R.E. Rudd, G.W. Collins, *Phys. Rev. Lett.* **102**, 075503 (2009).
20. M.A. Meyers, F. Gregori, B.K. Kad, M.S. Schneider, D.H. Kalantar, B.A. Remington, G. Ravichandran, T. Boehly, J.S. Wark, *Acta Mater.* **51**, 1211 (2003).
21. K.J. Frutsky, R.J. Clifton, *J. Mech. Phys. Solids* **46**, 1723 (1998).
22. J.S. Wark, R.R. Whitlock, A. Hauer, J.E. Swain, P.J. Solone, *Phys. Rev. B* **35**, 9391 (1987).
23. J.S. Wark, R.R. Whitlock, A. Hauer, J.E. Swain, P.J. Solone, *Phys. Rev. B* **40**, 5705 (1989).
24. D.H. Kalantar, E.M. Bringa, M. Caturia, J. Colvin, K.T. Lorenz, M. Kumar, J. Stolken, A.M. Allen, K. Rosolankova, J.S. Wark, M.A. Meyers, M. Schneider, T.R. Boehly, *Rev. Sci. Instrum.* **74**, 1929 (2003).
25. K. Rosolankova, J.S. Wark, E.M. Bringa, J. Hawreliak, *J. Phys. Condens. Matter* **18**, 6749 (2006).
26. A. Loveridge-Smith, A. Allen, J. Belak, T. Boehly, A. Hauer, B. Holian, D. Kalantar, G. Kyrila, R.W. Lee, P. Lomdahl, M.A. Meyers, D. Paisley, S. Pollaine, B. Remington, D.C. Swift, S. Weber, J.S. Wark, *Phys. Rev. Lett.* **86**, 2349 (2001).
27. W.J. Murphy, A. Higginbotham, G. Kimminau, B. Barbre, E.M. Bringa, J. Hawreliak, R. Kodama, M. Koenig, W. McBaron, M.A. Meyers, B. Nagler, N. Ozaki, N. Park, B. Remington, S. Rothman, S.M. Vinko, T. Whitcher, J.S. Wark, *J. Phys. Condens. Matter* **22**, 065404 (2010).
28. D.H. Kalantar, J.F. Belak, G.W. Collins, J.D. Colvin, H.M. Davies, J.H. Eggert, T.C. Germann, J. Hawreliak, B.L. Holian, K. Kadau, P.S. Lomdahl, H.E. Lorenzana, M.A. Meyers, K. Rosolankova, M.S. Schneider, J. Sheppard, J.S. Stolken, J.S. Wark, *Phys. Rev. Lett.* **95**, 075502 (2005).
29. M. Suggit, G. Kimminau, J. Hawreliak, B. Remington, N. Park, J. Wark, *Rev. Sci. Instrum.* **81**, 083902 (2010).
30. J. Hawreliak, H.E. Lorenzana, B.A. Remington, S. Lukezic, J.S. Wark, *Rev. Sci. Instrum.* **78**, 083908 (2007).
31. M.P. Allen, D.J. Tildesley, *Computer Simulation of Liquids* (Clarendon Press, Oxford, 1987).
32. J.N. Glosli, K.J. Caspersen, D.F. Richards, R.E. Rudd, F.H. Streitz, J.A. Gunnels, in *Proc. Supercomputing 2007* (2007).
33. K. Kadau, T.C. Germann, P.S. Lomdahl, *Int. J. Mod. Phys. C* **17**, 1755 (2006).

34. E.B. Tadmor, M. Ortiz, R. Phillips, *Philos. Mag. A* **73**, 1529 (1996).
35. R.E. Rudd, J.Q. Broughton, *Phys. Status Solidi B* **217**, 251 (2000).
36. R.E. Rudd, J.Q. Broughton, *Phys. Rev. B* **72**, 144104 (2005).
37. R.E. Miller, E.B. Tadmor, *Modell. Simul. Mater. Sci. Eng.* **17**, 053001 (2009).
38. J.A. Moriarty, L.X. Benedict, J.N. Glosli, R.Q. Hood, D.A. Orlikowski, M.V. Patel, P. Soderlind, F.H. Streitz, M. Tang, L.H. Yang, *J. Mater. Res.* **21**, 563 (2006).
39. A. Arsenlis, W. Cai, M. Tang, M. Rhee, T. Oppelstrup, G. Hommes, T.G. Pierce, V.V. Bulatov, *Modell. Simul. Mater. Sci. Eng.* **15**, 553 (2007).
40. W.G. Hoover, *Phys. Rev. Lett.* **42**, 1531 (1979).
41. B.L. Holian, G.K. Straub, *Phys. Rev. Lett.* **43**, 1598 (1979).
42. B.L. Holian, *Phys. Rev. A* **37**, 2562 (1988).
43. B.L. Holian, P.S. Lomdahl, *Science* **280**, 2085 (1998).
44. T.C. Germann, B.L. Holian, P.S. Lomdahl, R. Ravelo, *Phys. Rev. Lett.* **84**, 5351 (2000).
45. D. Tanguy, M. Mareschal, P.S. Lomdahl, T.C. Germann, B.L. Holian, R. Ravelo, *Phys. Rev. B* **68**, 144111 (2003).
46. T.C. Germann, D. Tanguy, B.L. Holian, P.S. Lomdahl, M. Mareschal, R. Ravelo, *Mater. Mater. Trans.* **35A**, 2609 (2004).
47. J.-B. Maillet, M. Mareschal, L. Souillard, R. Ravelo, P.S. Lomdahl, T.C. Germann, B.L. Holian, *Phys. Rev. E* **63**, 016121 (2000).
48. E.M. Bringa, J.U. Cazamias, P. Erhart, J. Stolken, N. Tanushev, B.D. Wirth, R.E. Rudd, M.J. Caturla, *J. Appl. Phys.* **96**, 3793 (2004).
49. R. Ravelo, B.L. Holian, T.C. Germann, P.S. Lomdahl, *Phys. Rev. B* **70**, 014103 (2004).
50. A. Kubota, D.B. Reisman, W.G. Wolfer, *Appl. Phys. Lett.* **88**, 241924 (2006).
51. G. Kimminau, P. Erhart, E.M. Bringa, B. Remington, J.S. Wark, *Phys. Rev. B* **81**, 092102 (2010).
52. E.M. Bringa, K. Rosolankova, R.E. Rudd, B.A. Remington, J.S. Wark, M. Duchaineau, D.H. Kalantar, J. Belak, *Nat. Mater.* **5**, 805 (2006).
53. E.M. Bringa, A. Caro, Y. Wang, M. Victoria, J.M. McNaney, B.A. Remington, R.F. Smith, B.R. Torralva, H. van Swygenhoven, *Science* **309**, 1838 (2005).
54. R.E. Rudd, *Mater. Sci. Forum* **633-634**, 3 (2010).
55. B.A. Remington, S.W. Haan, S.G. Glendinning, J.D. Kilkenny, D.H. Munro, R.J. Wallace, *Phys. Rev. Lett.* **67**, 3259 (1991).
56. A.C. Fisher, N.D. Masters, P. Dixit, D.J. Benson, A.E. Koniges, R.W. Anderson, B.T.N. Gunney, P. Wang, R. Becker, *J. Phys. Conf. Ser.* **112** 022027 (2008).
57. J. Belak, *J. Comput.-Aided Mater. Des.* **5**, 193 (1998).
58. R.E. Rudd, J.F. Belak, *Comput. Mater. Sci.* **24**, 148 (2002).
59. J.A. Moriarty, J.F. Belak, R.E. Rudd, P. Soderlind, F.H. Streitz, L.H. Yang, *J. Phys. Condens. Matter* **14**, 2825 (2002).
60. E.T. Seppala, J. Belak, R.E. Rudd, *Phys. Rev. B* **69**, 134101 (2004).
61. R.E. Rudd, *Philos. Mag.* **89**, 3133 (2009).
62. E.T. Seppala, J. Belak, R.E. Rudd, *Phys. Rev. Lett.* **93**, 245503 (2004).
63. E.T. Seppala, J. Belak, R.E. Rudd, *Phys. Rev. B* **71**, 064112 (2005).
64. R.E. Rudd, E.T. Seppala, L.M. Dupuy, J. Belak, *J. Comput.-Aided Mater. Des.* **14**, 425 (2007).
65. V.A. Lubarda, M.S. Schneider, D.H. Kalantar, B.A. Remington, M.A. Meyers, *Acta Mater.* **52**, 1397 (2004).
66. D.C. Ahn, P. Sofronis, R. Minich, *J. Mech. Phys. Solids* **54**, 735 (2006).
67. V. Dremov, A. Petrovtsev, P. Sapozhnikov, M. Smirnova, D.L. Preston, M.A. Zocher, *Phys. Rev. B* **74**, 144110 (2006).
68. S.G. Srinivasan, M.I. Baskes, G.J. Wagner, *J. Appl. Phys.* **101**, 043504 (2007).
69. S.N. Luo, Q. An, T.C. Germann, L.B. Han, *J. Appl. Phys.* **106**, 013502 (2009).
70. S.N. Luo, T.C. Germann, D.L. Tonks, *J. Appl. Phys.* **106**, 123518 (2009).
71. K. Kadau, T.C. Germann, P.S. Lomdahl, B.L. Holian, *Science* **296**, 1681 (2002).
72. J. Hawrelak, J.D. Colvin, J.H. Eggert, D.H. Kalantar, J.S. Stölken, H.M. Davies, T.C. Germann, B.L. Holian, K. Kadau, P.S. Lomdahl, A. Higginbotham, K. Rosolankova, J. Sheppard, J.S. Wark, *Phys. Rev. B* **74**, 184107 (2006).
73. J. Hawrelak, D.H. Kalantar, J.S. Stölken, B.A. Remington, H.E. Lorenzana, J.S. Wark, *Phys. Rev. B* **78**, 220101 (2008).
74. K. Kadau, T.C. Germann, P.S. Lomdahl, B.L. Holian, *Phys. Rev. B* **72**, 064120 (2005).
75. K. Kadau, T.C. Germann, P.S. Lomdahl, R.C. Albers, J.S. Wark, A. Higginbotham, B.L. Holian, *Phys. Rev. Lett.* **98**, 135701 (2007).
76. H. Sakagami, K. Nishihara, *Phys. Fluids B* **2**, 2715 (1990).
77. M.A. Meyers, B.A. Remington, B. Maddox, E.M. Bringa, *JOM* **62**, 24 (2010).
78. J.M. Walsh, *Bull. Am. Phys. Soc.* **29**, 28 (1954).
79. D. Bancroft, E.L. Peterson, S. Minshall, *J. Appl. Phys.* **27**, 291 (1956).
80. J.C. Jamieson, A.W. Lawson, *J. Appl. Phys.* **33**, 776 (1962). □

The Materials GatewaySM—www.mrs.org



DEDICATED PILOT PRODUCTION EQUIPMENT AND RESOURCES FOR YOUR ADVANCED MATERIALS

Powder Metallurgy · Rapid Solidification · Specialty Alloys Melt Spinning



- Pilot scale production as low as 5kg for trial
- Feasibility trials of melt spinning your materials
- Evaluation and expert advice upon request
- Opportunity to scale for commercialization
- Access to our jet casting facilities



We Specialise in

Post-casting heat treatment Handling and processing powder Processing ribbon, foil and powder
Melt spinning in vacuum and inert atmosphere Rapid quenching to generate nanocrystalline and amorphous alloys



We are the World's Largest Melt Spinner of Specialty Alloys

61 Science Park Road, #01-19 The Galen, Singapore Science Park II, Singapore 117525.

research@magnequench.com
ISO 14001:2004 and ISO 9001:2000 Certified





***In situ* characterization of metals at extremes**

N.D. Browning, G.H. Campbell, J.A. Hawreliak, and M.A. Kirk

The fundamental processes taking place in metals under extreme conditions can occur on ultrafast timescales (i.e., nanoseconds to picoseconds), and yet their result can continue to have a significant impact on the structural properties for many years to follow. The challenge in developing *in situ* methods for characterization under extreme conditions therefore involves both the modification of the instrumentation to implement the high-temperature, strain, and radiation conditions and the definition of the timescale over which the measurement must be made. While techniques are well established for characterization of the long-term effects of extreme conditions, experiments are only just beginning to probe the initial stages of structural evolution. This article reviews recent developments in optical, x-ray, and electron probes of metals under extreme conditions and also discusses the needs for future experiments and potential pathways to achieving these goals.

Introduction

The need to develop new materials that can perform well under the extreme conditions of high temperature, radiation dose, strain rate, and pressure (either individually or in combination) presents a unique set of challenges for structural characterization methods. Instrumentation must be modified to permit some semblance of the extreme condition(s) to be safely replicated in the experiment, while at the same time allowing the experiments to be performed on the critical time and length scales important for the materials' function. As methods to understand the long-term aging of components under extreme conditions are well established (simple before-and-after experiments are sufficient provided you can wait long enough), it is the short-timescale interactions that are at the forefront of new developments in *in situ* experimentation. In this article, the main issues involved in studying metals under extreme conditions are discussed for the current major methods of *in situ* characterization: transmission electron microscopy (TEM), synchrotron radiation, and short-pulse-laser-driven optical methods. For each of these methods, an example of the type of experiment that can be performed will be described, and the potential of each method for future advancements in the study of extreme conditions will be discussed.

The need for *in situ* measurements

Since post-mortem materials characterization techniques have been in existence for many years, the first thing we need to

address with this article is “Why are *in situ* studies necessary?”

This question takes on even more consequence for metals under extreme conditions that are very difficult to establish in the laboratory. So why should we struggle to do this? It is the very nature of the extreme conditions that makes *in situ* studies so valuable, even if the analyses do not achieve the same resolution as static experiments. In the extreme conditions where we need metals to function, structural changes are rapid, with many processes often occurring simultaneously (such as phase transitions, secondary phases, voids, and dislocations), and materials may progress through intermediate states that exist for only short periods of time. If we are to control the structure of materials under extreme conditions, we need to know the order in which the structural changes occurred and whether we can change the final outcome of the extreme conditions by changing the kinetics of the intermediate states.

Phase transformations with rapid thermal gradients

Since its invention, TEM has excelled at determining and quantifying the structure of materials and the presence of defects at small length scales.¹ The development of aberration correctors^{2,3} over the last 10 years has taken the available direct-imaging resolution in state-of-the-art microscopes into the deep sub-angstrom regime. Significant, but less publicized, progress is also being made by creating controlled experimental conditions

N.D. Browning, University of California–Davis, One Shields Ave., Davis, CA 95616, USA; nbrowning@ucdavis.edu
G.H. Campbell, Lawrence Livermore National Laboratory, MS L-356, PO Box 808, Livermore, CA 94550, USA; ghcampbell@llnl.gov
J.A. Hawreliak, Lawrence Livermore National Laboratory, PO Box 808 L-286, Livermore, CA 94550, USA; hawreliak1@llnl.gov
M.A. Kirk, Argonne National Laboratory, 9700 S. Cass Ave., Argonne, IL 60439, USA; kirk@anl.gov

at the specimen that allow *in situ* observations of the structure as it evolves in response to various forces. These observations have included oxidation reactions,⁴ catalytic reactions,^{5,6} and mechanical loading.⁷⁻⁹ At the length scales probed by TEM, the structure evolves rapidly because distances are short; this is especially true under extreme conditions, where the driving forces can be very large.

One such example of extreme conditions is pulsed-laser-induced heating of a material, where heating rates are typically $>10^{11}$ K/s and can be much higher. With these rates, a sample can be heated to a high temperature much faster than its structure can respond.¹⁰ Under these circumstances, subsequent structural evolutions typically fall into two categories.

In the first category, the change in the structure will be accompanied by dissipative processes, so if the evolution is reversed, it will leave a structure that is different from the initial condition. A specific example would be a phase transformation that introduces dislocations in the surrounding material to accommodate misfit strains. If the phase transformation is reversed, the accommodation dislocations will likely remain, leaving the original microstructure changed. These types of evolutions encompass phase transformations, chemical reactions, and the movement of dislocations, boundaries, and interfaces—the types of structural changes that are prevalent in metals under extreme conditions.

A more limited number of structural changes fall into the second category, those that are easily reversible or have very small dissipations, leaving the initial structure unchanged. Such reversible effects include elastic strains to a lattice, certain electronic transitions, and plasmon excitations. Although techniques have been developed for TEM that can study these transformations on the femtosecond timescale,¹¹⁻¹³ because they do not apply in general to metals under extreme conditions, they will not be discussed further here.

The development of the single-shot dynamic transmission electron microscope (DTEM) at Lawrence Livermore National Laboratory (LLNL),^{14,15} shown in **Figure 1**, permits the direct study of structural changes that occur in the presence of dissipative mechanisms, as just described. In the DTEM, a short (~ 15 ns) pulse of electrons is generated that contains enough electrons to acquire a whole diffraction pattern or image with a single shot. To form a high-quality image, $\sim 10^8$ electrons must reach the camera,¹⁶ implying a current at the specimen in excess of 10 mA, roughly a million times greater than the \sim nA current in normal operation of a TEM. To create this level of current from a small source, the LLNL DTEM uses photoemission from a pulsed laser focused on a photocathode, in which the wavelength of the photons has been converted to 211 nm to increase the efficiency of the emission.¹⁷ The emission proceeds for the duration of the laser pulse, which in this case is 10 ns (the electron pulse broadens in time to 15 ns at the specimen position). The *in situ* experimental conditions are typically created by a second laser pulse that heats the specimen to a certain temperature. The relative timing of the two laser pulses sets the arrival time of the electron pulse at the specimen. A series

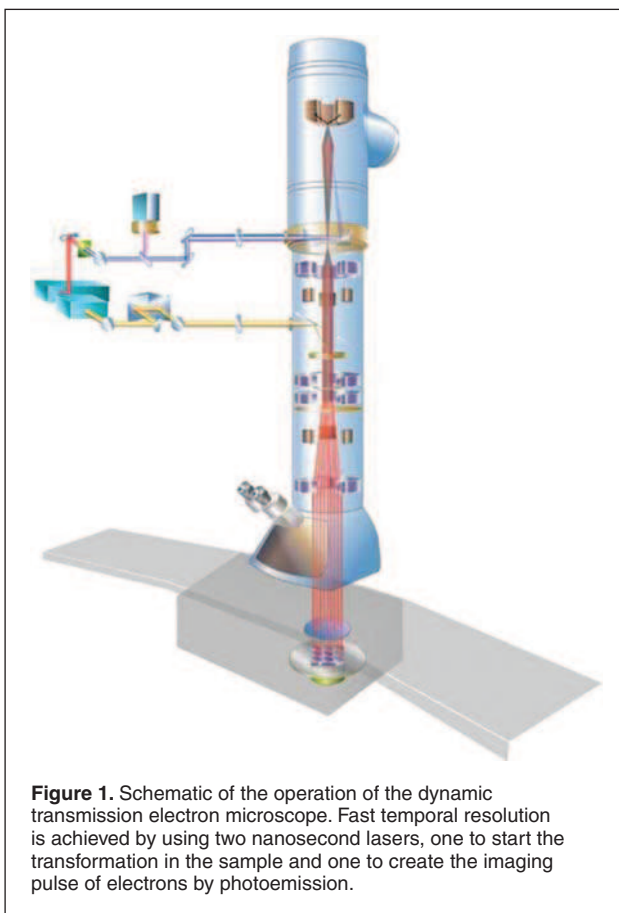


Figure 1. Schematic of the operation of the dynamic transmission electron microscope. Fast temporal resolution is achieved by using two nanosecond lasers, one to start the transformation in the sample and one to create the imaging pulse of electrons by photoemission.

of delays can be used in separate experiments to follow the evolution of the material structure in time.

An example of the microstructural evolution created by extreme heating rates is pulsed-laser-induced crystallization of an amorphous solid.¹⁸ In some intermetallic systems, films can be created with a completely amorphous structure by sputtering onto a room-temperature substrate. Subsequent heating can crystallize the amorphous films. The process has been studied thoroughly with differential scanning calorimetry (DSC)¹⁹ and by slow *in situ* heating experiments in the TEM.²⁰ In both of these approaches, the heating rate is $<10^2$ K/s, and the temperature of crystallization stays close to the threshold temperature.

Under pulsed-laser energy deposition in the DTEM, the volume of the 100-nm-thick TEM foils can be heated essentially uniformly. In most metals, the laser energy is deposited in a thin layer, typically on the order of 10 nm (the skin depth), and the through-thickness temperature equilibrates in 10s of nanoseconds within the irradiated spot, with rates $>10^{11}$ K/s. If the crystallization process is slower than the through-thickness temperature equilibration, the film can be heated to any temperature up to the melting temperature prior to any crystallization taking place. The film then stays at an elevated temperature, cooling much slower due to the limited thermal conduction through the small cross-sectional area of the film.

(The temperatures of interest are too low for radiation to be a strong effect.) In fact, for many of the time scales of interest for this high-temperature crystallization, the films can be treated as essentially isothermal.

An example of a DTEM observation of the crystallization process is shown in **Figure 2a**. In this image, the crystal nuclei are visible, and the interfaces between the crystalline and amorphous phase are clearly delineated, even though they are moving with a speed of up to 1 m/s. These observations give two quantities of direct relevance to the kinetics analysis of the process: the nucleation rate—by counting nuclei as a function of time—and the growth rate—by tracking the size of the crystalline islands as a function of time. These measurements are made as a function of temperature, and the time-temperature-transformation (TTT) diagram is mapped out (Figure 2b). The data from traditional methods are also shown in the figure, highlighting that the data acquired with the DTEM map out a section of the TTT diagram that is accessible by no other technique. In fact, the DTEM has revealed the “nose” in the C-curve section of the TTT diagram. Entropic effects limit the nucleation rate above the nose (thermodynamically limited), and temperature limits the growth rate below it (kinetically limited). This is arguably the most important and useful aspect of these data.

Structural materials under irradiation

Another area where TEM can provide useful *in situ* information is the study of materials under irradiation, which is particularly important for materials being developed for nuclear reactor applications.²¹ (See also the article by Demkowicz et al. in this issue of *MRS Bulletin*.) Candidate materials for structures in the next generation of fission reactors and first-generation fusion power reactors include ferritic-martensitic steels and also the more complex mechanically alloyed oxide-dispersion-strengthened (ODS) steels. The attraction of these alloys for nuclear applications includes relatively low swelling under high-fluence neutron irradiation, reduced radiation embrittlement, good strength at relatively high temperatures, and low activation. However, the fundamental understanding of the radiation damage under high-fluence neutron irradiation, especially at elevated temperatures, is quite limited at present. Recently, these materials (as well as simpler model alloys) have been the subject of studies by TEM with *in situ* ion irradiation over ranges of temperature and accumulated radiation damage equivalent in dpa (displacements per atom) to years of reactor exposure.

The mechanisms by which radiation damage develops in ferritic materials are still not well understood. In a program from the University of Oxford, the development of heavy-ion irradiation damage in Fe and FeCr alloys was followed by *in situ* electron microscopy and revealed some unexpected dynamic processes. Thin foils of pure Fe and FeCr alloys (with 5–11%Cr) were irradiated with 150 keV Fe⁺ ions at temperatures 30–500°C in the Argonne IVEM-Tandem Facility, which comprises an electron microscope linked to a heavy-ion accelerator. Dynamic observations under weak-beam diffraction conditions followed the evolution of damage over doses 0–13 dpa.^{22,23}

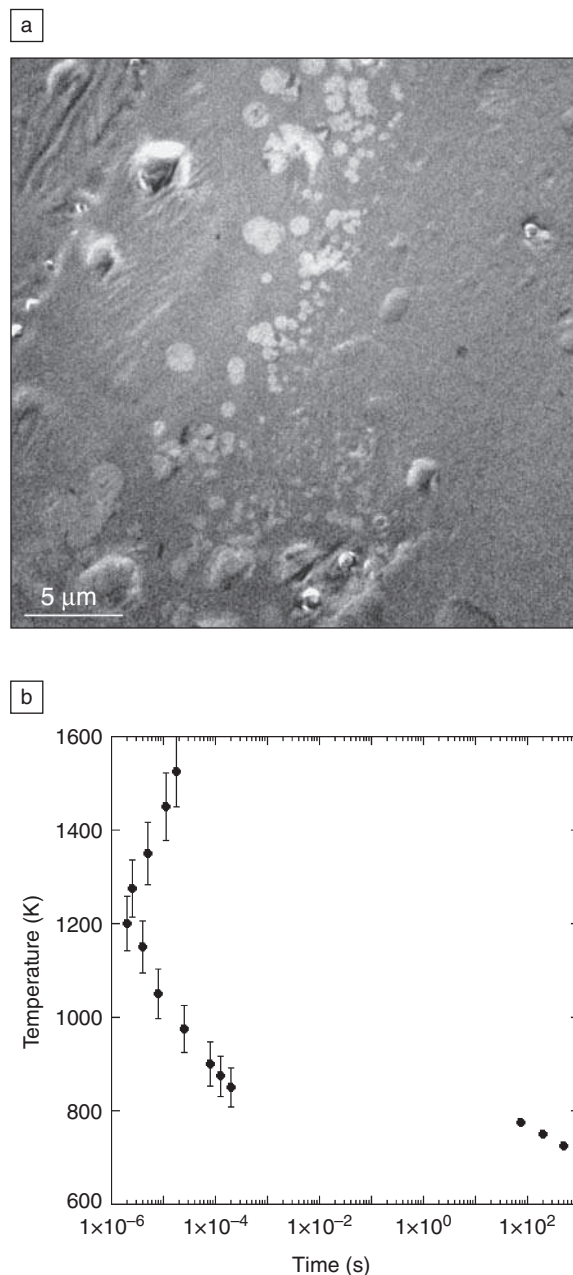


Figure 2. (a) A time-resolved plan-view image of an amorphous NiTi thin film, acquired in the dynamic transmission electron microscope (DTEM) 2 μ s after heating with a 10 ns pulse of 1064 μ m laser light. The Gaussian beam, centered out of the field of view to the left, creates a temperature gradient across the field, with higher temperatures on the left. The lighter-contrast circular spots are crystalline regions growing into the darker contrast amorphous matrix. At the left the film is too hot to nucleate, and at the right it is too cold to nucleate crystals in the 2 μ s interval since the laser irradiation. (b) The time-temperature-transformation diagram determined by DTEM experiments like those in (a) (points with error bars, left) and by traditional furnace-heating *in situ* experiments (points on right). The DTEM experiments probe extreme conditions that are inaccessible to characterization by any other means and reveal the “C-curve,” in which nucleation takes longer for temperatures that are either too high or too low.

At low doses, ≤ 1 dpa, damage in pure Fe took the form of small, isolated dislocation loops with Burgers vectors $\mathbf{b} = \langle 100 \rangle$ and $\frac{1}{2}\langle 111 \rangle$. Loops with $\mathbf{b} = \frac{1}{2}\langle 111 \rangle$ were highly mobile, moving by discrete hops from one position to another, both during and after ion irradiation.²² Similar loops formed in FeCr alloys but were less mobile than in pure Fe. At temperatures $\leq 300^\circ\text{C}$ and doses ≥ 1 dpa, complex microstructures developed in thicker regions of the foils, both in pure Fe and FeCr alloys. First, strings of several loops formed, all with the same $\frac{1}{2}\langle 111 \rangle$ Burgers vector, involving cooperative movement of individual loops. Then, larger loops were produced by the coalescence of loops in a string. In high-purity Fe irradiated at 300°C , further coalescence and complex glide and climb processes led to the formation of large (several μm) finger-shaped loops with $\mathbf{b} = \frac{1}{2}\langle 111 \rangle$ and large shear components. By this stage, the loop nature could be shown to be interstitial.²³ In pure Fe at temperatures higher than 300°C , square-shaped sessile edge interstitial loops with $\mathbf{b} = \langle 100 \rangle$ nucleated and grew to large sizes. At temperatures $\leq 450^\circ\text{C}$, these $\langle 100 \rangle$ loops co-existed with $\frac{1}{2}\langle 111 \rangle$ loops, but at 500°C , only $\langle 100 \rangle$ loops formed. Mobile $\frac{1}{2}\langle 111 \rangle$ loops formed at temperatures just below 500°C were seen to move to, and be subsumed by, large $\langle 100 \rangle$ loops.²⁴ This change in the predominant Burgers vector type with temperature is consistent with recent theoretical work by Dudarev et al.²⁵

ODS steels owe their favorable mechanical properties to their special microstructure, especially the oxide precipitates. The investigation of the irradiation-altered phase stability of this microstructure, in particular of these nanosize particles, is thus necessary to determine whether these properties are maintained under irradiation. These alloys are under consideration for fuel-cladding applications in future, Gen-IV reactors, so neutron-irradiation-induced damage is a critical issue. A recent study by a group from Penn State University addressed this, one of the main materials research issues for this class of steels identified by the Gen-IV working groups.²⁶

In that study, several ODS ferritic/martensitic steels, produced by mechanical alloying with Y_2O_3 particles, are being considered for advanced nuclear power applications. Characterization of the initial precipitate population revealed (within the limitations of the technique) two populations of nanoparticles in term of size: small nanoclusters less than 10 nm in size and larger nanoparticles up to a few hundred nanometers. The alloys were irradiated, in the IVEM-Tandem facility at Argonne National Laboratory (ANL), with Fe and Kr ions at 25°C and 500°C . The use of 1 MeV Kr ions allowed high doses (more than 100 dpa) to be achieved. Various effects of ion irradiation were observed as they occurred, including amorphization of large particles at 25°C , dislocation-loop formation, voids, and precipitate dissolution and formation. At 500°C , amorphization does not occur, and the fine particles are still present at the end of the irradiations. Another important observation is that the alloys retain their microstructural grain morphology even after reaching doses as high as 100 dpa; this is very important for assessing whether the properties relying on grain microstructure can be retained under high doses.²⁷

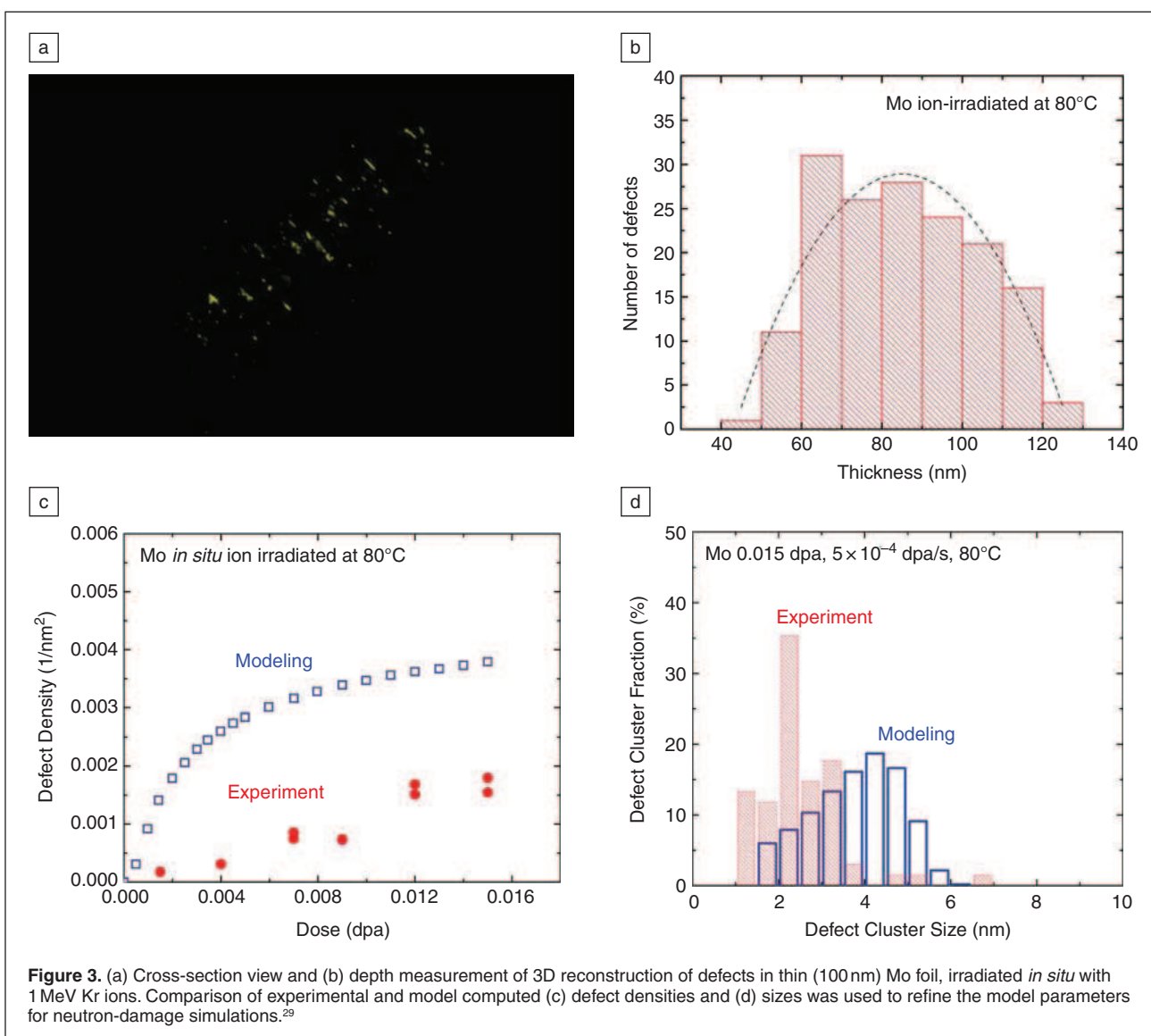
A new effort has been initiated to use *in situ* ion irradiation to improve and validate computer-model simulations for predicting neutron irradiation effects. The nature of neutron irradiation experiments has limited their use in providing direct experimental evidence for these computational models, while *in situ* TEM ion irradiation has significant advantages. However, the different aspects of damage produced by neutron irradiation and *in situ* ion irradiation must be appreciated, and one of the most critical aspects is the role of the loss of mobile defects and defect clusters to nearby foil surfaces in *in situ* ion irradiated thin foils. Previously, the effect of foil surfaces was measured indirectly in the electron microscope in the usual plane view images.²⁸ In a recent experiment using the IVEM-Tandem facility for comparing and benchmarking computer simulations of radiation damage in *in situ* ion-irradiated thin foils, the defect density was measured in three dimensions by electron tomography.

While electron tomography has been used in biological specimen examinations for several decades, only recently has it been applied in materials science to image structures in 3D on the nanometer scale. Here we use diffraction contrast, with precise control of constant diffraction conditions over a high tilt range, and apply this technique to *in situ* ion irradiation of thin foils.²⁹ The nanometer-sized defects are expected to vary strongly in density with foil depth, but there are no chemical differences that would allow use of other imaging techniques.

Both plane view and 3D images were analyzed and compared in detail with computer model simulations of *in situ* ion irradiated molybdenum under the exact experimental conditions (Figure 3). Experimental results were used to refine model parameters until improved agreement of defect densities and sizes was achieved. This validated model can then be utilized in simulations of neutron damage in bulk materials under extreme conditions of high radiation dose and temperature. The irradiation defect study in molybdenum serves as an example to show the important role of the *in situ* TEM ion irradiation and tomography techniques in advancing the fundamental understanding of irradiation damage by a coordinated approach of computational modeling and experimental validation. The experiments are intended to show an emerging new research direction in using the IVEM-Tandem facility to measure defect structures in 3D and to validate computational modeling for simulating neutron irradiation damage.

Materials under extreme pressure

A consistent theme of this article is the use of lasers to create the extreme conditions used for the *in situ* experiments. At the top end of the scale, high-power laser systems have the capability of generating short-lived (~ 10 ns) high-energy density ($> 10^9 \text{ J/m}^3$) states of matter.^{30,31} Understanding materials properties at these extreme conditions is critical for planetary studies ($> 1000 \text{ GPa}$)³⁴ and inertial confinement fusion ($> 10^5 \text{ GPa}$).³⁵ To study the atomic structure of materials requires single shot nanosecond *in situ* x-ray diffraction while the material is in the high-pressure state.^{31–33}



The basis of these experiments is a pump-probe configuration.³⁶ We use one collection of laser beams to provide the material state through dynamic ablative compression. The simplest form of ablative compression is directly exposing the target surface with a constant laser energy to create a Hugoniot state.³⁰ The optical laser light also can be converted to x-rays in a hohlraum, and varying the temporal profile of the x-ray distribution can provide a loading history closer to the isentrope.³⁷ These quasi-isentropic drives are being developed for the National Ignition Facility to achieve a solid-state compression greater than 1000 GPa.³⁷

A second set of beams is focused on a small (<0.1 mm diameter) spot to generate a bright burst of quasi-monochromatic x-rays, which are used to probe the state of atomic structure using *in situ* x-ray diffraction. Typically these experiments use thermal K-shell emission from mid-Z elements (V, Ti, Fe, Cu) as backlighters because the photon energy is high enough to record diffraction from multiple lattice planes and can be generated on mid-level laser systems with $\sim 10^{15}$ W/cm² laser intensities.³⁸

The other regime is using K- α emission from a short pulse laser beam incident on a foil target, where the x-ray energy can exceed 22 keV (Ag K- α)³⁹ and pulse duration is ~ 10 ps. One great benefit of using a laser system is the exquisite time resolution. Typically the jitter set between the drive and backlighter beams will be on the order of 50 ps, with the ability to measure it to higher precision during the actual experiment. This is ideal for measuring material kinetic processes initiated during the dynamic loading.

Schematic of typical experimental setups are shown in **Figure 4** for both (a) single-crystal⁵³ and (b) polycrystalline materials.⁴¹ The single-crystal geometry takes advantage of the divergent source to probe the crystal with a range of incident angles. Diffraction occurs where the Bragg condition is met on the sample surface; when pressure is applied, the interatomic plane spacing changes, causing an associated shift in the Bragg angle. Typically the diffracted signal is recorded on large-area-image-plate detectors. In the polycrystalline case, the x-ray source is collimated using a series

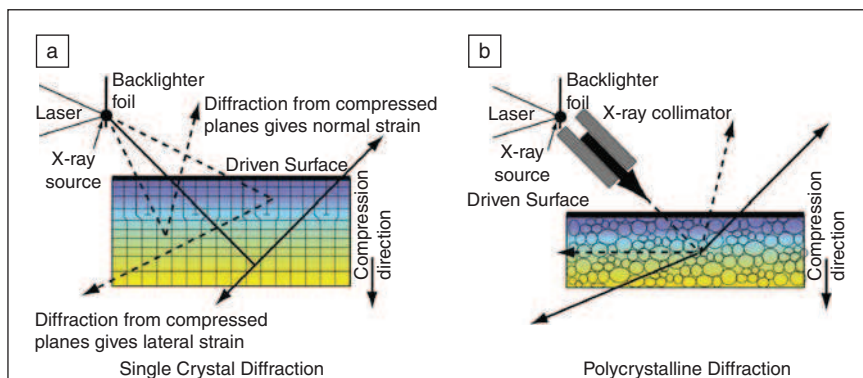


Figure 4. Schematic representation of *in situ* x-ray diffraction experiments on large-scale lasers. A high-intensity focused beam will generate a point source of x-rays at wavelengths characteristic of the material irradiated. In the single-crystal case (a), a wide range of angles are incident on the crystal surface, and wherever the Bragg condition is met, diffraction occurs. For polycrystalline materials (b), the x-ray beam is collimated, and a large detector is placed around the sample to record the Debye-Scherrer rings. VISAR: Velocity interferometer system for any reflector.

of pinhole apertures, and the diffraction angle 2θ is measured relative to the incoming beam. In the shock case, the x-ray pulse is timed so that the finite penetration depth and probe time will give a record of the unshocked sample, which provides a reference from which to measure the lattice change. **Figure 5** schematically represents how to record both static and dynamic data on a single shot. **Figure 6** shows example *in situ* x-ray diffraction data from (a) single crystals³² and (b) polycrystals.⁴² The single-crystal data show a series of arcs from the conic section that meets the Bragg condition on the surface of the crystal. The position and curvature of the arcs give plane spacing and orientation. Forward calculations and knowledge of the initial sample structure and orientation can be used to identify the planes associated with each arc. Positions

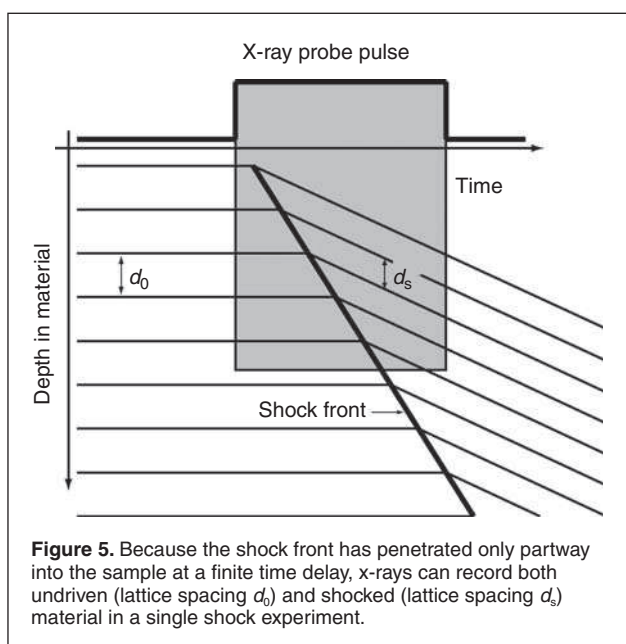


Figure 5. Because the shock front has penetrated only partway into the sample at a finite time delay, x-rays can record both undriven (lattice spacing d_0) and shocked (lattice spacing d_s) material in a single shock experiment.

along the arc give spatial resolution along the surface of the sample. The polycrystalline data are spatially integrated over an area of $\sim 1 \text{ mm}^2$. By measuring the associated change in 2θ , we can determine the compression of the material.

Summary and future directions

Although *in situ* methods require a great deal of time and effort to establish meaningful and reproducible conditions, the effort is beginning to pay off with unprecedented scientific information about materials under extreme conditions. For the future, the overarching goals are clear: we need to look at larger samples, increase the speed at which measurements can be achieved, investigate samples under higher irradiation doses, pressures, and temperature gradients, and couple these measurements directly with

first-principles simulations. In the near term, there are obvious new experiments that can be performed.

In the case of electron microscopy, *in situ* irradiation capabilities can be coupled with aberration-corrected microscopes to increase the spatial resolution and sensitivity of the analyses. Additionally, coupling the irradiation capabilities with a dynamic transmission electron microscope (DTEM) may allow the individual irradiation tracks to be analyzed while they occur. For DTEM, the goal is clearly to move to faster timescales. By moving to higher voltages, using concepts such as pulse compression and incorporating new gun designs, it may be possible to increase temporal resolution into the picosecond regime with a spatial resolution that will permit the observation of structural dynamics (although atomic resolution is unlikely). The higher voltages will allow for thicker samples that may permit shocks to be established in the TEM samples and a closer connection established with the other experimental methods.

In the case of x-ray scattering, current time-resolved results are limited by both the detector geometry and inherent limitations of the laser drive system. Results of two-dimensional scattering experiments on recovered material indicate that the end-state voids are not spherical. Whether this is true throughout the process will be addressed in future experiments using a two-dimensional detector, along with a beam-shuttering system to allow a much longer read-out interval. Ultimately, there is much to be gained by tighter synchronization between the laser and x-ray source pulses, and this is the long-term direction to be pursued at either a synchrotron or an x-ray free-electron laser-based source (such as the Linac Coherent Light Source), which offers much higher single-pulse x-ray intensity. Such advances will allow an investigation of the early time behavior of void nucleation and growth as well as void compression in foam materials, both of which require detection of very small changes in the shape of the overall scattering curve.

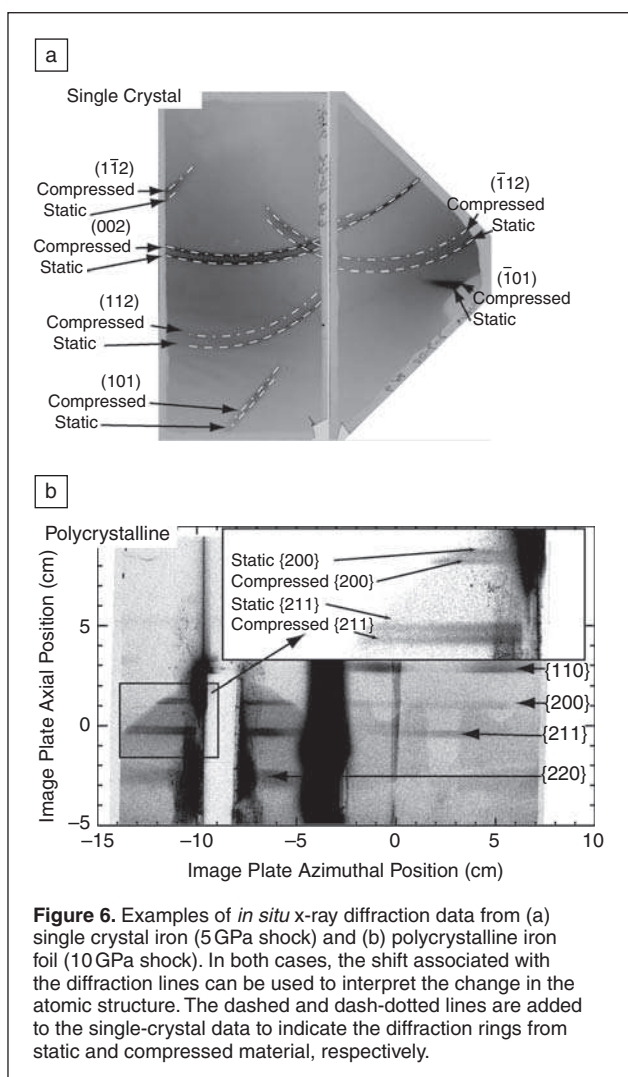


Figure 6. Examples of *in situ* x-ray diffraction data from (a) single crystal iron (5 GPa shock) and (b) polycrystalline iron foil (10 GPa shock). In both cases, the shift associated with the diffraction lines can be used to interpret the change in the atomic structure. The dashed and dash-dotted lines are added to the single-crystal data to indicate the diffraction rings from static and compressed material, respectively.

Finally, with the commissioning of the National Ignition Facility and its expanding science program,⁴³ there are opportunities to achieve unprecedented high pressures in a controlled laboratory setting. At these ultrahigh pressures, a new scientific opportunity to study materials at extremes is forming. This new pressure regime will allow us to address questions such as what is a solid at >1000 GPa? Do all materials form a close-packed structure? How large a role do the inner-shell electrons play in determining material structure when the material is compressed to four times solid density? The ability to record atomic structure *in situ* will play a key role in answering these questions, and many others, as we explore new regimes of ultrahigh pressure. As with all the methods for *in situ* analysis, we will continue to discover new structural features and processes that will help in the development of advanced materials systems to work under extreme conditions.

Acknowledgments

Aspects of this work were performed under the auspices of the U.S. Department of Energy by Lawrence Livermore

National Laboratory and supported by the Office of Science, Office of Basic Energy Sciences, Division of Materials Sciences and Engineering, of the U.S. Department of Energy under Contract DE-AC52-07NA27344. Aspects of this work were performed under the auspices of the U.S. Department of Energy by Lawrence Livermore National Laboratory under Contract DE-AC52-07NA27344. Aspects of this work were also supported by the U.S. Department of Energy Office of Science under Contract No. DE-AC02-06CH11357.

References

1. P.B. Hirsch, R.W. Horne, M.J. Whelan, *Philos. Mag.* **1**, 677 (1956).
2. M. Haider, S. Uhlemann, E. Schwan, H. Rose, B. Kabius, K. Urban, *Nature* **392**, 768 (1998).
3. P.E. Batson, N. Dellby, O.L. Krivanek, *Nature* **418**, 617 (2002).
4. G.W. Zhou, J.C. Yang, *J. Mater. Res.* **20**, 1684 (2005).
5. S. Hofmann, R. Sharma, C. Ducati, G. Du, C. Mattevi, C. Cepek, M. Cantoro, S. Pisana, A. Parvez, F. Cervantes-Sodi, A.C. Ferrari, R. Dunin-Borkowski, S. Lizzit, L. Petaccia, A. Goldoni, J. Robertson, *Nano Lett.* **7**, 602 (2007).
6. R. Sharma, *J. Mater. Res.* **20**, 1695 (2005).
7. A.M. Minor, S.A.S. Asif, Z.W. Shan, E.A. Stach, E. Cyranowski, T.J. Wyrobek, O.L. Warren, *Nat. Mater.* **5**, 697 (2006).
8. Z.W. Shan, R.K. Mishra, S.A.S. Asif, O.L. Warren, A.M. Minor, *Nat. Mater.* **7**, 115 (2008).
9. B.G. Clark, I.M. Robertson, L.M. Dougherty, D.C. Ahn, P. Sofronis, *J. Mater. Res.* **20**, 1792 (2005).
10. D.J. Siwick, J.R. Dwyer, R.E. Jordan, R.J.D. Miller, *Science* **302**, 1382 (2003).
11. T. LaGrange, M.R. Armstrong, K. Boyden, C.G. Brown, G.H. Campbell, J.D. Colvin, W.J. DeHope, A.M. Frank, D.J. Gibson, F.V. Hartemann, J.S. Kim, W.E. King, B.J. Pyke, B.W. Reed, M.D. Shirk, R.M. Shuttlesworth, B.C. Stuart, B.R. Torralva, N.D. Browning, *Appl. Phys. Lett.* **89**, 044105 (2006).
12. T. LaGrange, G.H. Campbell, B. Reed, M. Taheri, J.B. Pesavento, J.S. Kim, N.D. Browning, *Ultramicroscopy* **108**, 1441 (2008).
13. M.R. Armstrong, K. Boyden, N.D. Browning, G.H. Campbell, J.D. Colvin, W.J. DeHope, A.M. Frank, D.J. Gibson, F.V. Hartemann, J.S. Kim, W.E. King, T.B. LaGrange, B.J. Pyke, B.W. Reed, R.M. Shuttlesworth, B.C. Stuart, B.R. Torralva, *Ultramicroscopy* **107**, 356 (2007).
14. B.W. Reed, M.R. Armstrong, N.D. Browning, G.H. Campbell, J.E. Evans, T. LaGrange, D.J. Masiel, *Microsc. Microanal.* **15**, 272 (2009).
15. O. Bostanjoglo, T. Rosin, *Mikroskopie* **36**, 344 (1980).
16. O. Bostanjoglo, T. Rosin, *Phys. Status Solidi A* **57**, 561 (1980).
17. V.A. Lobastov, R. Srinivasan, A.H. Zewail, *Proc. Nat. Acad. Sci. U.S.A.* **102**, 7069 (2005).
18. T. LaGrange, D.S. Grummon, B.W. Reed, N.D. Browning, W.E. King, G.H. Campbell, *Appl. Phys. Lett.* **94** (2009).
19. J.M. Ting, P. Chen, *J. Vac. Sci. Technol., A* **19**, 2382 (2001).
20. H.J. Lee, H. Ni, D.T. Wu, A.G. Ramirez, *Appl. Phys. Lett.* **87** (2005).
21. J.A. Hinks, *Nucl. Instrum. Methods Phys. Res., Sect. B* **267**, 3652 (2009).
22. Z. Yao, M. Hernandez-Mayoral, M.L. Jenkins, M.A. Kirk, *Philos. Mag.* **88**, 2851 (2008).
23. M. Hernandez-Mayoral, Z. Yao, M.L. Jenkins, M.A. Kirk, *Philos. Mag.* **88**, 2881 (2008).
24. Z. Yao, M.L. Jenkins, M. Hernández-Mayoral, M.A. Kirk, *Philos. Mag.* **1–12** (2010).
25. S.L. Dudarev, R. Bullough, P.M. Derlet, *Phys. Rev. Lett.* **100**, 135503 (2008).
26. U.S. DOE Nuclear Energy Research Advisory Committee, "A Technology Roadmap for GenIV Nuclear Technology Systems" (2002); http://gif.inel.gov/roadmap/pdfs/gen_iv_roadmap.pdf.
27. D. Kaoumi, A.T. Motta, M. Kirk, T. Faney, B. Wirth, "Microstructure Evolution of a Model F/M Steel Irradiated with Ions In-Situ in a TEM and Modeling," Electron Microscopy and Multiscale Modelling 2009 (EMMM09), Zurich, Switzerland, 2009.
28. M. Kirk, M. Li, P. Baldo, *Microsc. Microanal.* **15** (Suppl. 2), 1348 (2009).
29. M. Kirk, M. Li, P. Baldo, *Microsc. Microanal.* **16** (Suppl. 2), 1608 (2010).
30. A. Ng, D. Parfeniuk, L. DaSilva, *Phys. Rev. Lett.* **54**, 2604 (1985).
31. D.H. Kalantar, B.A. Remington, J.D. Colvin, K.O. Mikaelian, S.V. Weber, L.G. Wiley, J.S. Wark, A. Loveridge, A.M. Allen, A.A. Hauer, *Phys. Plasmas* **7**, 1999 (2000).
32. A. Loveridge-Smith, A. Allen, J. Belak, T. Boehly, A. Hauer, B. Holian, D. Kalantar, G. Kyrila, R.W. Lee, P. Lomdahl, M.A. Meyers, D. Paisley, S. Pollaine, B. Remington, D.C. Swift, S. Weber, J.S. Wark, *Phys. Rev. Lett.* **86**, 2349 (2001).

33. D.H. Kalantar, J.F. Belak, G.W. Collins, J.D. Colvin, H.M. Davies, J.H. Eggert, T.C. Germann, J. Hawreliak, B.L. Holian, K. Kadau, P.S. Lomdahl, H.E. Lorenzana, M.A. Meyers, K. Rosolankova, M.S. Schneider, J. Sheppard, J.S. Stolken, J.S. Wark, *Phys. Rev. Lett.* **95**, 075502/1-4 (2005).
34. J. Hawreliak, J. Colvin, J. Eggert, D.H. Kalantar, H.E. Lorenzana, S. Pollaine, K. Rosolankova, B.A. Remington, J. Stölken, J.S. Wark, *Astrophys. Space Sci.* **307**, 285 (2007).
35. J. Lindl, *Phys. Plasmas* **2**, 3933 (1995).
36. J.S. Wark, R.R. Whitlock, A.A. Hauer, J.E. Swain, P.J. Solone, *Phys. Rev. B* **40**, 5705 (1989).
37. B.A. Remington, R.M. Cavallo, M.J. Edwards, D.D.M. Ho, B.F. Lasinski, K.T. Lorenz, H.E. Lorenzana, J.M. McNaney, S.M. Pollaine, R.F. Smith, *Astrophys. Space Sci.* **298**, 235 (2005).
38. D.W. Phillion, C.J. Hailey *Phys. Rev. A* **34**, 4886 (1986).

39. H.S. Park, N. Izumi, M.H. Key, J.A. Koch, O.L. Landen, P.K. Patel, T.W. Phillips, B.B. Zhang, *Rev. Sci. Instrum.* **75**, 4048 (2004).
40. D.H. Kalantar, E. Bringa, M. Caturia, J. Colvin, K.T. Lorenz, M. Kumar, J. Stolken, A.M. Allen, K. Rosolankova, J.S. Wark, M.A. Meyers, M. Schneider, T.R. Boehly, *Rev. Sci. Instrum.* **74**, 1934 (2003).
41. J. Hawreliak, H.E. Lorenzana, B.A. Remington, S. Lukezic, J.S. Wark, *Rev. Sci. Instrum.* **78**, 083908 (2007).
42. J. Hawreliak, M. Butterfield, H. Davies, B.El-Dasher, A. Higginbotham, D.H. Kalantar, G. Kimminau, J. McNaney, D. Milathianaki, W.J. Murphy, B. Nagler, N. Park, B. Remington, L. Thorton, T. Whitcher, J.S. Wark, H. Lorenzana, *AIP Conf. Proc.* **955**, 1327 (2007).
43. "For Users: Science at the National Ignition Facility;" https://lasers.llnl.gov/for_users. □



www.materialsforenergy.org


MATERIALS RESEARCH SOCIETY
Advancing materials. Improving the quality of life.

Join the Conversation on the Materials for Energy Blog

- READ** about bioremediation for oil spills, materials availability for electric vehicles, or the hottest superconductors
- CONTRIBUTE** your thoughts to the developing stories
- SUBSCRIBE** to the Materials for Energy RSS feed
- SHARE** the news with friends and colleagues—Link to Facebook, LinkedIn, Twitter and other social media

Valveless

NEW!

Programmable, Digital Dispensing & Metering

PDS-100



Ideal for...
**Analytical Lab, Process,
& Production**

- Many Dispense & Metering Modes
- Intuitive Set-up & Programming
- Single, Dual Channel & "Pulseless Flow"
- Easy Integration with Process Controls
- Dispense from 500 nL

FMI Pumps feature:
One Moving Part
Ceramic Internals
1% Accuracy




FLUID METERING, INC.

516-922-6050 / 800-223-3388
 or visit us at www.fmipump.com



UPCOMING GSAS SESSION



Global School for Advanced Studies
Training Global Leaders in Science and Engineering

GRAPHENE FUNDAMENTALS AND APPLICATIONS

June 20-26, 2011 ■ Grenoble, France



GSAS Sessions foster innovative research in critical global challenge areas and prepare young researchers from around the world to lead global research initiatives.

This Session will include: systems-based lectures, team research planning and mentoring by leading international experts such as **Harry Kroto, Sumio Iijima, Daniel Neumaier**, and others.

Members of the winning research team(s) will be hired as postdocs to implement their project(s) at CEA laboratories in Grenoble.

Senior graduate students and postdocs from all related disciplines are invited to apply.

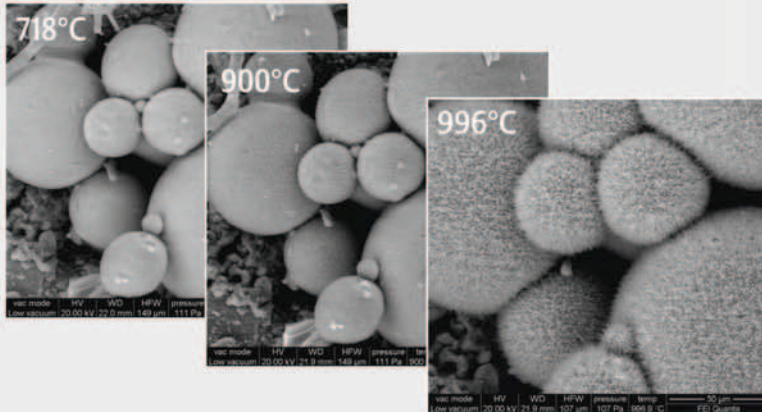
www.gsasprogram.org

Email Contact: mri@northwestern.edu





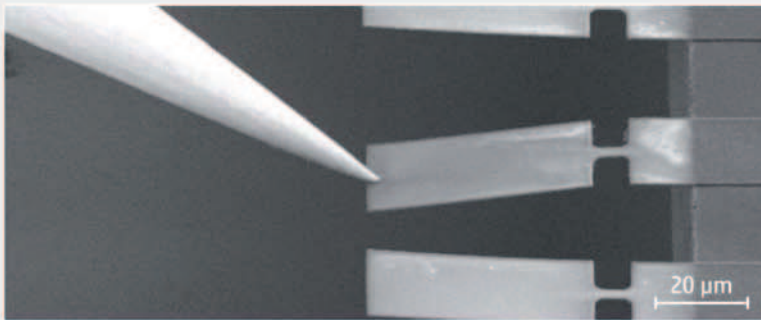

in situ NanoProcesses



Courtesy of FEI
NanoPort,
The Netherlands

Heating effects

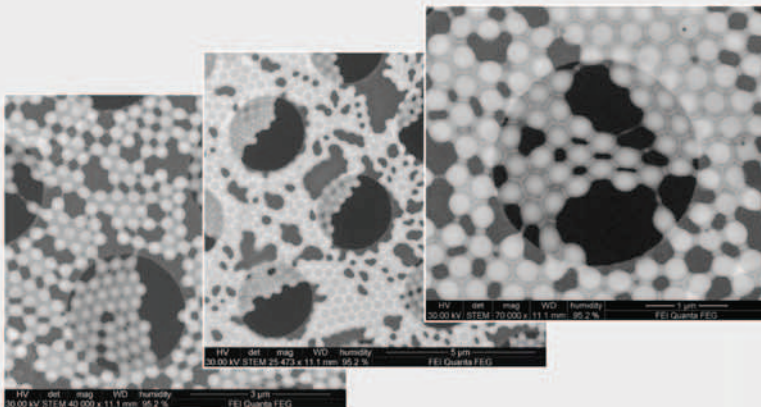
in situ heating of metal spheres allows monitoring of surface morphology development



Courtesy of Ghodssi
et al, University of
Maryland, USA

Mechanical testing

in situ probing of a nanocantilever at cryogenic temperatures gives valuable insight into mechanical properties



Courtesy of the
Cavendish Laboratory,
Cambridge University,
United Kingdom

Wet samples

in situ wetSTEM observation of latex spheres shows formation of crystallographic clusters

Learn more at FEI.com/research

© 2010. We are constantly improving the performance of our products, so all specifications are subject to change without notice.

